HIGH RESOLUTION TECHNIQUES FOR THE MEASUREMENT OF COMPONENT AND DEVICE PERFORMANCE

by

KURT ANDRE APRIL

Submitted to the University of Cape Town in
fulfilment of the requirements for the degree of
Masters of Science in Electrical Engineering

April 1996

SYNOPSIS

This aim of this thesis was to conduct an investigation into the performance of components and devices, whilst focusing on specific parameters and characteristics, by making use of high precision measurement techniques and incorporating a PC-based data acquisition system.

An accurate and versatile measurement-card, employing a 12-bit analogue-to-digital converter, was designed and developed. The card, which plugs directly into the I/O bus of any computer, has an accuracy of one least significant bit (approximately 0.02%), which is remarkably better than most A/D cards available on the market at present. Executable software was written in Pascal and TurboVision to facilitate the proper operation of the card, and to provide a platform for the user to define certain parameters during experimentation. The measurement-card has been used, with success, during all of the investigative experiments conducted for this thesis.

An experiment using a computer, the measurement-card, and a pressure/temperature unit, employing a MPX100AP pressure sensor and LM35 temperature sensor, was set up to act as a "weather station" over short periods (minutes, hours) and long periods (days, weeks). Analogue device, viz., a barometer and thermometer, were used as control instruments in order to verify the readings taken. The results obtained from this experiment were highly satisfactory.

The negative feedback of operational amplifier circuits result in the output resistance being "negligibly" low. The LF351 voltage follower, with 100% negative feedback, was chosen as being the most challengingly low value available. The circuit used to determine this output resistance was developed over various stages, employing many methods of calibration and redesign. To measure this resistance meaningfully, high gain was needed, the output currents had to be kept below the non-linear region of the device, and the load

resistance covered the full range of positive and negative current. The presence of noise, during experimentation, indicated that the experiment-under-test was virtually at the limit of measurement. The final output resistance of the operational amplifier, determined in this manner, was found to be 3.83mΩ. The change in output response of the operational amplifier as a result of power supply fluctuations was also investigated. With the operational amplifier connected as an unity-gain inverting amplifier, it was found that by lowering the power supply voltage from ±12V to ±8V, the deviation from unity (error) increased from 0.345ppt to 1.255ppt, i.e., a 3.5 times degradation in output.

The change in component values and integrated circuit performance as a function of temperature is conspicuously low for those currently used. The changes, usually summarised by a simple temperature coefficient, are measurable and can be of design importance. Seven different types (and variants) of components were studied, i.e., carbon film- and metal-film resistors, Polyester capacitors and piezo-ceramic capacitors, soft ferrite Pot- and E-cores, and a range of zener diodes. The instrumentation amplifier was the central component of these experiments. The primary feature of all these experiments was the symmetry of two channels. They were virtually identical, but one was subject to the various parameter changes and the other was held constant (reference). Measurements were targeted at parts per thousand and parts per million. As the work progressed, it became evident that the symmetry idea was quite widely applicable to precision measurements, e.g., using two crystal oscillators, the temperature coefficient which is less than 1ppm/°C is quite measurable. Calibration, directly related to the instrumentation amplifier's output and measured in parts per thousand and parts per million, were carried out right at the circuit itself, avoiding intermediate steps such as measuring the overall gain of the circuit. Minimum early experiments were valuable in arriving at a final design and experiment plan. For temperature cycling, an aluminium plate was used, which was large enough to accommodate the sensitive components of the circuit, the temperature sensor, and heater resistors. The heater was located so as to minimise temperature gradients which could exist, whilst the temperature sensor and unit-under -test was kept in very close proximity. Temperature cycling gave good insight into thermal hysteresis, which was due to reversal of heat flow on heating and cooling. The thermal effect became of great interest

when rather bulky capacitors and inductors were studied. Techniques to correct for the thermal hysteresis were developed. The carbon film resistor, the most common and cheapest, had the least impressive performance, compared to the metal-film resistors, and exhibited a negative temperature coefficient of : -383.67ppm/°C ± 0.22ppm/°C, whilst the metal-film resistors displayed a positive temperature coefficient of +52.26ppm/°C ± 0.107ppm/°C. Due to its high temperature coefficient, i.e., +342.47ppm/°C ± 10ppm/°C, the Wima polyester capacitors proved unsuitable for applications where a stable, low-loss component is required. Experimental results led to the belief that there might be a case for heatsinking or recessing capacitors when used in circuits which require precise measurement. The expected temperature dependence of the piezo-ceramics were evident in the investigations, and the temperature coefficient was found to be +212.9ppm/°C,. However, the exponential increase in capacitance with temperature was alarming, viz., as the temperature was increased, the change in capacitance increased to nearly infinity. An exponential extrapolation was done until, theoretically, the Curie point was reached around 200°C. The pot- and E-cores has similar temperature coefficients, i.e., +117.4ppm/°C and +103.7ppm/°C respectively. Both of these cores are extremely temperature dependent, which was expected, and exhibited quadratic output responses when heated, with maximums at 75°C. A full range of zener diodes were also studied, from the 3.9V (with a -771ppm/°C temperature coefficient) to one of the 9.1V zener diodes, with a very high positive temperature coefficient. The 6.8V zener diode was virtually independent of temperature (+0.86ppm/°C temperature coefficient) and, in addition, had only 2ppm of noise. It therefore represented the best choice out of the batch studied, for applications where temperature is an important feature. A crossover voltage between the negative temperature coefficients of the 4.7V zener and the positive temperature coefficient of the 6.8V zener diode were confirmed experimentally.

For most non-critical applications, the best choice for a voltage regulator is the simple 3-terminal type, and typical of this type is the 78xx and the 79xx series, for positive and negative voltages respectively. The output response with temperature for the +5V, -5V and

+12V regulators in the series were investigated. All the regulators exhibited a quadratic response to temperature increase, with their maximum and minimum values situated at 36°C for the +5V regulator, 22.6°C for the -5V regulator and 11°C for the +12V regulator. These temperatures are reasonably adjacent to temperatures encountered in practice, and thus should be of interest to any designer or user of these regulators. A set of expected outputs has been produced, through experimentation, to assist potential users to take corrective action when using these devices, e.g., in the form of offsets. Repeated experiments showed that negative regulators are significantly more noisy than positive ones. Other regulators of the same series were also tested, but the +5V regulators had by far the most stable characteristics. Since the +5V regulator had a near perfect quadratic output, it was decided to build a temperature-compensating circuit to emulate the quadratic, in the opposite sense, so as to nullify the change in regulator output with temperature. By making use of skilful circuit design, and ingenuity, the temperature-compensating circuit was able to nullify the regulator's output to a mere 20ppm change over a 20°C temperature range, compared to 400ppm without this circuitry.

ACKNOWLEDGEMENTS

I wish to express my sincere gratitude to the following people, whom have assisted me, directly and indirectly, in the completion of my Masters thesis :

My supervisor, John F.W. Bell, Honorary Professor of Electrical and Electronic Engineering at the University of Cape Town, who provided continuing encouragement and academic insight, and who was always available to provide constructive assistance.

Amanda, my wife, for her infinite patience, kind suggestions and ceaseless encouragement, as well as being an excellent advisor concerning the intricacies of the English language.

For his skilful ability and input regarding software development, Mr Christo Kleyn.
Mr Henry Brown for the use of his personal Laserjet printer and assistance during printing.

My parents, for their tremendous understanding and moral support.

TABLE OF CONTENTS

	Page
SYNOPSIS	(i)
ACKNOWLEDGEMENTS	(v)
TABLE OF CONTENTS	(vi)
LIST OF ILLUSTRATIONS	(viii)
LIST OF TABLES	(x)
LIST OF PHOTOGRAPHS	(xi)
GLOSSARY	(xiii)
Chapter 1 : INTRODUCTION	
Chapter 2 : MEASUREMENT SYSTEMS	
2.1 : Objectives of Engineering Measurement	Page 2
2.2 : Components of Measuring Systems	Page 3
Chapter 3 : DATA CAPTURE AND STORAGE	
3.1 : Investigating the PC On-Board Power Supply	Page 2
3.2 : The Analogue-to-Digital Converter (ADC)	Page 4
3.3 : The Programmable Peripheral Interface (PPI)	Page 5
3.3.1 : Programming the 8255	Page 5
3.3.2 : Initiating Conversions with the ADC	Page 7
3.4 : Enhancing the Compatibility of the Card	Page 8
3.4.1 : Base-Address Selection	Page 8
3.4.2 : Decoder Facility	Page 9
3.4.3 : Multiplexing Facility	Page 9
3.5 : The Completed Card	Page 9
3.6 : The Weather Station	Page 12
Chapter 4 : THE INSTRUMENTATION AMPLIFIER	
4.1 : The LF351 Op-Amp	Page 2
4.2 : Output Resistance	Page 3
4.3 : The Amplifier's Response	Page 6

Chapter 5 : COMPONENTS TEMPERATURE COEFFICIENTS

5.1 : The Common Experimental Layout Page 1
5.2 : Resistors Page 5
5.2.1 : Calibration for Resistor Experiments Page 6
5.2.2 : Thermal Hysteresis Page 8
5.2.3 : Resistors Temperature Coefficients Page 10
5.2.4 : In Summary Page 14
5.3 : Capacitors Page 15
5.3.1 : Experimental Details Page 15
5.3.2 : The Wima Polyester Capacitors Page 16
5.3.3 : The Piezo-Ceramic Capacitors Page 22
5.4 : Soft Ferrite Cores Page 27
5.5 : Zener Diodes Page 35

Chapter 6 : VOLTAGE REGULATORS

6.1 : Experimental Details Page 1
6.2 : Experimental Results Page 3
6.3 : The LM7905 (-5V) Regulator Page 7
6.4 : The 12V Regulator Page 13
6.5 : The General Temperature Characteristics Page 16
6.6 : Temperature Compensation Page 18
6.6 : In Summary Page 22

Chapter 7 : CONCLUSIONS

APPENDICES

APPENDIX A1 : Software Code
APPENDIX A2 : Software Graphics
APPENDIX B : Photographs
APPENDIX C : Circuit Diagrams

REFERENCES

BIBLIOGRAPHY

LIST OF ILLUSTRATIONS

Figure 2.2a : A typical PC-based Data Acquisition System — Page 3/Chapter 2
Figure 3a : Block diagram of the ADC measuring unit — Page 2/Chapter 3
Figure 3.1a : Circuit diagram of the RLC Network — Page 3/Chapter 3
Figures 3.1b-c : Noise waveforms on the computer power supplies — Page 3/Chapter 3
Figures 3.1d-e : "Cleaned up" waveforms on the supplies of the computer — Page 4/Chapter 3
Figure 3.3a : The 8255 functions — Page 5/Chapter 3
Figure 3.3.1a : Control word format of the 8255 — Page 6/Chapter 3
Figures 3.5a-b : The printed circuit board layouts — Page 10/Chapter 3
Figure 3.6a : Pressure Variations monitored by the weather station — Page 12/Chapter 3
Figures 3.6b-e : "Exploded time frames" of the Pressure Variations — Page 13/Chapter 3
Figures 3.6f-g : The Weather Station: Pressure- and Temperature Variations — Page 14/Chapter 3
Figure 4a-b : The basic differential op-amp circuit (open loop) and a plot of the op-amp's response — Page 1/Chapter 4
Figure 4.1a-b : (a) A typical connection when using the LF351, (b) Simplified schematic of the op-amp — Page 2/Chapter 4
Figure 4.1c : Connection diagram for the LF351 — Page 3/Chapter 4
Figure 4.2a : Circuit for determining the output resistance of a LF351 op-amp — Page 4/Chapter 4
Figure 4.2b : Output voltage change for the LF351 op-amp — Page 4/Chapter 4
Figure 4.2c : A possible circuit for expanding the usefulness of the test - circuitry — Page 6/Chapter 4
Figure 4.3a : The Unity-gain inverting amplifier set-up used — Page 6/Chapter 4
Figures 4.3b-e : Output response and detrend plots of the LF351 op-amp : ±12V supplies — Page 7/Chapter 4
Figures 4.3f-i : Output response - and detrend plots of the LF351 op-amp : ±8V supplies — Page 8/Chapter 4
Figure 5.1a : Heating Plate used in experiments — Page 2/Chapter 5
Figure 5.1b : Temperature Sensing Circuitry — Page 3/Chapter 5
Figure 5.1c : Connection diagram for the AD620 — Page 3/Chapter 5
Figure 5.1d : Circuitry used to determine the temperature characteristics — Page 4/Chapter 5
Figure 5.2a : Wheatstone bridge configuration used — Page 5/Chapter 5
Figure 5.2.1a : Calibration of the bridge — Page 6/Chapter 5
Figure 5.2.1b : Calibration output plot : Metal-film resistors — Page 7/Chapter 5
Figure 5.2.1c : Calibration output plot : Carbon resistors — Page 8/Chapter 5
Figure 5.2.2a : Temperature cycling : Metal-film resistors — Page 9/Chapter 5
Figure 5.2.2b : Temperature cycling : Carbon resistors — Page 9/Chapter 5
Figure 5.2.3a : Temperature characteristic of the metal-film resistors — Page 10/Chapter 5
Figure 5.2.3b : Metal-film resistors : temp. characteristic and regressed plot — Page 11/Chapter 5
Figure 5.2.3c : Metal-film resistors : Detrend graph — Page 11/Chapter 5
Figure 5.2.3d : Temperature characteristic of the carbon resistors — Page 12/Chapter 5
Figure 5.2.3e : Carbon resistors : temp. characteristic and regressed plot — Page 13/Chapter 5
Figure 5.2.3f : Carbon resistors : Detrend graph — Page 13/Chapter 5
Figure 5.3.1a : Connection diagram of the AD637 — Page 15/Chapter 5
Figure 5.3.2a : Circuit used to determine the temperature characteristic of the Wima polyester capacitors — Page 16/Chapter 5
Figure 5.3.2b : Temperature cycling ..... on capacitors — Page 17/Chapter 5
Figure 5.3.2c-f : Comparison of temperature changes on bottom and top of the capacitors — Page 18/Chapter 5
Figure 5.3.2g : Temperature characteristic of the polyester capacitor — Page 19/Chapter 5
Figure 5.3.2h : Capacitors : experimental and regressed plots — Page 19/Chapter 5

Figure 5.3.2i : Polyester capacitor : Detrend graph Page 20/Chapter 5
Figure 5.3.3a : Calibration of the system Page 23/Chapter 5
Figure 5.3.3b : Temperature cycling : Piezoelectric transducer Page 24/Chapter 5
Figure 5.3.3c : Extrapolated plot for the piezoelectric transducer Page 24/Chapter 5
Figure 5.3.3d : Piezoelectric transducer : Linear regression Page 25/Chapter 5
Figure 5.3.3e : Exponential extrapolation until Curie Point Page 26/Chapter 5
Figure 5.4a : Circuit used to obtain Q-values for the inductors Page 29/Chapter 5
Figure 5.4b : Calibration output plot Page 30/Chapter 5
Figure 5.4c : Pot core : temperature cycling Page 30/Chapter 5
Figure 5.4d : Temperature hysteresis plot of the pot core Page 31/Chapter 5
Figure 5.4e : Reducing of thermal hysteresis in the pot core Page 31/Chapter 5
Figure 5.4f : Change in inductance of the pot core ferrite Page 32/Chapter 5
Figure 5.4g : Change in inductance of the E-core ferrite Page 32/Chapter 5
Figure 5.4h : Pot core : parabolic change in inductance Page 33/Chapter 5
Figure 5.4i : E-core : parabolic change in inductance Page 34/Chapter 5
Figure 5.5a-e : Plots of temperature slopes for a range of zener diodes Page 37/Chapter 5
Figure 5.5f-i : Linear regressions of experimental data of a range of zeners Page 38/Chapter 5
Figure 5.5j-m : Detrend graphs for a range of zener diodes Page 39/Chapter 5
Figure 5.5n : Zener reverse breakdown voltage-current characteristic Page 40/Chapter 5
Figure 5.5o-p : Zener slope resistances and temperature coefficients Page 41/Chapter 5
Figure 6.1a : Layout used for temperature cycling Page 1/Chapter 6
Figure 6.1b : Circuit used to condition the "temperature signal" Page 2/Chapter 6
Figure 6.1c : Circuit used to determine the temperature characteristics of the regulators Page 2/Chapter 6
Figure 6.2a : Calibration Method : LM7805 Page 3/Chapter 6
Figure 6.2b : Calibration Output : LM7805 Page 3/Chapter 6
Figure 6.2c : Temperature Cycling : LM7805 Page 4/Chapter 6
Figure 6.2d : Plot of the temperature characteristic of the LM7805 Page 5/Chapter 6
Figure 6.2e : An expanded view of the upper portion of the parabolic plot Page 5/Chapter 6
Figure 6.2f : Experimental values overlaid by the regressed polynomial Page 6/Chapter 6
Figure 6.2g : Detrend graph : LM7805 Page 7/Chapter 6
Figure 6.3a : Dynamic calibration technique on LM7905 Page 8/Chapter 6
Figure 6.3b : Calibration output : LM7905 Page 8/Chapter 6
Figure 6.3c : Temperature Cycling : LM7905 Page 9/Chapter 6
Figure 6.3d : Noise levels on the LM7905 output Page 10/Chapter 6
Figure 6.3e : Temperature characteristic of the LM7905 Page 10/Chapter 6
Figure 6.3f : A graphical comparison of the experimental data and the theoretical parabola Page 11/Chapter 6
Figure 6.3g : Detrend graph : LM7905 Page 12/Chapter 6
Figure 6.4a : Calibration technique : +12V regulator Page 13/Chapter 6
Figure 6.4b : Calibration output plot : LM7812 Page 13/Chapter 6
Figure 6.4c : Temperature characteristic of the +12V regulator Page 14/Chapter 6
Figure 6.4d : Departure from linearity for the +12V regulator Page 15/Chapter 6
Figure 6.4e : Detrend graph : LM7812 Page 15/Chapter 6
Figure 6.5a : Connection diagram for the AD633 Multiplier Page 18/Chapter 6
Figure 6.5b : Block diagram of the temperature-compensating circuit Page 19/Chapter 6
Figure 6.5c : Temperature-compensating circuitry output Page 19/Chapter 6
Figure 6.5d : Complete circuit diagram of the compensated testing-circuitry Page 20/Chapter 6
Figure 6.5e : Both multiplier - and regulator output Page 21/Chapter 6
Figure 6.5f : A plot of the summed output response (compensated) Page 21/Chapter 6

LIST OF TABLES

Table 6.5I : The actual deviation from +5V for a LM7805 (+5V) voltage regulator, near the axis of its output response Page 16/Chapter 6

Table 6.5II : The actual deviation from -5V for a LM7905 (-5V) voltage regulator, near the axis of its output response Page 17/Chapter 6

Table 6.5III : The actual deviation from +12V for a LM7812 (+12V) voltage regulator , near the axis of axis of its output response Page 17/Chapter 6

LIST OF PHOTOGRAPHS

Photograph 3.5α : Photograph of the completed Measurement PC-Interface Card, which employs a 12-bit ADC, built on double sided printed circuit board. Notice that the power supply regulation circuitry, and filter network, is located very close to the connector end of the card. Also, the clock crystal is situated away from the rest of the components on the board. Careful examination of the card will reveal that the analogue input circuitry, i.e., the analogue input multiplexer, ADC, etc., is designed to be on one half of the board, whilst the digital circuitry and signals, i.e., address decoding IC's data to/from the computer, etc., are on the other half of the board. Another feature is that the multiplexer was built as close to the ADC as the design and board space would allow. Components were kept as close as possible to the printed circuit board's surface. Page 11/ Chapter 3

Photograph Bα : This double sided printed circuit board is a bottom view of the 12-bit PC-interface card. The only components on this side (for the sake of saving space) are the red dipswitch, and the LM7905 (-5V) regulator. Also evident in this photograph in the protruding input jack, mounted on the top side of the board. The dimensions of the card is 135mm × 110mm, and the card plugs directly into the I/O bus of any computer. Notice the widespread ground throughout the board, which reduces the amount of noise. Appendix B

Photograph Bβ : This photograph shows the two resistors that were used during the investigation into the temperature coefficients of metal-film resistors and carbon film resistors. They are both 100Ω resistors, and the 5% tolerance carbon film resistor is shown on the left, whilst the 1% tolerance metal-film resistor is shown on the right. Notice the difference in the size of the two resistors. Also included in the photograph is the LM35 temperature sensor, which was employed in virtually all the experiments. This 3-legged device provides a voltage output with +10mV/°C slope.....it has an internal offset such that the output is 0 volts at 0°C. Appendix B

Photograph Bχ : The three devices shown are the AD633, the LF351 high speed, JFET-input operational amplifier, and the AD620 high accuracy, instrumentation amplifier. The LF351 is normally used in applications such as high speed integrators, fast D/A converters, sample-and-hold circuits, and many other circuits requiring low input offset voltage, low input bias current, high input impedance, high slew rate and wide bandwidth. The high accuracy AD620, with its low offset voltage, high common-mode rejection and extremely low offset drift of 0.6μV/°C, is ideally suited for use in precision data acquisition systems such as transducer interfaces. Appendix B

Photograph Bδ : The two voltage regulators that were studied, i.e., the LM7805 (+5V) regulator, and the LM7905 (-5V) regulator. Both these regulators exhibited parabolic output responses to increased temperature. Other regulators in the series were also tested, but the LM7805 had by far the most stable characteristics. Appendix B

Photograph Bε : The MPX100AP pressure sensor, which was used during experiments with the "weather station". The MPX100AP sensor is a silicon piezo-resistive pressure sensor. It provides a very accurate and linear voltage output, which increases with increasing pressure relative to ambient pressure (approximately 100kPa) applied to the pressure side of the device. Appendix B

Photograph Bϕ : The white 5W resistors is similar to the "heater resistors" used during experiments conducted and components to establish their temperature coefficients. The plate, onto which the unit-under-test was secured, was heated with the aid of two (white 5W) 100Ω resistors, which were connected in parallel to a 30V power supply. The 1.5μF Wima polyester capacitor (red) was studied for its thermal properties. Notice the bulky size of the capacitor. Appendix B

Photograph Bγ : A "mixed bag" of components and devices that were used, and studied, during experiments. Appendix B

GLOSSARY

C	Capacitance [Farads]
f	Frequency [hertz]
f_s	Sampling frequency [hertz]
I	Current [amperes]
L	Inductance [Henries]
t	Time [seconds]
V	Voltage [volts]
V_{FS}	Full-scale voltage
μ	Micro
μP	Micro-processor
Ω	Ohms
dV/dt	Rate of change
ADC	Analogue-to-Digital Converter
A/D	Analogue-to-Digital
Bus	A set of data-carrying wires to connect devices
D/A	Digital-to-Analogue
HP	Hewlett-Packard
IC	Integrated Circuit
I/O	Input/Output
INTEL	A company that manufactures integrated circuits
LED	Light-emitting diode
LSB	Least significant bit
MSB	Most significant bit
Op-Amp	Operational Amplifier
PASCAL	A computer programming language
PC	Personal computer

1. INTRODUCTION

"The engineer is inevitably confronted with measurements, whether he merely uses them as a tool to obtain information or becomes involved in fundamental studies of measurement theory. He must be acquainted with apparatus, methods, limitations, techniques, and accuracy capabilities of measurements. A strong foundation in principles provides the structure that supports and engenders the comprehension necessary for solution of specific problems. The important thing is to learn the discipline of analytical thought. Without such discipline, individual progress in any scientific field is likely to become frustrated and opportunities for achievement improbable. With such discipline, the horizons are virtually unlimited"

Ernest Frank, in his book : "Electrical Measurement Analysis", 1959.

This report sets out the results of an investigation into the performance of components and devices, with the aid of high precision measurement techniques and by making extensive use of a PC-based data acquisition system.

The overall concept of the work was to measure selected parameters of commonly encountered passive and active electronic components and devices. The parameters selected were those which are regarded as zero (e.g., the output resistance of an operational amplifier) or invariant (e.g., the temperature coefficient of resistors, and the sensitivity of the performance of integrated circuits to supply voltages). Most of the measurements consisted of comparing the signals from two of the circuits under test. One was held under steady conditions, which served as a reference, and the other was subjected to parameter changes. The difference between them, as a function of the changes, was measured with high precision and logged to a personal computer. The out-of-balance component was amplified by as much as was needed to do the measurement.

Although many important systems, e.g., computers, can be considered as entirely digital electronic devices, the real world is, for the most part, analogue and non-electronic. Real-world interfacing challenges engineers to produce circuits which maximise the features of the personal computer, as replacements for traditional analogue designs. The experiments used up to four channels of a 12-bit analogue-to-digital converter plug-in board with independent voltage regulator and clock. This versatile and accurate PC-interface card was designed and developed to accommodate the necessary measurements. The basic knowledge and understanding necessary to develop this card was acquired during my undergraduate thesis, which is entitled : "A study of the fundamental performance and limitations of Analogue-to-Digital Converters", where the limitations, specifications and capabilities of analogue-to-digital converters were investigated. The design and board layout eliminates the internally generated noise, which frequently bedevils commercial units. For the ultimate resolution there was a noise limitation, and this proved to be an instructive encounter.

For the experiments described, the voltage limits were ±5 volts, giving 2.4 millivolt reading steps. The experiments were designed around these limits and the high resolution needed, i.e., a few parts-per-thousand or -million, could easily be obtained. Whatever the sensor or circuit being used, the final outputs had to cover as much as the ±5 volts as possible, subject to avoiding the saturation limits. Matching the readings to the analogue-to-digital converter's input requirements required gain selection and appropriate offset. Care was taken in designing the circuits. The circuits had to be soldered throughout, and crocodile clips and similar attachments, which could have been major sources of noise, had to be avoided if parts-per-thousand and -million were to be achieved. Minimum early experiments were valuable in arriving at the final design and experiment plan.

Software was developed, using Pascal and TurboVision, to facilitate the real-time interface between circuits and the computer. The versatility of Pascal allows it to be run on personal 8-bit computers or Pentiums. The software permits the four multiplexed inputs to be displayed on the monitor of the computer, and the captured data is stored on the hard-drive.

The information on which this report is based was obtained from laboratory experiments performed, as well as published media. The laboratory experiments were limited to using the equipment available in the Electrical Engineering Department at the University of Cape Town.

At the outset, the report discusses the objectives and composition of measuring systems, and in particular, the PC-based acquisition system. This provides the theoretical background necessary for understanding many of the motives, concepts and reasons for particular laboratory set-ups used during calibration and experimentation. In addition, it describes the method of the laboratory experiments performed on various components and devices, and proceeds to an analysis of the results of these experiments.

Furthermore, conclusions were drawn regarding the performance and use of the components and devices investigated, and recommendations made.

2. MEASUREMENT SYSTEMS

"... hence we must believe that all the sciences are so interconnected, that it is much easier to study them all together than to isolate one from all the others. If, therefore, anyone wishes to search out the truth of things in serious earnest, he ought not to select one special science, for all the sciences are co-joined with each other and interdependent."

Rene Descartes (1596-1650), in his 1629 text, *"Rules for the Direction of the Mind"*. A mathematician and philosopher, Descartes systematised analytical geometry and is sometimes called the father of modern philosophy.

Ever since human beings began to think, we have exchanged information and have given measures to quantities in an attempt to understand our surroundings. In a continual process towards perfection, we are still developing and refining our tools to improve our understanding of all kinds of mechanisms. The field of engineering and scientific instrumentation encompasses activities in many engineering sciences. Among these are the branches of electronic, electrical, optical, and mechanical measurement, and data transmission, data processing, and computation. Each of these functions may take place by manual, semi-automatic, or automatic means. According to W. Wildhack, Proc. 1953 National Conference on Instrumentation : "Instrumentation in general has been considered as being the art and science of designing, constructing, and applying physical devices and systems for extending, refining, or supplementing the sensory, perceptual, or communicative facilities of man".

2.1 OBJECTIVES OF ENGINEERING MEASUREMENT

There are many reasons for testing physical systems. The aims of a data collection program may be to :

(1) measure the correctness and completeness of design;

(2) evaluate the performance of the system;

(3) permit system improvement with minimum acceptable tolerance on each component;

(4) uncover system defects at an early stage;

(5) increase the understanding of the operation of the system;

(6) determine data for new design;

(7) determine data for improved design;

(8) perform integrated control analysis; and

(9) confirm theoretical calculations.

It is generally necessary to carry out careful measurements to accomplish these aims. In conducting experimental work on engineering prototypes, these are, therefore, the common goals continually sought.

The testing procedure that is almost universally followed consists of these four steps :

(1) planning the tests,

(2) selecting the test equipment,

(3) making the tests, and

(4) analysing recorded data.

The test planning is governed by the purpose of the test and should define the input and output variables for the system. Limitations imposed by the nature of the experimental measurement are those imposed by the theory, capabilities of the system, and quantities that are incapable of measurement. The latter may occur either because of lack of knowledge of the physical theory or the technology has not uncovered a practical method. Interpretation of the data depends not only on the engineer's experience in performing tests, but also on his/her understanding of the test vehicle under test and the instrumentation capabilities and limitations.

2.2 THE COMPOSITION OF MEASURING SYSTEMS

In the last few years, industrial PC I/O products have become increasingly reliable, accurate and affordable. Also, with the development of software packages that are geared toward better productivity, speed, and ease-of-use, the computer's processing capabilities are being exploited more and more. As a result of this, PC-based data acquisition and control systems are widely used in areas such as industrial monitoring and control, laboratory experiments, data acquisition and automated testing. Data acquisition includes everything from gathering data, to transporting it, and storing it. The term *data acquisition* is described as the "phase of data handling that begins with sensing of variables and ends with a magnetic recording of raw data, and may include a complete telemetering link" ("Dictionary of Scientific and Technical Terms", 1978). Here the term "variables" refers to those physical quantities that are associated with a natural or artificial process. A data acquisition phase involves a real-time computing environment, where the computer must be keyed to the time scale of the process. Figure 2.2a below shows a layout of a typical PC-based data acquisition system.

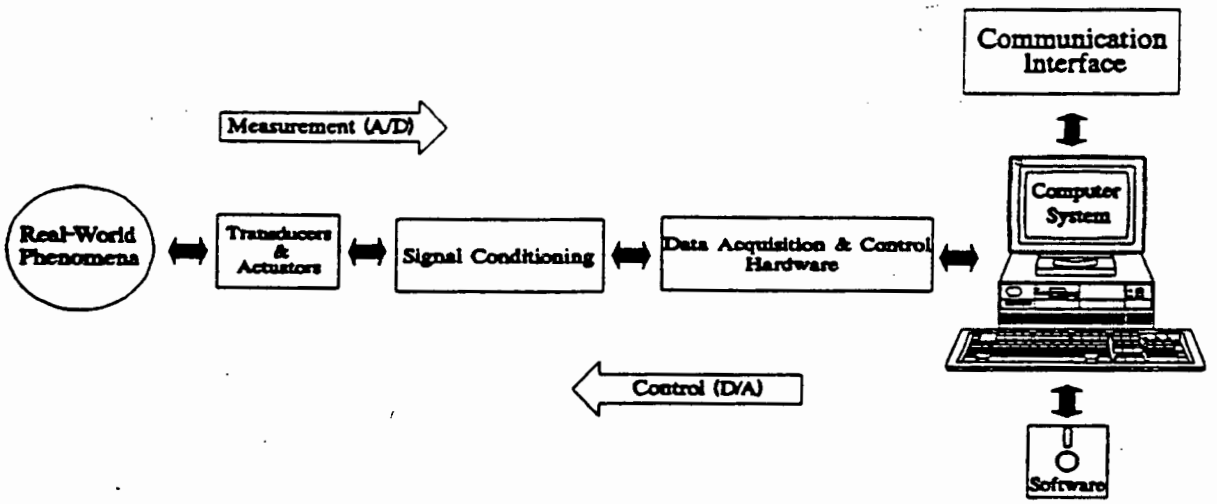

Figure 2.2a : A typical PC-based data acquisition system. This system (or part thereof) was used during all the experiments described in this thesis.

The following discussion, concerning the PC-based data acquisition system, has been adapted from : "Total Solution for PC-based Industrial Automation", by Advantech.

- *Real-world Phenomena* :

Data acquisition systems measure real-world phenomena such as temperature, pressure, level and flow rate. Although many important systems, e.g., computers, can be considered as entirely digital electronic devices, the real world is, for the most part, analogue and non-electronic. To utilise the power of digital systems to process information from this non-digital world requires transducers to convert the information to analogue electronic signals and encoders to change these to digital signals. The main advantages of a digital system over an analogue one are that the problems associated with non-linearity and gain change in the analogue system are eliminated once the signals are digitised, and the digital system can provide much greater and more flexible processing power.

- *Transducers* :

The most widely used definition of a transducer is that which has been applied to electrical transducers by the Instrument Society of America (ANSI MC6.1, 1975) : *Transducer - a device which provides a usable output in response to a specified measurand* (the *measurand* is the physical quantity, property, or condition which is measured). A transducer is more generally defined as a device which converts energy from one form to another, e.g., a transducer converts temperature, pressure, level, length, position, etc., into voltage, current, frequency, pulses or other signals.

- *Signal Conditioning* :

Signal conditioning circuits improve the quality of signals generated by transducers before they are converted into digital signals by the PC's data-acquisition hardware. Examples of signal conditioning are signal scaling, amplification, linearisation, filtering, attenuation, excitation, common-mode rejection, etc. One of the most common signal conditioning functions is amplification (converting transducer signals to high level voltage). Amplification expands the range of the transducer signals so that they match the input

range of the A/D converter, for maximum resolution. The amplifier is frequently followed by a low-pass active filter which reduces the high frequency signal components, unwanted electrical interference noise or electronic noise from the signal. The amplifier is sometimes also followed by a special non-linear analogue function circuit, which performs a non-linear operation on the high level signal. Such operations include squaring, multiplication, division, RMS conversion, log conversion, or linearisation.

- *Data Acquisition and Control Hardware* :

For maximum performance and flexibility, most data acquisition and control hardware integrates such functions as : analogue input, multiplexing, A/D converters, peripheral interface devices, analogue output, digital input and output, etc. The specific hardware used for data capture and storage during experimentation for this Masters is fully described in Chapter 3.

- *Computer Systems* :

Today's rapidly growing industrial PC market offers a great variety of industrial PC hardware and peripherals. Different applications require different system performance levels : 286, 386, 486, and Pentium CPU's are now available, allowing the user to select system performance ranging from a landmark speed of 20MHz to over 200MHz. Most measurement and process control applications usually need no more than a computer system with a 80286 CPU.

- *Software* :

The driving force behind any data acquisition and control system is software control. Programming your data acquisition and control system can be accomplished in the following three ways : hardware-level programming, driver-level programming, and package-level programming. For the experiments described in this thesis, software was written in Pascal and TurboVision, and then compiled into a "package". Hence, the application program does the work for the user, and the user simply has to tell it what to do. The software package integrates data analysis, presentation and instrument control capabilities into a single interface. The program offers a multitude of features, such as

pull-down menus, data logging and analysis, use of a mouse, real-time display, user-specified inputs, and real-time display.

To summarise, the experiments and measurements described in further chapters were all done using a PC-based data acquisition system. The objectives of engineering measurement described in Section 2.1, the adherence to the universal testing procedures, and the data acquisition system, together with careful circuit design, contributed to the high resolution techniques required to measure component and device performance.

3. DATA CAPTURE AND STORAGE

Data acquisition and conversion systems interface between the real world, which is analogue, and the 'artificial world' of digital computation and control. With current emphasis on digital systems, the interfacing function has become an important one. The devices which perform the interfacing function are analogue-to-digital converters (ADC's) and digital-to-analogue converters (DAC's). It was found that certain 12-bit ADC cards, when fitted into a computer, appear to have inherent noise of as much as 2 or 3 bits. This could be a feature of the compatibility of card and computer as, in all likelihood, the cards passed their production tests. It was therefore decided to investigate this and possibly produce a more generally compatible card. After consultation with a number of post-graduate students, university staff and people in industry, it was decided to design and produce a relatively inexpensive, robust and accurate plug-in card, which employs a 12-bit ADC and which directly interfaces with a computer. Initial investigation into the capabilities, limitations and hardware requirements surrounding the use of various analogue-to-digital converters were conducted during my final-year undergraduate thesis titled : "A critical study of the fundamental performance and limitations of Analogue-to-Digital Converters".

The approach used was to initially identify the sources and causes of electrical noise and interference. Once this was established, practical methods for the elimination of this interference was investigated. These methods were then employed in the design and building of a prototype for the final design, which was then investigated to determine its performance and limitations. Great care was taken to eliminate noise on signals and power supply rails, and keep the designs as simple as possible. Results showed that the conversion process, accuracy, and maximum conversion rate of the ADC, was dependent on a few factors such as : the clock frequency used to drive the ADC, the voltage reference to the ADC, the speed of the chips used in the periphery to make the ADC work correctly, and the internal circuitry of the ADC (e.g., how good the comparator of the ADC was, and

whether or not the converter had features such as auto-zeroing, self calibration, etc., as well as its dependence on noiseless signals and clean power supplies). The following describes how a 12-bit card, accurate to one least significant bit (approximately 0.02%), was built. Figure 3a shows the card in block form :

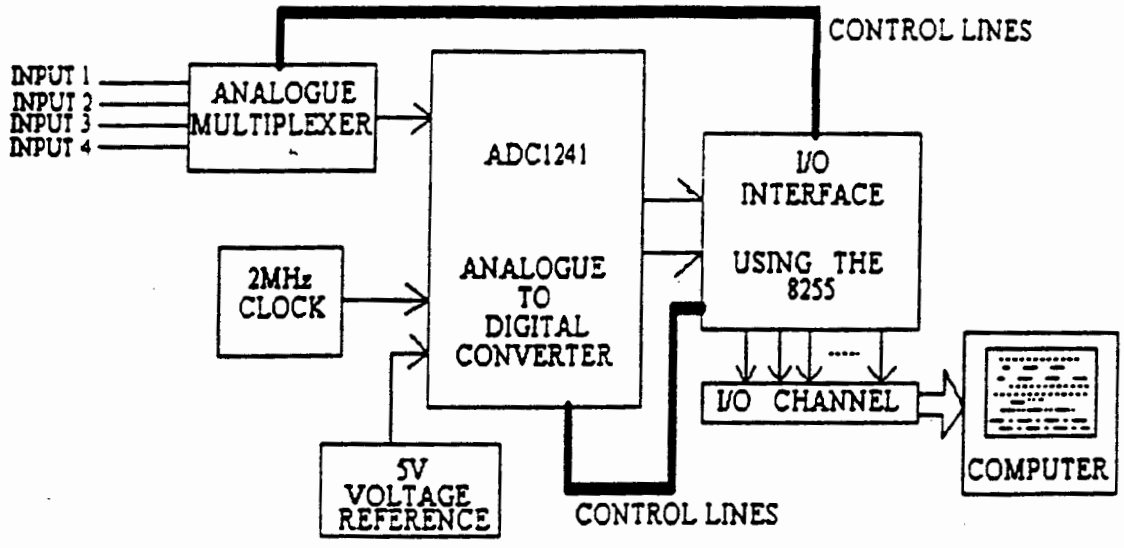

Figure 3a : Block diagram of the ADC Measuring Unit, which acted as the interface between the analogue inputs and the digital computer. With the use of the multiplexer, four analogue inputs were sampled in turn.

3.1 INVESTIGATING THE PC ON-BOARD POWER SUPPLY

An important source of error for most computer I/O devices is the noise associated with the computer's power supply rails. With the aid of a spectrum analyser, a thorough investigation revealed that the noise, superimposed onto the computer's supplies, was caused by: the switching action of the computer's switched-mode power supply, the computer clock, and mains power supply interference. A passive resistor-inductor-capacitor (RLC) network was designed to filter out the unwanted frequencies that corrupted the computer power supply rails, as shown in Figure 3.1a below. Even though the figure only shows filtering of the positive 12V supply line, this filter network was employed on the negative 12V supply rail as well.

The programming model of the 8255 consists of four 8-bit registers : ports A, B, and C, and a control register. Depending on which address the device is located in the available I/O space, the register model appears as four addresses, as shown below.

ADDRESS	/CS	A_1	A_0	SELECTED
Base	0	0	0	Port A
Base + 1	0	0	1	Port B
Base + 2	0	1	0	Port C
Base + 3	0	1	1	Control Register
—	1	X	X	8255 is not selected

The operation of the I/O ports is controlled by the format of the 8-bit word written to the control register, located at address Base + 3. The control word format of the 8255 is shown in Figure 3.3.1a.

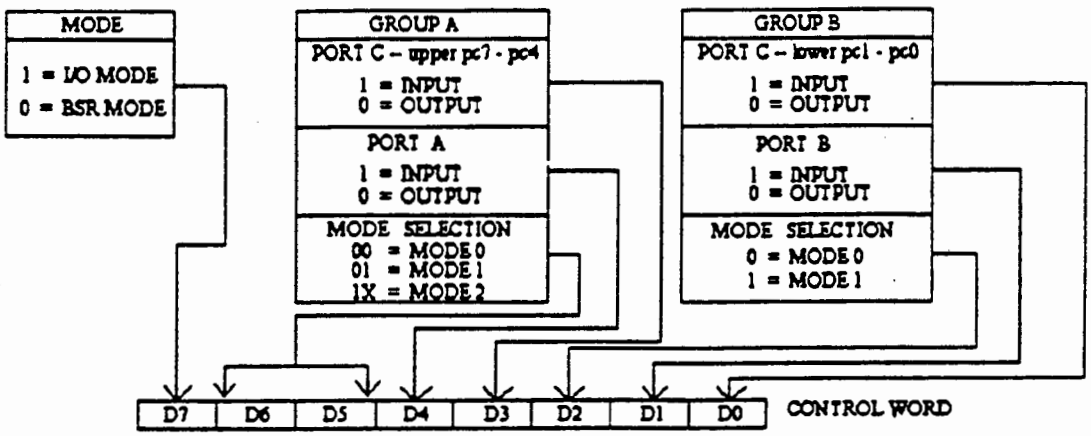

Figure 3.3.1a : Control word format for the I/O Mode, as used by the 8255.

3.3.2 Initiating Conversions with the ADC

The 8255 peripheral interface is operated in Mode 0 on the card. The input/output features in Mode 0 are as follows :

- outputs are latched;
- inputs are not selected;
- ports do not have handshake or interrupt capability.

Ports A and B are configured as inputs, and port C as an output. The lower 8 least significant bits of the ADC are read into port A, while the upper 4 bits, the sign bit, and the end-of-conversion (EOC) bit are read into port B. The 4 least significant bits of port C are used for initiating conversions and putting data onto the bus lines, from the ADC to the ports of the 8255. They are in the following order, starting from the LSB of port C : /WR (Write), /RD (Read), /CS (Chip select), and /CAL (Auto-calibration). The 5th- and 6th-bit of port C are used to control the select lines of the analogue switch (multiplexer), in order to choose amongst the four possible analogue inputs to the ADC.

On power up, a calibration sequence is initialised by pulsing /CAL low with /CS, /RD and /WR high. To acknowledge the /CAL signal, EOC goes low after the falling edge of /CAL, and remains low during the calibration cycle of 1396 clock periods. During the calibration sequence, first the comparator's offset is determined, then the capacitive DAC's mismatch error is found. Correction factors for these errors are then stored in internal RAM.

A conversion is initialised by taking /CS and /WR low. The /AZ (auto-zero) signal line is tied low during the conversion process. Thus, before the actual conversion is started, the ADC goes through an auto-zero cycle, which takes 26 clock periods. The auto-zero cycle determines the correction factors for the comparator's offset voltage. However, provision has also been made on the card to skip the auto-zero cycle, i.e., by shifting a jumper on the card. Next, the analogue input is sampled for 7 clock periods, and held in the capacitive DAC's ladder structure. The EOC then goes low, signalling that the analogue input is no longer being sampled and that the A/D successive approximation conversion has started.

During a conversion, the sampled input voltage is successively compared to the output of the DAC. First, the acquired input voltage is compared to analogue ground to determine its polarity. The sign bit is set low for positive input voltages and high for negative voltages. Next the MSB of the DAC is set high with the rest of the bits low. If the input voltage is greater than the output of the DAC, then the MSB is left high; otherwise it is set low. The next bit is set high, making the output of the DAC three quarters or one quarter of full-scale. A comparison is done, and if the input is greater than the new DAC value this bit remains high; if the input is less than the new DAC value, the bit is set low. This process continues until each bit has been tested. The result is then stored in the output latch of the ADC. Next EOC goes high, and INT goes low, to signal the end of the conversion. The result can now be read by taking /CS and /RD low, to enable the tristate output buffers (DB0 - DB12).

3.4 ENHANCING THE COMPATIBILITY OF THE CARD

Many features have been provided on the card, in order to meet the requirement for a generally compatible card. A few of these features are described below :

3.4.1 Base-Address Selection

Computers allow I/O devices to only use the I/O space it makes available (exceptions are made in certain cases, for example, memory-mapped I/O). Therefore, any I/O device that is added to the computer's motherboard needs to be able to slot into 'free' I/O space in that particular computer, and the start address of this 'free' space will naturally differ from computer to computer. The card therefore needs to be able to change its base address according to the available I/O space allocated by a specific computer. A dipswitch was therefore employed on the card, which makes provision for manual base-address selection, thus, there is no reason for any computer to experience an address clash.

3.4.2 Decoder Facility

The card includes a Dual 2-to-4 Line Decoder, which is used to select the programmable peripheral interface. The decoder has been included, in case the need arises, to select other chips and RAM, e.g., very fast ADC's uses RAM to store the digital equivalent of the input, so that the computer is able to read the RAM at its own (slower) speed; hence, the decoder can be used to select chips like these. The decoder is well-suited to memory address decoding and data routing applications. It possesses the high noise immunity and low power consumption usually associated with CMOS circuitry, yet has speeds comparable to low power Schottky TTL logic. Thus, together with software techniques, the decoder provides the facility to expand and enhance the usefulness of the card.

3.4.3 Multiplexing Facility

Analogue multiplexers are circuits which time-share an ADC among a number of different analogue channels. Since the ADC is the most expensive component of the whole data acquisition unit, multiplexing analogue inputs to the ADC makes good economical sense. The multiplexer used is a differential four-channel device, having two binary control inputs and an inhibit input. The device has a low 'on' impedance and very low 'off' leakage currents. The two binary input signals select 1 of 4 pairs of channels to be turned on, and connect the differential analogue inputs to the differential outputs. Analogue signals from -5V to +5V can be controlled, and resistors have been added to each input in order to minimise the possibility of crosstalk. Having four analogue inputs is a desirable feature in any laboratory set-up where measurements are taken and experiments conducted.

3.5 THE COMPLETED CARD

The completed circuit design was incorporated on a 135mm x 110mm double-sided printed circuit board. All components were kept as close as possible to the board's surface. Figures 3.5a-b shows the actual-size, of both the top (a) and bottom (b) sections, and layout of the double-sided printed circuit board (pcb) design, which was created using the software pcb- and schematic-design program TANGO.

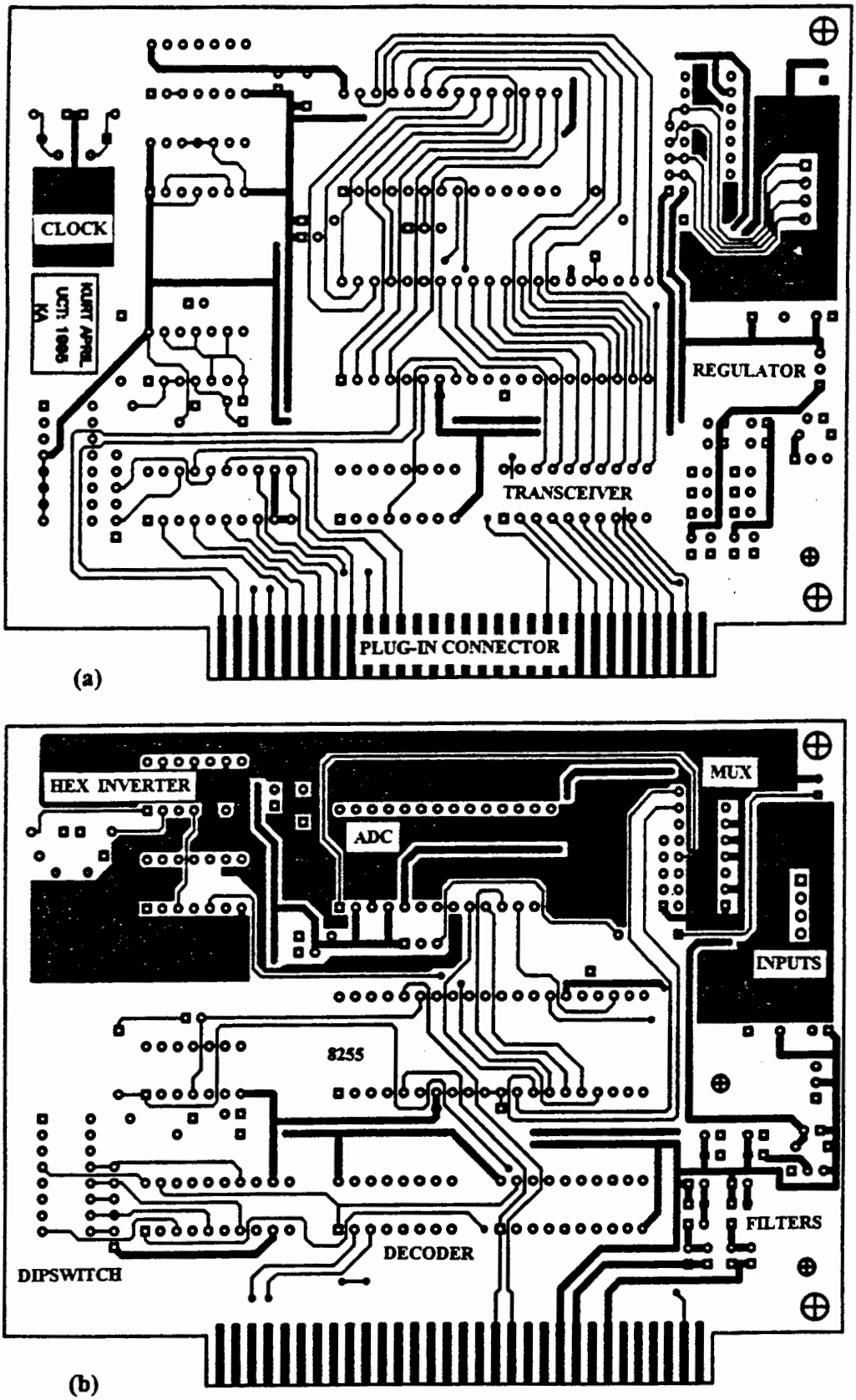

Figures 3.5a-b : The top/component-side (a) and bottom-side (b) of the double-sided printed circuit board, showing the actual dimensions of the PC-interface card. Some labels have been added to indicate the component positions. Notice the spread of the ground plane throughout the board, especially in the facinity of the analogue components, which have intentionally been placed as far from the digital circuitry as the design would allow.

Great care was taken to have sufficient spread of the ground plane throughout the design of the board, especially in the vacinity of the ADC, multiplexer, and power supply regulation circuitry. The analogue multiplexer was built close to the ADC, and the digital and analogue circuitry was separated as far from each other as the pcb-design would allow. The power supply regulation circuitry, and filter network, was built as close as possible to the connector-end of the card, i.e., the end-piece which plugs directly into the I/O channel of the computer. Software (presented in the appendices) was developed to be user-friendly, using Pascal and TurboVision, i.e., colour, use of a mouse, pull-down menus, etc. The software was written to facilitate the real-time interface between the analogue circuitry and the computer. The four multiplexed inputs to the interface-card are displayed on the computer's monitor, and the captured data is stored on the computer's hard drive.

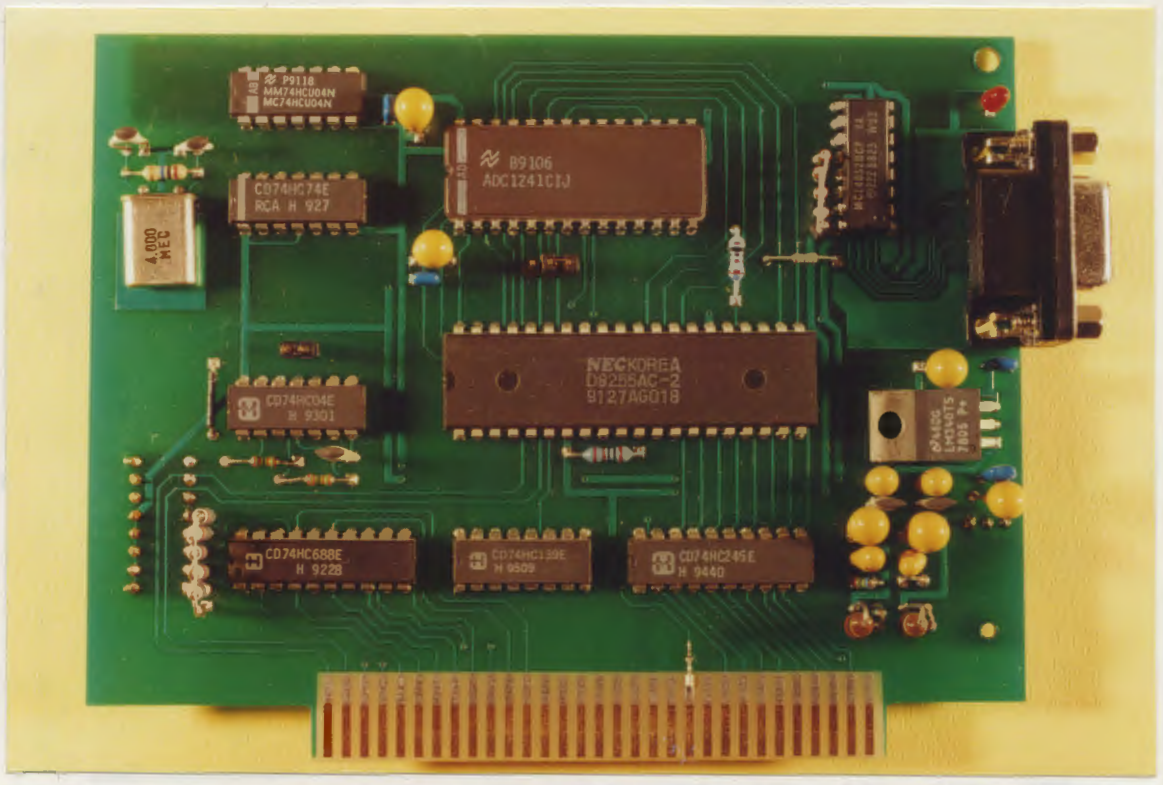

Photograph 3.5α : Photograph of the completed Measurement PC-Interface Card, which employs a 12-bit ADC, built on double sided printed circuit board. Notice that the power supply regulation circuitry, and filter network, is located very close to the connector end of the card. Also, the clock crystal is situated away from the rest of the components on the board. Careful examination of the card will reveal that the analogue input circuitry, i.e., the analogue input multiplexer, ADC, etc., is designed to be on one half of the board, whilst the digital circuitry and signals, i.e., address decoding IC's data to/from the computer, etc., are on the other half of the board. Another feature is that the multiplexer was built as close to the ADC as the design and board space would allow. Components were kept as close as possible to the printed circuit board's surface.

3.6 THE WEATHER STATION

An experiment using a computer, the interface card, and a pressure/temperature unit which employed a MPX100AP pressure sensor and LM35 temperature sensor, was set up. The LM35 sensor is a precision integrated circuit whose output voltage is linearly proportional to the Centigrade temperature, and has a sensitivity of 10mV per degree starting at 0°C. The MPX100AP sensor is a silicon piezo-resistive pressure sensor which provides a very accurate and linear voltage output, which increases with increasing pressure relative to ambient pressure (approximately 100kPa) applied to the pressure-side of the device. Analogue devices, viz., a barometer and thermometer, were used as control instruments in order to verify the readings taken.

Firstly, it was decided to monitor the pressure changes over an entire week. The software was arranged to take readings every 90 seconds, from 18h13 on Sunday 30th July 1995 to 17h01 on Monday 7th August 1995. The figures below show the pressure changes over the time range mentioned, as well as smaller detailed segments of the changes.

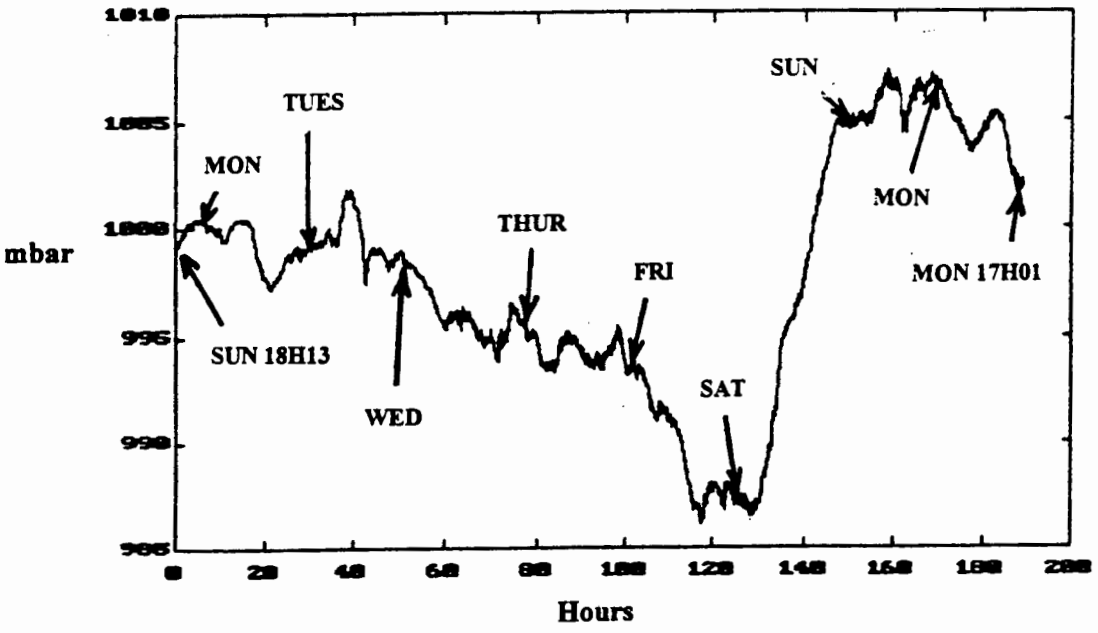

Figure 3.6a : Plot of the pressure variations in millibar from 18h13 on Sunday 30th July 1995 to 17h01 on Monday 7th August 1995. The plot illustrates a 20mbar change in pressure for the 200 hour time span shown. This plot is shown in "exploded time frames" in figures below.

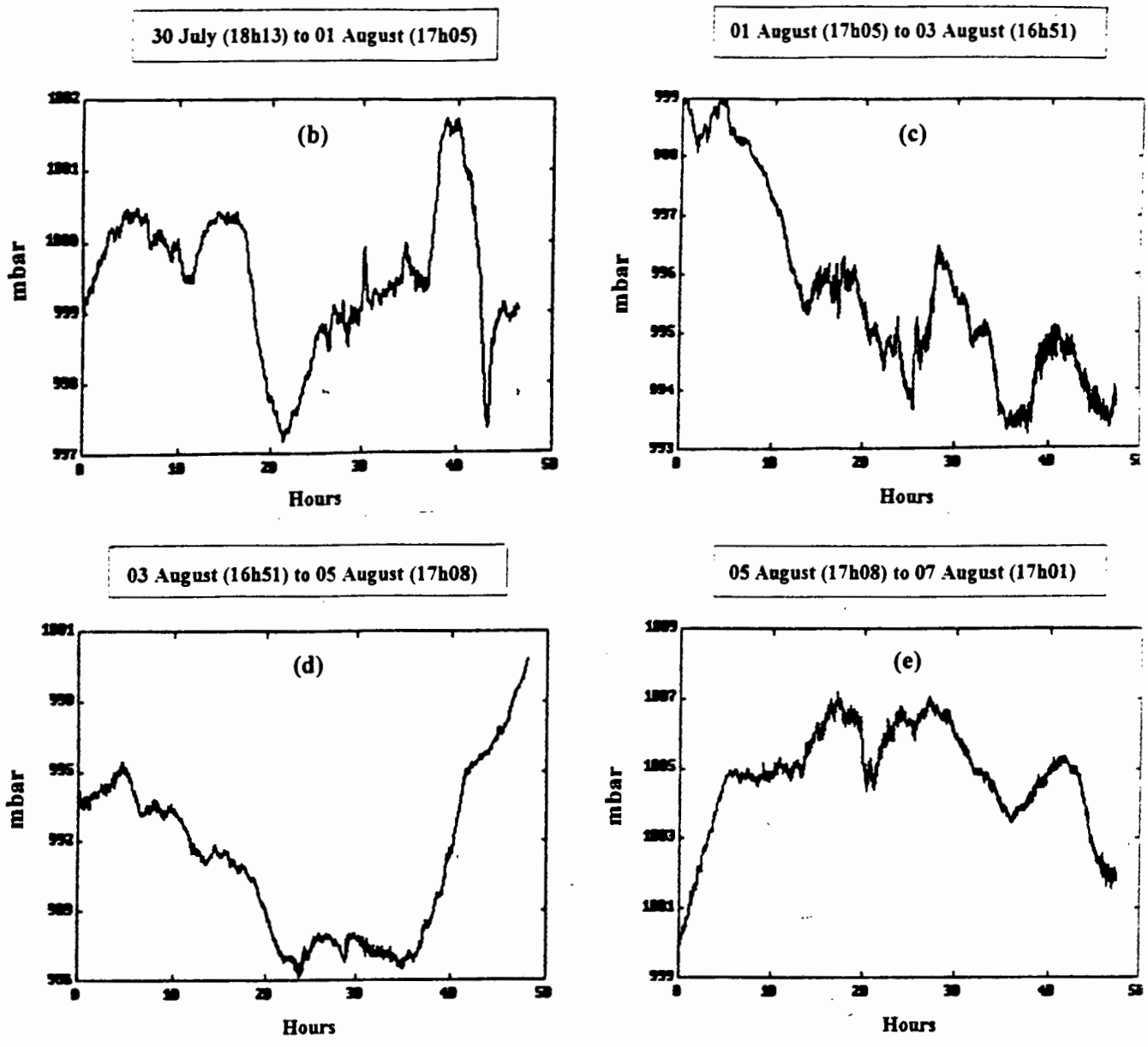

Figures 3.6b-e : "Exploded time frames" of the pressure-variation plot shown in Figure 3.6a. Figure (b) shows the 5mbar pressure variations from 18h13 on a cold and wet Sunday evening of the 30th July 1995, to 17h05 on the slightly warmer, but windier, evening of Tuesday 1st August 1995. Figure (c) represents the 6mbar pressure change from 17h05 on the evening of Tuesday 1st August 1995, to 16h51 of the cold and rainy late afternoon of Thursday 3rd August 1995. Figure (d) illustrates the 14mbar change in pressure over the period 16h51 on Thursday 3rd August 1995, to the wet and cold evening at 17h08 on Saturday 5th August 1995. The 7mbar pressure variation shown in Figure (e) was measured from 17h08 on Saturday 5th August 1995, to the cold evening of Monday 7th August 1995.

The figures below illustrate both temperature and pressure variations for the period from 19h38 on Wednesday 16th August 1995 to 11h41 on Tuesday 22nd August 1995. Once again, readings were taken every 90 seconds and stored to the computer's hard drive.

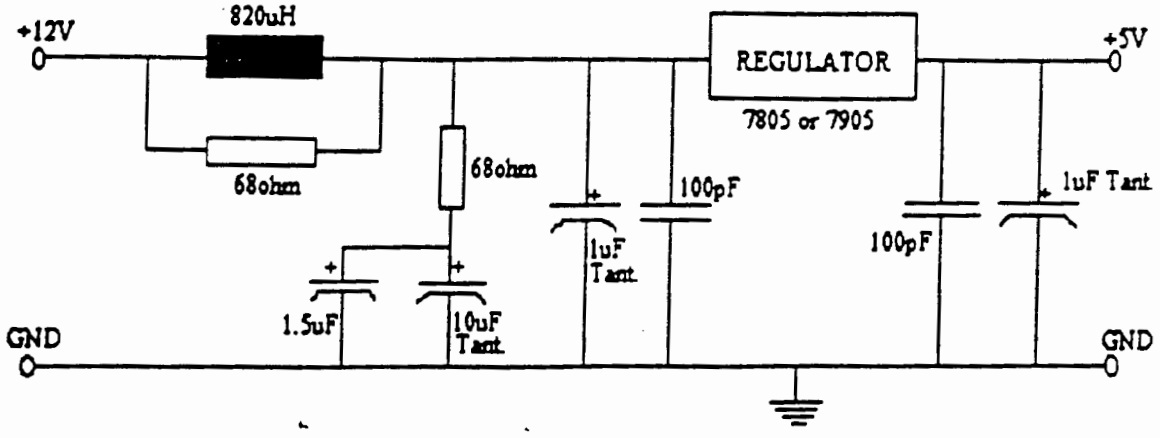

Figure 3.1a : Circuit diagram of the RLC Network used to filter out noise on the power rails of the IBM PC. This filter set-up can be used, with advantage, on any computer using I/O peripherals.

The +5V and -5V power rails, necessary for use on the interface-card, were obtained by using the LM7805 and LM7905 voltage regulators respectively. For maximum ripple rejection, two capacitors in parallel and de-coupled to ground, 100pF ceramic and 1μF tantalum, were employed on the inputs and outputs of the regulators. This filter network can be used, with advantage, in/with any I/O device that makes use of the power lines in a computer. Figures 3.1b-c shows an oscilloscope image of the noise waveforms that were measured on the computer's power supplies. The amount of noise, which proved excessive and would definitely cause errors in the ADC's conversion process, were calculated to be : ±200mVp-p for the +12V and -12V rails, and ±50mVp-p for the +5V and -5V rails.

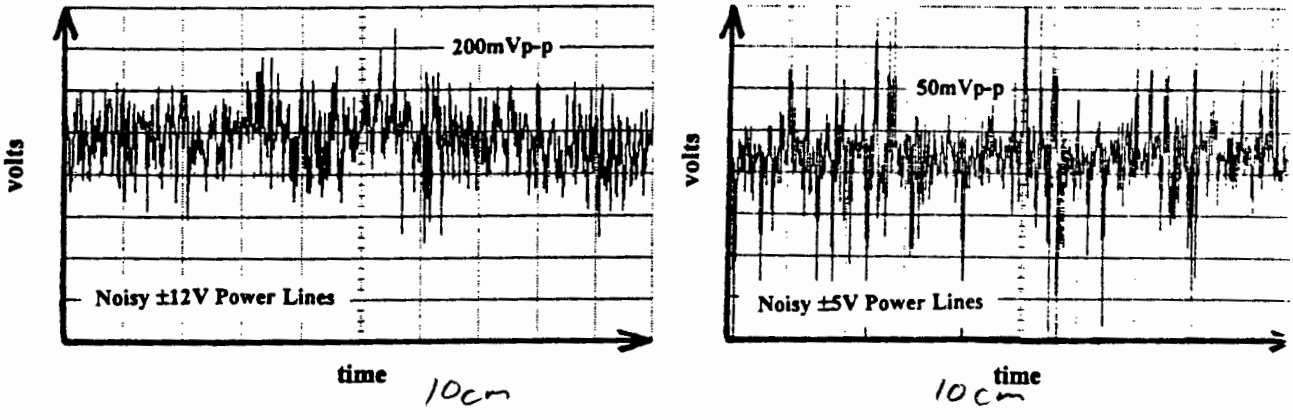

Figures 3.1b-c : The noise waveforms on the computer power supplies was found to be ±200mVp-p for the +12V and -12V rails (b), and ±50mVp-p for the +5V and -5V rails (c). This noise proved to be excessive, and would definitely cause errors in the conversion process of the analogue-to-digital converter.

Figures 3.1d-e shows the "cleaned up" power supply rails. Using the RLC network, it was possible to reduce the noise on the ±12V to 0.5mVp-p and to 0.02mVp-p on the ±5V rails.

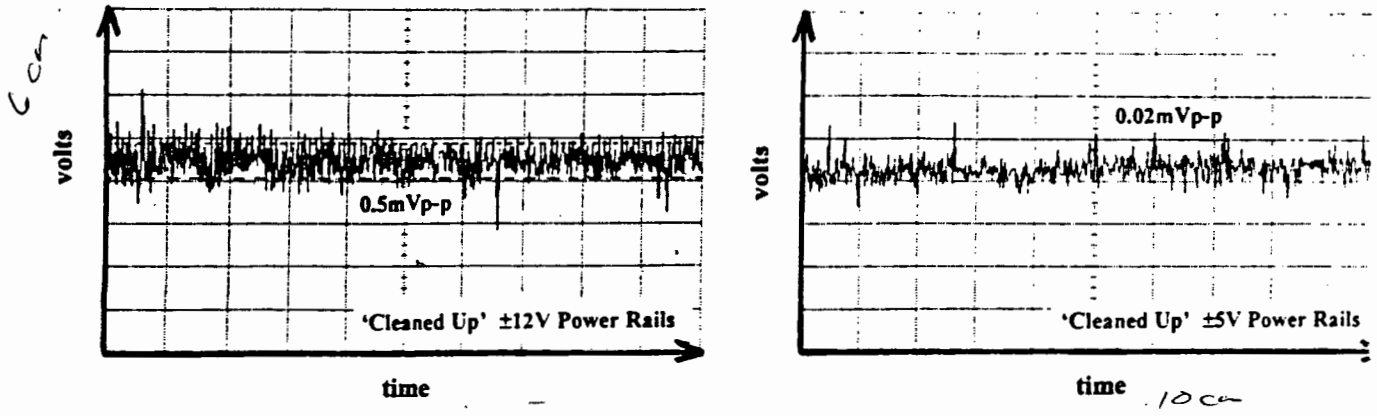

Figures 3.1d-e : The figures represent the "cleaned up" waveforms on the supplies of the computer. With the use of the RLC filter network, the noise on the ±12V rails was reduced to 0.5mVp-p (d) and to 0.02mVp-p (e) in the case of the ±5V.

3.2 THE ANALOGUE-TO-DIGITAL CONVERTER (ADC)

National Semiconductor manufactures an integrated-circuit analogue-to-digital converter, the ADC1241, which (theoretically) meets the criteria for speed, accuracy and cost. It is a CMOS 12-bit plus sign successive approximation ADC, with a conversion time of 13.8μs, i.e., its conversion frequency = 72 463 Hz. On request, the converter will go through a self-calibrating cycle that adjusts positive linearity and full-scale error to less than ±1/2 LSB each, and zero error to less than ±1 LSB. The ADC also has the ability to go through an Auto-Zero Cycle that corrects the zero error during every conversion. The analogue input to the ADC is tracked and held by the internal circuitry, and therefore does not require an external sample-and-hold. A unipolar analogue input voltage range (0V to +10V) or a bipolar range (-5V to +5V) can be accommodated. The 13-bit word, on the ADC's output, gives a 2's complement representation of negative analogue inputs. The digital inputs and outputs of the ADC are compatible with TTL and CMOS logic levels.

3.3 THE PROGRAMMABLE PERIPHERAL INTERFACE (PPI)

The Intel 8255 chip is a widely used, programmable, parallel I/O device that can be programmed to transfer data under various conditions, from simple I/O to interrupt I/O. It is flexible, versatile, and economical (when multiple I/O ports are required), but somewhat complex. It is an important general purpose I/O device that can be used with almost any microprocessor. The 8255 has 24 I/O pins that can be grouped primarily into two 8-bit parallel ports: A and B, with the remaining eight bits as port C. The functions of the ports are defined by writing a control word in the control register. Figure 3.3a shows all the functions of the 8255 classified according to two modes : the Bit Set/Reset (BSR) mode and the I/O mode.

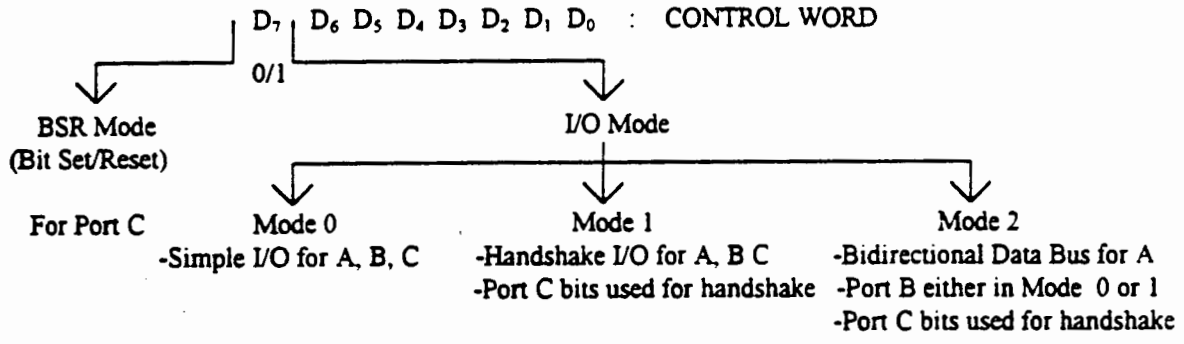

Figure 3.3a : The ports functions are defined by writing a control word in the control register. All the functions of the 8255 are classified according to the Bit Set/Reset Mode and the I/O Mode, as is illustrated in this figure.

3.3.1 Programming the 8255

To communicate with peripherals through the 8255, three steps are necessary :

(1) Determine the address of ports A, B, and C, and of the control register according to the Chip Select logic and address lines A_0 and A_1.

(2) Write a control word in the control register.

(3) Write I/O instructions to communicate with peripherals through ports A, B, and C.

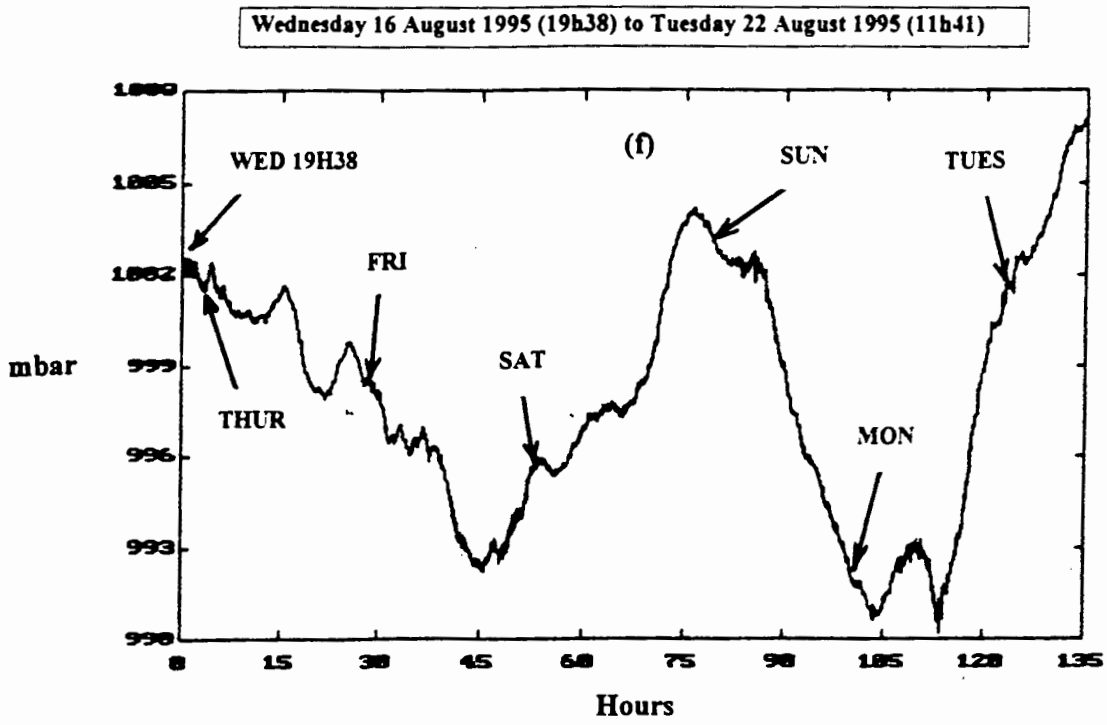

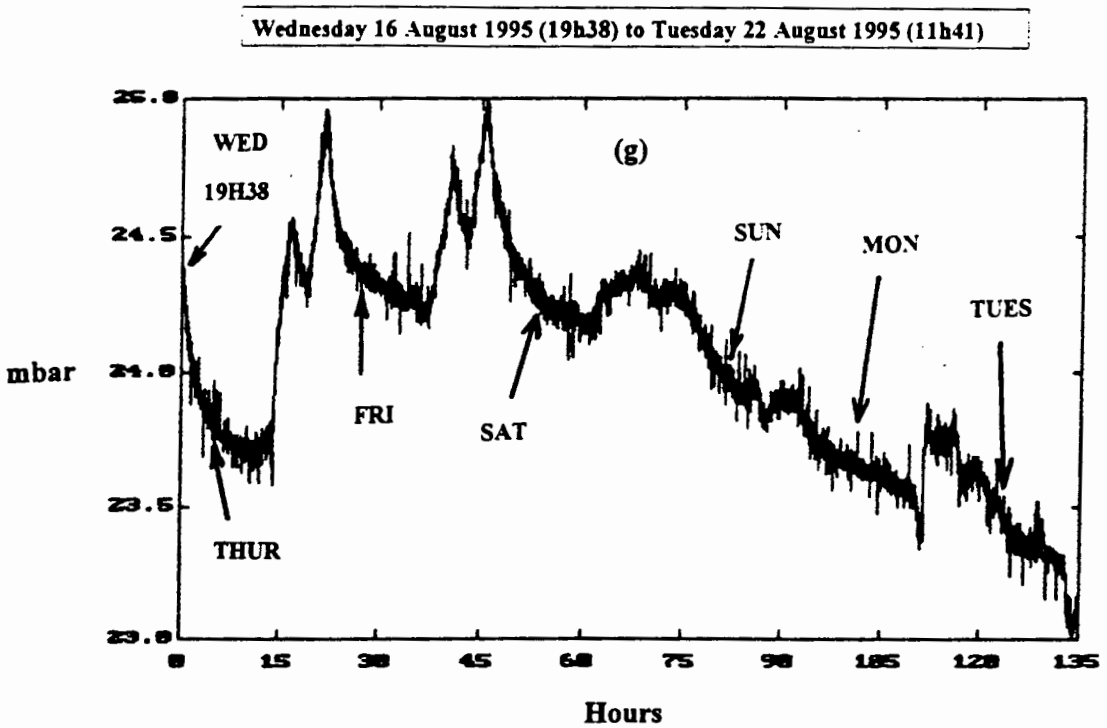

Figures 3.6f-g : An 18mbar pressure change is shown in Figure (f), over a 135 hour time span from 19h38 on Wednesday 16th August 1995 to Tuesday 22nd August 1995. Figure (g) illustrates the temperature change, in degrees Celsius, over the same period. The weather conditions for each day in over the period shown in August 1995 was as follows: Wednesday the 16th was warm during the day, but the readings were started in the evening when the temperature was cooling down; Thursday the 17th was sunny, but windy; Friday the 18th was sunny and warm all day; Saturday the 19th was cold and windy; A cold wind blew on a sunny Sunday the 20th; Monday the 21st was rainy, cold, wet and windy; Tuesday the 22nd was cold, wet and rainy.

To summarise, the completed board met all the requirements and design criteria initially specified, i.e., well-engineered, relatively inexpensive, generally compatible, and accurate to one least significant bit. The card together with a personal computer, has the capacity to be used in many useful applications within a laboratory, performing monitoring functions, in control situations, and other engineering environments. The card was employed successfully during experiments described in further chapters, and is presently being used for data acquisition by the Process Computing Department at Koeberg Nuclear Power Station in Melkbossrand (Cape).

4. THE OPERATIONAL AMPLIFIER

Transducers usually require amplifiers or related devices for buffering, isolation, gain, level translation, and current-to-voltage or voltage-to-current conversion. The operational amplifier is the basic building block for analogue circuits, and most of the functions mentioned are performed by this amplifier. The operational amplifier (op-amp) is a high-gain amplifier designed for use in feedback circuits to perform stable, predictable operations, which are inherently determined by the external components and configuration rather than by the amplifier's open-loop gain magnitude. Figure 4a-b, taken from "Transducer Interfacing Handbook" by D. H. Sheingold, shows the symbol of a differential operational amplifier and its basic open-loop response.

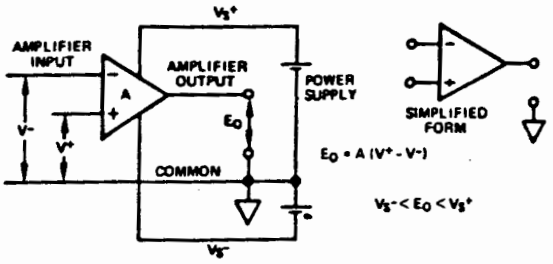

(a)

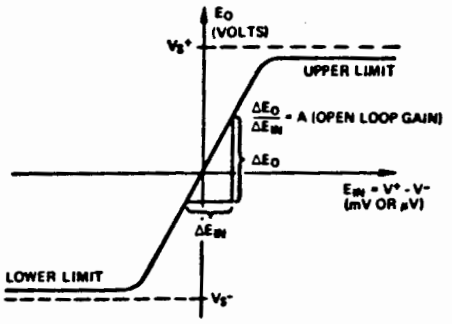

(b)

Figure 4a-b : The diagram in (a) shows the basic differential op-amp circuit (open loop), and (b) is a plot of the op-amp's response, i.e., output versus its input, for the circuit in (a). ***(taken from : "Transducer Interfacing Handbook", by Daniel H. Sheingold)***

4.1 THE LF351 OP-AMP

The following set of characteristics defines the ideal op-amp : infinite open-loop gain, infinite bandwidth, infinite input impedance, zero input offset voltage and bias current, zero output impedance, compatibility between different manufacturers, zero noise contribution, arbitrarily small supply current, absolute insensitivity to temperature, power rail and common-mode input fluctuations, and perfect reliability. Since none of these features are achievable, one has to select a practical op-amp, by making some trade-offs, from the multitude of types available to suit a given application. Device data sheets contain some, but not all, of the necessary information, and the functional characteristics often need some interpretation for one to make these trade-offs.

It was decided to investigate the op-amp response, together with its sensitivity to supply changes, as well as the output resistance of the commonly used LF351 high speed, JFET-input operational amplifier. The LF351 is normally used in applications such as high speed integrators, fast D/A converters, sample-and-hold circuits, and many other circuits requiring low input offset voltage, low input bias current, high input impedance, high slew rate and wide bandwidth. Figure 4.1a-c shows a typical connection, simplified schematic, and connection diagram for the LF351 (taken from : National Semiconductor Data Book)

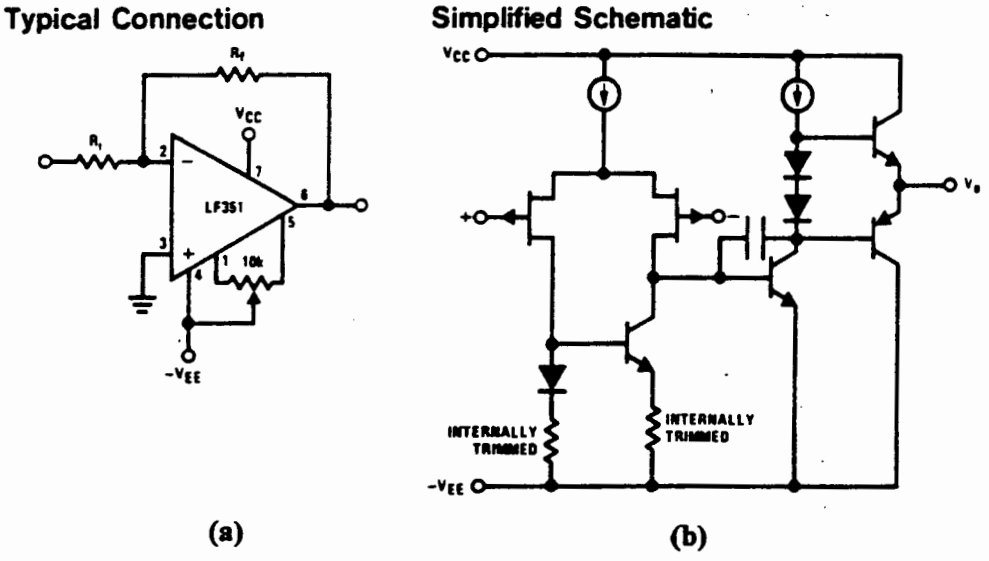

Figure 4.1a-b : Figure (a) is a typical connection when using the LF351, whilst figure (b) shows a simplified schematic of the operational amplifier.
(taken from : National Semiconductor Data Book)

Connection Diagram

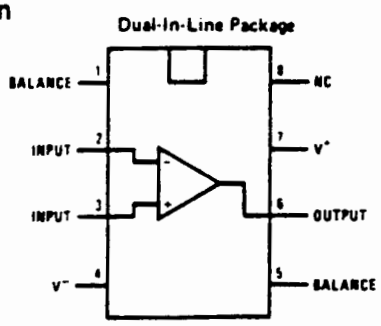

Figure 4.1c : Connection diagram for the LF351 high speed, JFET-input operational amplifier.

4.2 OUTPUT RESISTANCE

The negative feedback of operational amplifier circuits result in the output resistance being "negligibly" low. The voltage follower, with 100% negative feedback, was chosen as being the most challengingly low value available. The circuit used to determine this output resistance was developed over various stages, employing many methods of calibration and redesign. The final circuitry used is shown in Figure 4.2a below. To measure this resistance meaningfully, the output currents had to be kept below the non-linear region of the device, i.e., with the one end of the 1K resistor (toward point A in Figure 4.2a) virtually at zero volts, and the one end of the resistor being switched between +12V and earth, ±12mA was used. The load resistance covered the full range of positive current. Also, high gain was needed to obtain this characteristically low value of output resistance, viz., the gain formula for the AD620 is : $G = 1 + \frac{49.4K}{R_g} = 1 + \frac{49K}{22} = 2246.$

(See further, i.e., page 3 of chapter 5, for details on the AD620 instrumentation amplifier)

Twenty readings were taken at 1 second intervals with the 1KΩ resistor connected to earth, and then twenty more readings with the resistor connected to +12V. This process was repeated for a total of 80 readings, and the resultant output is shown in Figure 4.2b below. The presence of noise in Figure 4.2b indicates that the experiment-under-test was virtually at the limit of measurement.

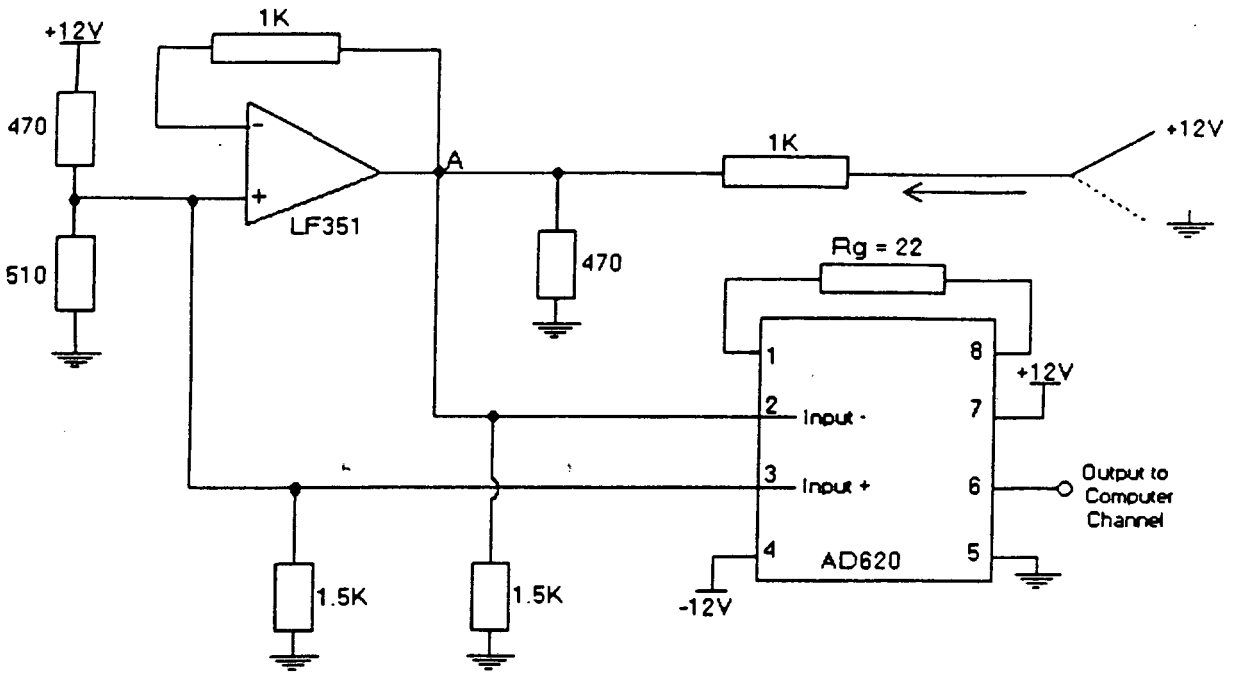

Figure 4.2a : Circuit for determining the output resistance of a LF351 operational amplifier. High gain (2246) was needed to obtain this characteristically low value of output resistance. The output current was kept below the non-linear region of the device, and the one end of the 1KΩ resistor was switched between +12V and earth. The final output resistance of the operational amplifier was found to be 3.83 mΩ.

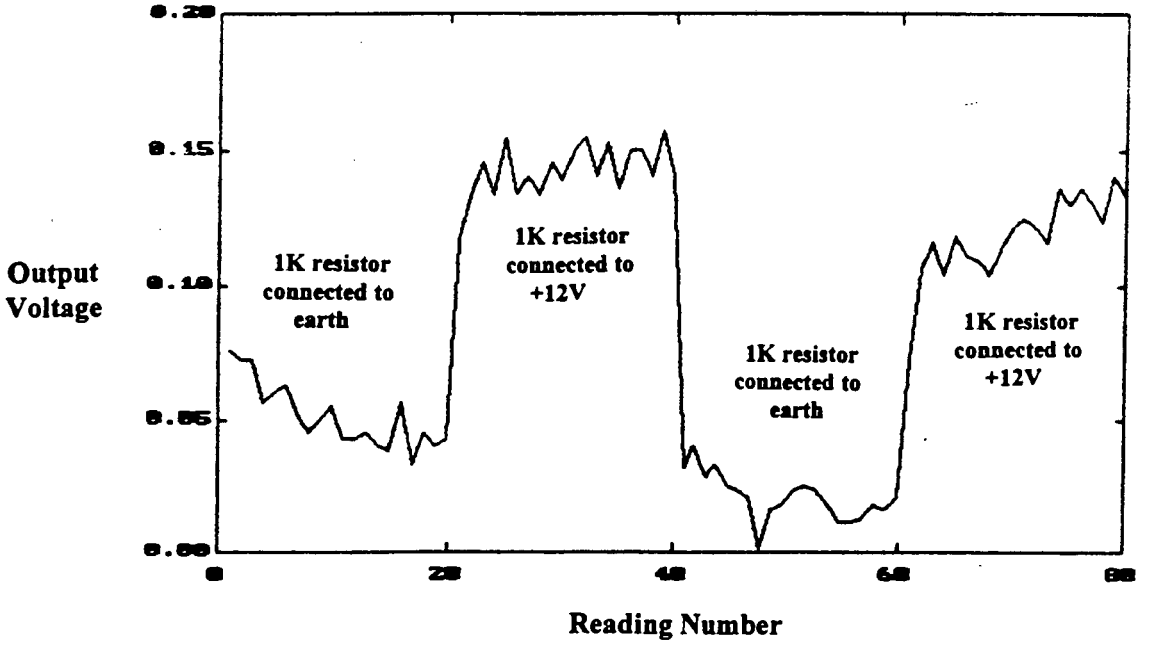

Figure 4.2b : Plot of the output voltage change, as the one end of the 1KΩ resistor was switched, every 20 readings, between +12V and earth, whilst readings were taken at 1 second intervals. The presence of noise in the figure indicates that the experiment-under-test was virtually at the limit of measurement. As can be seen from the figure, ΔV_{out} = 0.10329.

The following calculations were done on the results shown in Figure 4.2b :

$\Delta V_{out} = 0.10329$. Therefore, $\Delta V_{true} = \frac{\Delta V_{out}}{Gain} = \frac{0.10329}{2246} = 45.99\mu V$.

Current when switched to +12V : v = 12V - 5.37V = 6.63V, $\therefore$

$$i = \frac{V}{R} = \frac{6.63V}{1K\Omega} = 6.63mA.$$

Current when switched to earth : v = 12V - 6.63V = 5.37V, $\therefore$ $i = \frac{V}{R} = \frac{5.37V}{1K\Omega} = 5.37mA$.

Therefore, $\Delta i = 6.63mA + 5.37mA = 12mA$.

The final output resistance of the operational amplifier, determined in this manner, was

thus $r = \frac{\Delta V_{true}}{\Delta i} = \frac{45.99\mu V}{12mA} = 0.00383\Omega$, or <u>3.83mΩ.</u>

There are a few avenues that one can pursue with this topic, e.g.,

- One may find it useful to add a small resistor in the feedback loop, i.e., do the same process with and without a 0.1-1Ω resistor situated from the output of the LF351 operational amplifier to point A (as shown in Figure 4.2a). Also, to make the 1.5K resistors on pins 2 and 3 of the AD620 very much higher in value.
- Another option is to modify the circuit so that it has high- and low-current capabilities, since the limitation of the circuit in Figure 4.2a was that it could only deliver and sink a certain, limited amount of current. In fact, initial experiments with the circuit in Figure 4.2a produced unreliable results, as a result of the circuit being driven too hard for current. Figure 4.2c below, is a possible step forward in this direction. A good feature of this circuit is its ability to maintain its low source impedance for both scenarios.

The book : "Electronic Measurement", by Barney, Oliver and Cage, has some excellent examples of circuits employing op-amps, and gives good insight into the practical limitations and usage of these operational amplifiers.

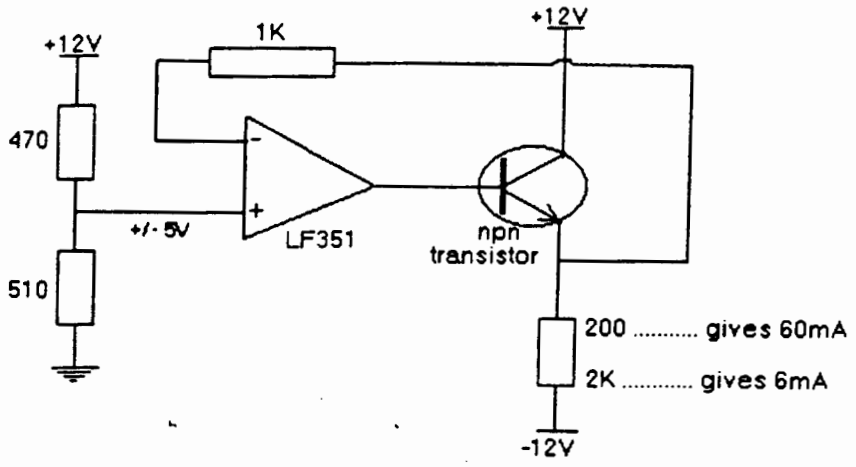

Figure 4.2c : A possible circuit for expanding the usefulness of the test-circuitry used in determining the output resistance of an op-amp (as shown in Figure 4.2a). This configuration overcomes the limited current available, since it has both low- and high-current capabilities. A good feature of this circuit is its ability to maintain its low source impedance for both cases.

4.3 THE AMPLIFIER'S RESPONSE

The influence of the gain resistors, and power supplies on the response of an op-amp was investigated. Once again, the LF351 op-amp was used, and the simple set-up is shown in Figure 4.3a. In all the cases presented below, a slowly varying ramp waveform, with a maximum and minimum value of +4.5V and -4.5V respectively, was inputted to the circuit shown in the figure, and 400 readings were taken at 1ms intervals.

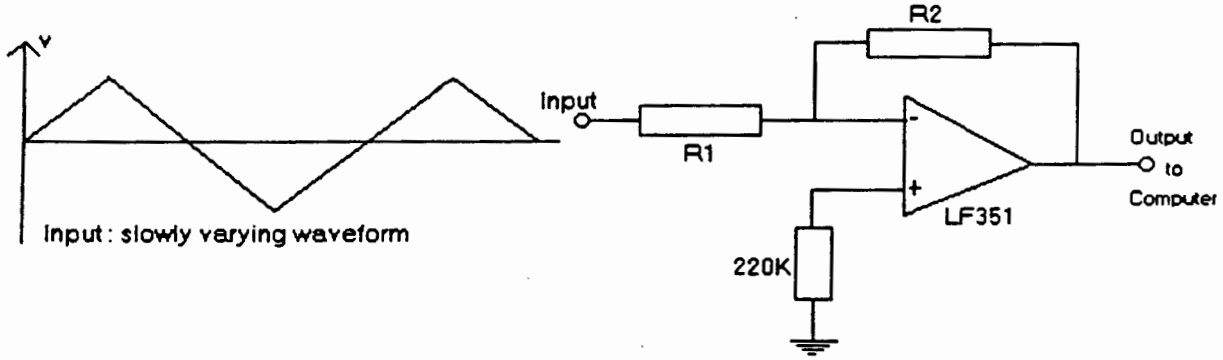

Figure 4.3a : The unity-gain inverting amplifier set-up used to determine whether or not the gain resistors and power supplies of an op-amp effects its response, and if so, what the increase in error would be. A slowly varying ramp waveform, with a maximum and minimum of +4.5V and -4.5V respectively, was fed into the input of the circuit. A total of 400 readings were taken for each case studied, at a sampling interval of 1ms.

- *Case I : ±12V supplies to the op-amp*

In this case, two 1KΩ (1%) metal-film resistors were taken "off-the-shelf". One of these resistors, R1, was then measured to be exactly equal to 995Ω and the other, R2, equal to 998Ω. Thus the gain = R2/R1 = 1.003015, and the supplies to the op-amp was ±12V. Figure 4.3b shows the op-amps response, i.e., output voltage vs. input voltage. A linear regression was then done on this data, and the slope for the line was found to be : -1.00218 ± 0.00025. The regressed line was then superimposed onto the experimental values and their difference was calculated, shown in the detrend graph of Figure 4.3c. Keeping all the other variables as before, R1 and R2 was then swopped around, i.e., the gain was now 0.996994. Once again, having done a linear regression on the experimental data, this slope was calculated to be -0.99748 ± 0.00022, and a detrend graph plotted.

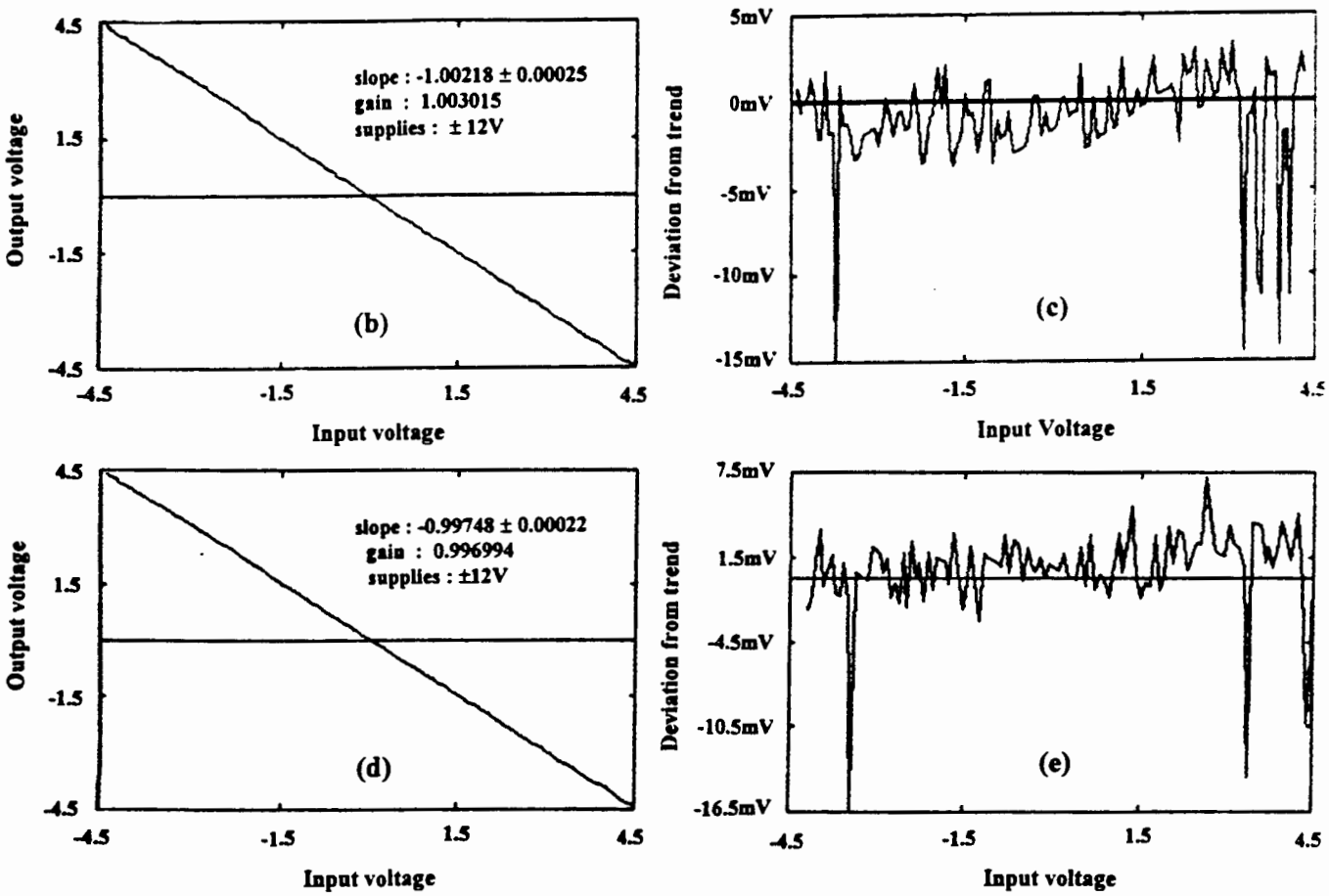

Figures 4.3b-e : These plots are shown for the case where ±12V supplies were used by the LF351 operational amplifier. Figures (a) and (c) shows two output response plots of the op-amp, i.e., input vs. output. In the case of Figure (a), the gain of the amplifier was set to 1.003015, by the two resistors of value 998Ω and 995Ω. Using the same resistors, but changing them around in the circuit, the gain was adjusted to 0.996994, and the output response using this configuration is shown in Figure (c). Linear regressions were done on the experimental data of both Figure (a) and (c). The slopes of each of these graphs were determined : in the case of Figure (a) it is -1.00218 ± 0.00025, and for Figure (c) it is -0.99748 ± 0.00022. The difference values between the theoretical straight lines and the actual experimental data are plotted in the detrend graphs of Figures (b) and (d).

- *Case II : ±8V supplies to the op-amp*

Here, the process in *Case I* was repeated with all the variables kept constant, except, the supply voltage to the operational amplifier was set down to ±8V. This was done in order to establish whether the actual supplies to the op-amp would affect its response. Hence, as before, the same two resistors were placed in the circuit so that the gain = R2/R1 = 998Ω/995Ω = 1.003015, and then the response of the the op-amp was determined. Figure 4.3f shows this response, and by doing a linear regression on the experimental data, the slope was found to be : -1.00159 ± 0.00031. Once again, the difference was calculated between the experimental data and the data calculated for the theoretical straight line, as illustrated in the detrend graph of Figure 4.3g. Thereafter, R1 and R2 was swopped around, giving a gain of 0.996994. The response of the op-amp for this set-up was plotted (Figure 4.3h), a linear regression done on the data, the slope calculated to be : -0.99716 ± 0.00025, and a detrend graph drawn (Figure 4.3i).

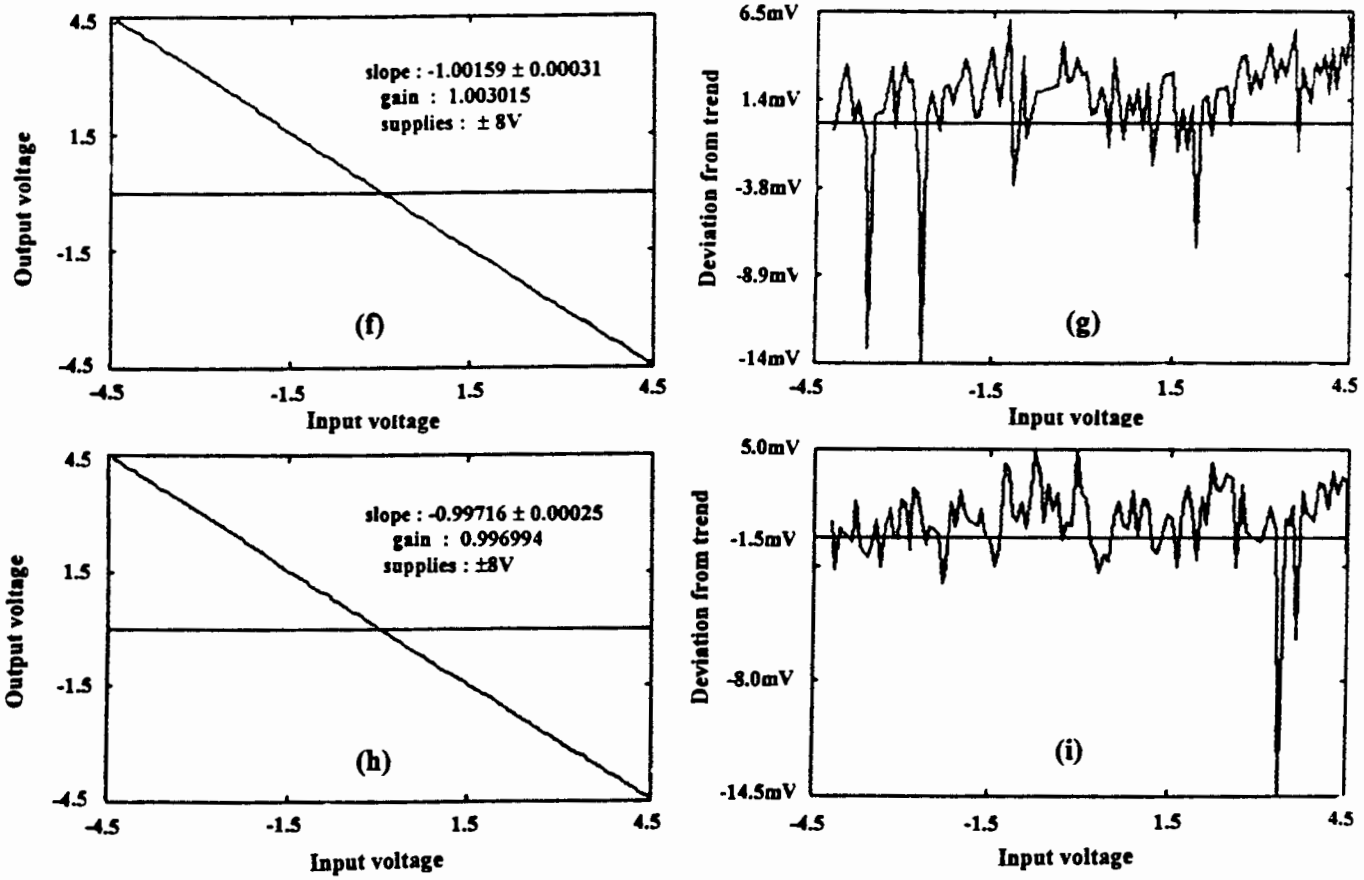

Figures 4.3f-i : Figures (f) and (h) shows two output response plots of the LF351 op-amp, i.e., input vs. output, for the case where ±8V supplies were used. In Figure (f), the gain of the amplifier was set to 1.003015, by two resistors of value 998Ω and 995Ω respectively. Swopping the resistors around in the circuit, the gain was adjusted to 0.996994, and the output response using this configuration is shown in Figure (h). Linear regressions were done on the experimental data of both Figure (f) and (h). The slopes of each of these graphs were determined : in the case of Figure (f) it is -1.00218 ± 0.00025, and for Figure (h) it is -0.99748 ± 0.00022. The difference values between the theoretical straight lines and the actual experimental data are plotted in the detrend graphs of Figures (g) and (h).

- *Analysis and summary :*

For the ±12V power supplies

(a) Unity-gain inverting amplifier : gain = 1.003015
slope 1 = -1.00218 ± 0.00025
intercept = -0.039591

(b) Unity-gain inverting amplifier : gain = 0.996994
(R1 and R2 reversed) slope 2 = -0.99748 ± 0.00022
intercept = +0.016620

Therefore, slope 1 × slope 2 = 0.9996554506.

Hence, 1 - 0.9996554506 = 0.00034455.

Therefore, the ERROR = 0.345 parts per thousand.

For the ±8V power supplies

(a) Unity-gain inverting amplifier : gain = 1.003015
slope 1 = -1.00159 ± 0.00031
intercept = +0.016611

(b) Unity-gain inverting amplifier : gain = 0.996994
(R1 and R2 reversed) slope 2 = -0.99716 ± 0.00025
intercept = +0.017363

Therefore, slope 1 × slope 2 = 0.998745484

Hence, 1 - 0.998745484 = 0.001254515.

Therefore, the ERROR = 1.255 parts per thousand. It is obvious, based on the calculations, that the error has increased by 3.5 times, when the supply voltages to the operational amplifier is dropped from ±12V to ±8V. In general, as long as the signal voltage is not more than 70% of the supply voltage, the error is a minimum.

There are many ways in which one could pursue this issue, however, I will not do so as my readings are accurate and precise. This chapter has demonstrated that the analogue techniques employed in the experiments, together with the PC-interface card and a personal computer are sufficient to effectively carry out the high resolution measurements required to characterise components and device performance.

5. COMPONENTS TEMPERATURE COEFFICIENTS

The change in the performance of components can be measured as a function of temperature, supply voltages and other parameters. Extensive data on these components are available from the manufacturers. Data sheet specifications of the individual components normally give average values of the components' major parameters. Here the temperature coefficients, which are given in broad terms, were investigated in specific detail.

5.1 THE COMMON EXPERIMENTAL LAYOUT

A range of these components, e.g., carbon- and metal-film resistors, capacitors and inductors (which are both very dependent on the dielectric and permeability of the material used), and zener diodes, selected for their particular interest and importance were studied. The actual temperature coefficient has some dependence on the manufacturing process and also on the value of the component. Temperature changes can come either from ambient variations or from self-heating during use. Any application which requires good value stability must keep within the level required by the manufacturers.

Temperature cycling gives a good insight into thermal hysteresis, which is due to the reversal of heat flow on heating and cooling. For temperature cycling an aluminium plate, which was large enough and of sufficient heat capacity to accommodate the components-under-test, the LM35 temperature sensor, as well as the "heater resistors", were used. The reason for using aluminium is because of its very high thermal conductivity. Heating of the plate was achieved with the aid of two 100Ω resistors, which were connected in parallel to a 30V power supply. In positioning all the components on the plate, the "heating resistors" were at one end, whilst the components-under-test together with the LM35 temperature sensor were at the other end of the plate. In this way the temperature gradients arising from heating and cooling were minimised. This feature reduced the thermal hysteresis unavoidable during the investigation. The output of the LM35 sensor, which gives a

proportional output voltage to the temperature being sensed, was fed to temperature-sensing circuitry. Figure 5.1a shows how the components were arranged on the aluminium plate, which was about 20cm × 15cm in area.

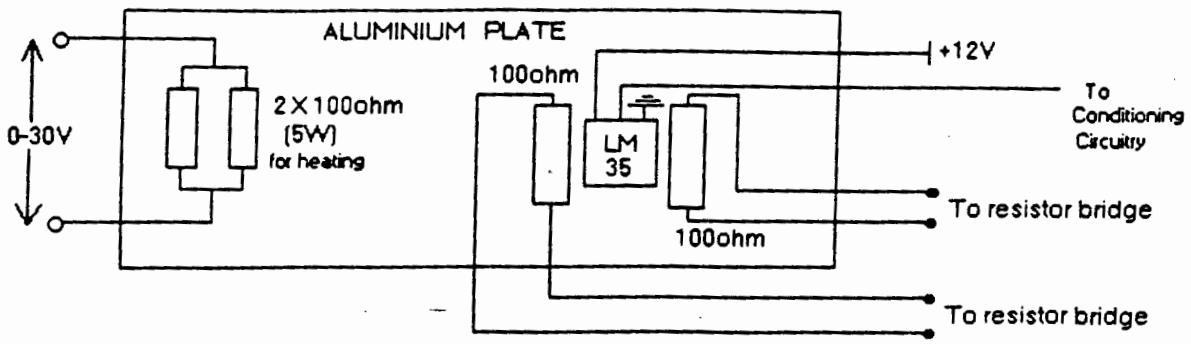

Figure 5.1a : An aluminium plate, large enough and of sufficient heat capacity to accommodate the components-under-test, the LM35 temperature sensor as well as the "heater resistors", were used for temperature cycling (the components-under-test in this figure are resistors). The heater was remotely placed so as to minimise temperature gradients, whilst the LM35 temperature sensor was placed in between (or next to) the components-under-test. The LM35's output was fed to temperature-sensing circuitry, whilst the resistors (in this case) occupied the diagonal positions of a Wheatstone Bridge.

For every experiment conducted, signal-conditioning circuitry was built so as best to interface the data to the computer's inputs. The circuits were initially calibrated experimentally, as described below. For most of the temperature-coefficient experiments however, certain basic circuitry were common. The LM35 (integrated circuit temperature sensor) provided a voltage output of +10mV/°C, and this output was amplified and adjusted to interface to the P.C., so as to make the best use of the 12-bit A/D interface and thus ensuring that no data was lost. The final signal presented to the computer was held to the range +5V to -5V (the design range of the A/D interface card). It was a matter of compromise, just as it is in choosing the range of a multimeter. A convenient two-amplifier circuit for doing the conditioning of the temperature signal is shown in Figure 5.1b. In the first stage, the op-amp was used in the non-inverting mode to avoid loading the input signal from the LM35 and R1 was chosen to give the gain. In the second stage, a summing amplifier of unity gain was used and R3 gave control of the offset voltage.

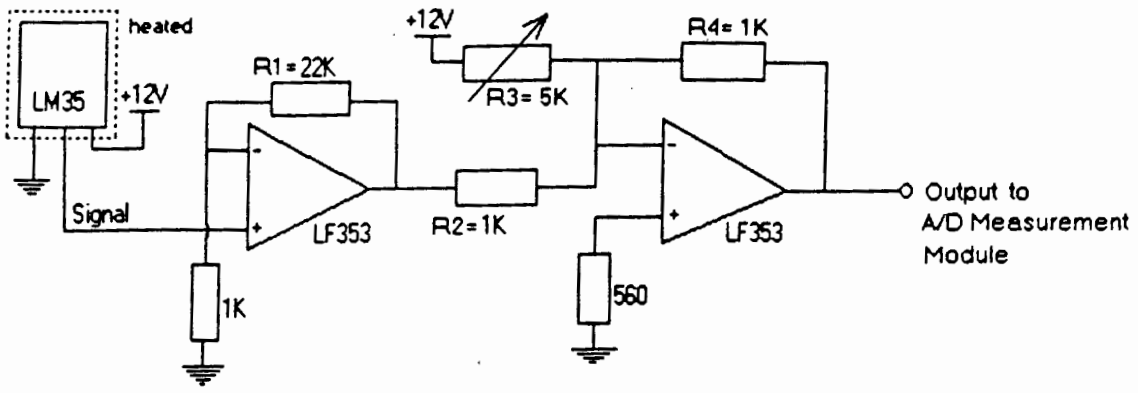

Figure 5.1b : The temperature sensing circuitry used to convert temperature changes in degrees, to signal changes in volts. The LM35 has an output voltage of +10mV/°C, and this was arranged to meet the computer channel requirements by a two-amplifier circuit. Typically, zero volts was set to the centre of the temperature range.

As far as interfacing the components-under-test to the computer were concerned, a board containing an instrumentation amplifier (AD620) was used, set to a gain of 50-2000. This instrumentation amplifier was the central component of these experiments, and has two voltage inputs of high impedance and a voltage output, which is the amplified difference between the two inputs. Its gain is resistor programmed by R_G, or more precisely, by whatever impedance appears between pins 1 and 8. The gain equation is : $G = \frac{49.4K\Omega}{R_G} + 1$.

The high accuracy AD620, with its low offset voltage and extremely low offset drift of 0.6μV/°C, is ideally suited for use in precision data acquisition systems such as transducer interfaces. It also offers high common-mode rejection, which is a measure of the change in output voltage when both inputs are changed by equal amounts.

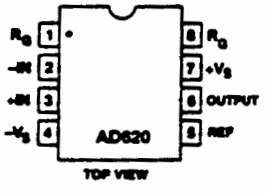

Figure 5.1c : A connection diagram for the AD620 instrumentation amplifier. The resistor controlling the gain is placed between pins 1 and 8, and the reference (Ref), which was set to earth in these experiments, does allow a precise control of output voltage offset.

The instrumentation amplifier was followed by an operational amplifier, which provided offset and gain control. It also acted as a filter, and the voltage outputs from this circuitry matched the analogue-to-digital converter's input, i.e., it was set to a range of ±5 volts, giving a resolution of 2.4mV (the value appropriate to the 12-bit board). A circuit diagram of this is shown in Figure 5.1d below.

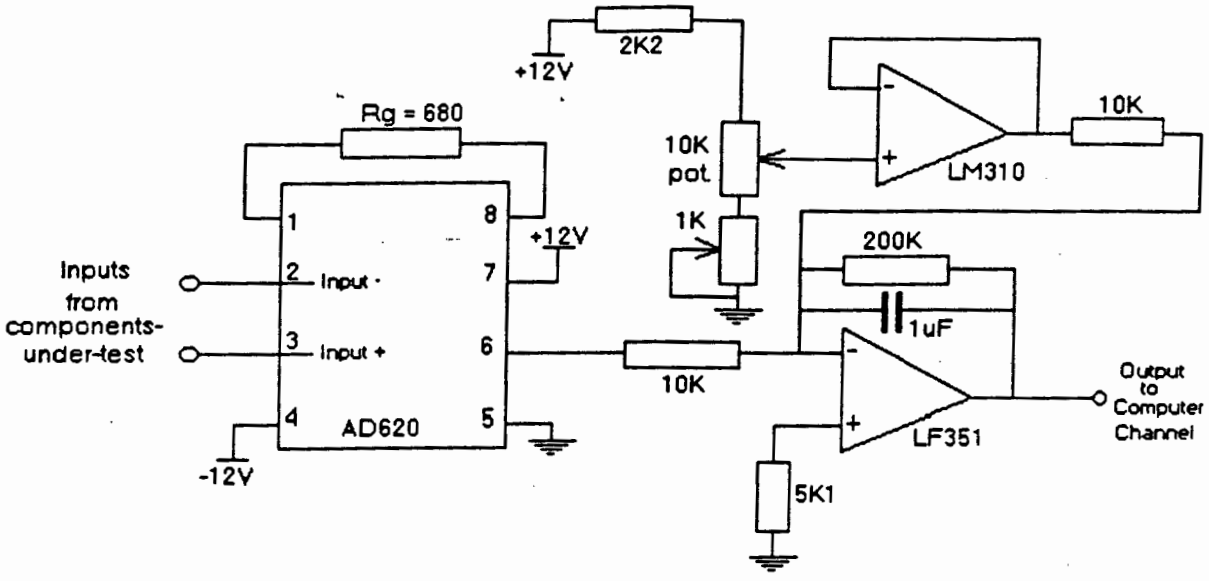

Figure 5.1d : The circuit used to determine the temperature characteristics of the components. The outputs from the components-under-test were inputted to pin 2 (negative input) and pin 3 (positive input) of the instrumentation amplifier. One of the inputs from the components was a reference input, whilst the other underwent parameter changes. The two potentiometers were necessary for course and fine adjustments during set-up.

The hardware and software for an experiment were carefully matched to the results expected. In this way, a high resolution was obtained. In many components, the temperature coefficients were small enough to be expressed in parts per million per degrees Celsius. Of necessity, signal leads were soldered as clip connections can be embarrassingly large generators of noise. During an experiment, the data acquired was stored on the computer's hard drive under filenames specified by the user. As an experiment was completed, the data was transferred to a floppy disk for analysis and subsequent presentation elsewhere.

5.2 RESISTORS

Resistors are ubiquitous, and because of this their performance is taken for granted. This is a reasonable assumption, provided the resistors are operated within their power, voltage and environmental ratings. However, there are measurement applications where one has to exercise some caution when specifying and applying resistors, especially where precision resistors are needed. This is when their resistive temperature coefficient, expressed in parts per million/°C, becomes particularly important. The temperature coefficient of a resistor is defined as : "The change in electrical resistance of a resistor per unit change in temperature". The circuit used is shown in Figure 5.2a :

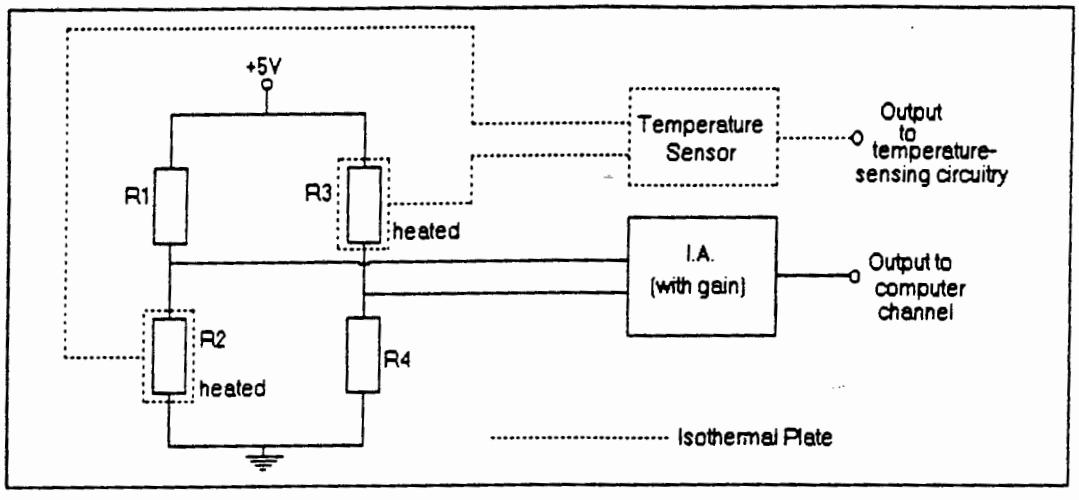

Figure 5.2a : Circuit used for determining the temperature coefficients of the metal-film resistors (1/4W), as well as the carbon resistors (1/4W). The use of the Wheatstone bridge is evident, but only the two diagonal resistors in the bridge are heated up. The out-of-balance signal is fed to the instrumentation amplifier circuitry (I.A.), whilst the temperature data is sensed by the LM35 and conditioned by the temperature-sensing circuitry. The outputs of the two circuits are acquired by the computer and stored for subsequent processing.

5.2.1 Calibration for Resistor Experiments :

The temperature coefficients of the two most common resistor types, viz., carbon- and metal film-resistors (1/4W), were investigated. In calibrating the systems before experimentation took place, the absolute values were known and the changes in parts per thousand or million were obtained from data sheets. A four arm Wheatstone bridge, with equal arms, was used in the calibration procedure. Typically a resistor, one thousand times larger than that being used, was placed in parallel with one arm (decreasing the value of the resistance by 0.1%) of the bridge, thus enabling the sensitivity in output voltage in ppm to be calculated. This method of calibration is convenient as it does not require any intermediate measurement of another parameter, such as gain for example. This dynamic calibration technique was conducted on one of the resistors that was to be heated up. Figure 5.2.1a illustrates the technique employed.

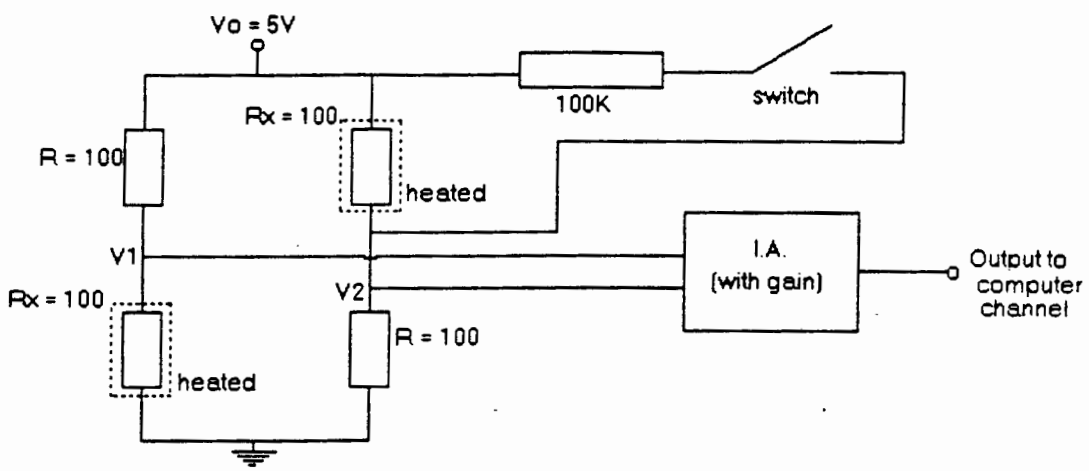

Figure 5.2.1a : To calibrate the bridge, a 100kΩ resistor was put in parallel with one of the 100Ω resistors. This resistor was switched in and out of the circuit by means of a switch, thus causing a change in output voltage – this was done every 20 readings whilst taking readings at 1 second intervals. The presence of the second resistor on the heating plate doubled the sensitivity of the measurements.

The following mathematical analysis was used to assist with the calibration analysis :

Let $R_x = R(1 - \delta)$. Now : $V_1 = V_0 \frac{R_x}{R_x + R} = V_0 \frac{R(1-\delta)}{R(1-\delta)+R} = V_0 \frac{1-\delta}{2-\delta} = V_0 \frac{1-\delta}{2(1-\frac{\delta}{2})}$

Thus, $\frac{V_1}{V_0} = \frac{1}{2}(1-\delta)(1+\frac{\delta}{2}) = \frac{1}{2}(1-\frac{\delta}{2}-\frac{\delta^2}{2})$, however $\frac{\delta^2}{2}$ is small enough to be neglected.

Hence, $\frac{V_1}{V_0} = \frac{1}{2}(1-\frac{\delta}{2})$. Similarly, $\frac{V_2}{V_0} = \frac{1}{2}(1+\frac{\delta}{2})$.

Hence, $\frac{V_2 - V_1}{V_0} = \frac{\delta}{2}$, which means that $\frac{\delta V_{out}}{V_0} = \frac{\delta}{2}$ (referred to 5V). It is worth noting that, while each resistor changes by δ, the practical change in voltage is only $\frac{\delta}{2}$.

The calibration results for the **metal-film resistors** is shown in Figure 5.2.1b

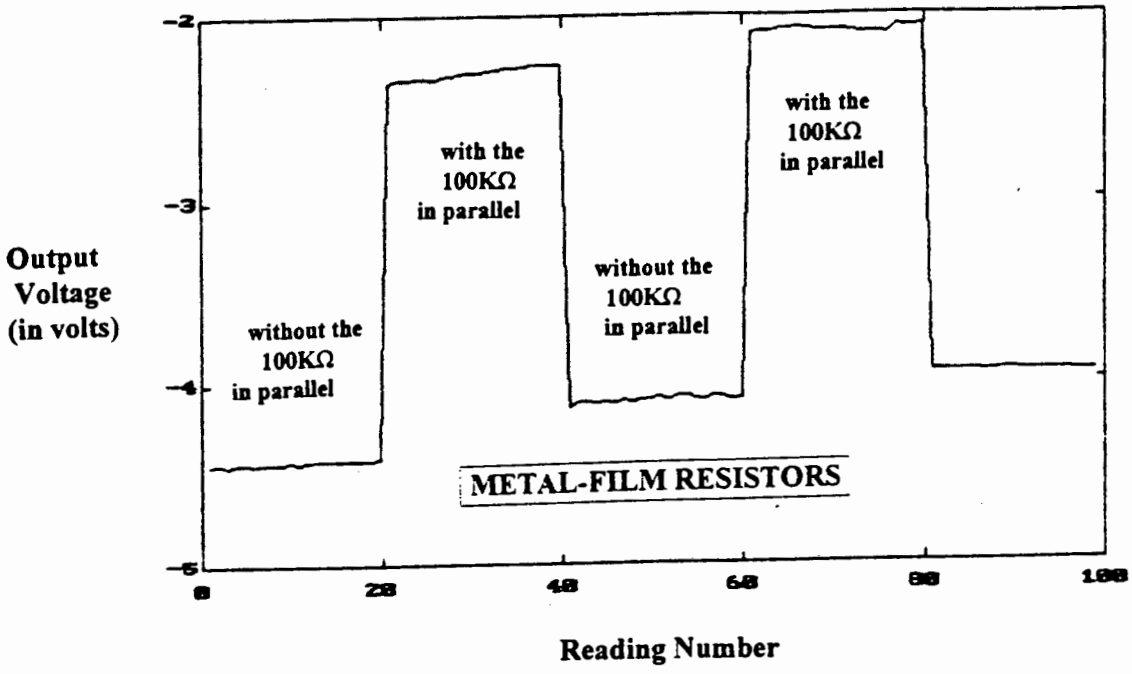

Figure 5.2.1b : Plot of output voltage change for METAL-FILM RESISTORS, as the resistance in one arm of the Wheatstone Bridge was increased and decreased during calibration. The sensitivity was calculated to be 2.01mV/ppm. A very slow drift in voltage with time is evident.

As a result of the switching in and out of the "calibration resistor" in the Wheatstone Bridge, the value of the resistance in the bridge was changed by 0.1%. This 0.1% change resulted in an average output voltage change of 2.075V, making the sensitivity 4.15 volts per parts per thousand (taking into account the two resistors which were heated).

The same calibration procedure was carried out for the **carbon resistors**, and the results thereof is shown in Figure 5.2.1c. In this case, the 0.1% change in resistance in one arm of the bridge -- and thus in voltage, resulted in an output voltage change of 1.72V.

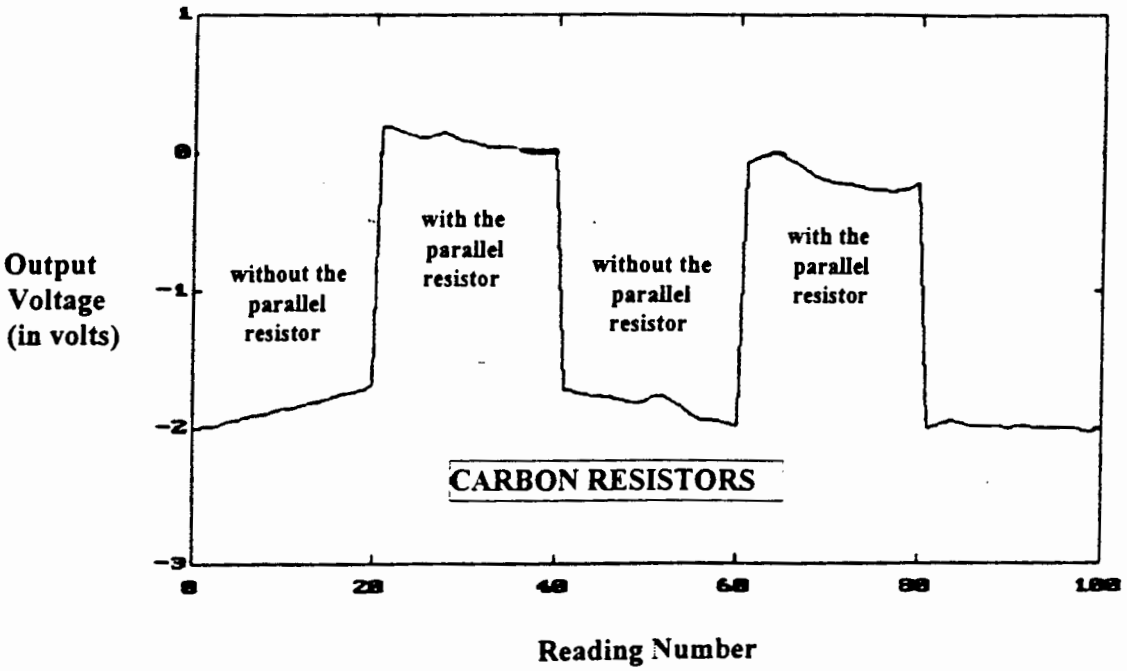

Figure 5.2.1c : Plot of output voltage change for CARBON RESISTORS, as a 100KΩ resistor was switched in- and out-of-parallel with the 100Ω resistor in one arm of the Wheatstone Bridge. The sensitivity was calculated to be 1.72mV/ppm. A drift in time of the output voltage is evident in the plot.

5.2.2 Thermal Hysteresis

In order to gain an understanding of the thermal hysteresis (the rate of heating and cooling) as far as the two resistor types were concerned, the temperature cycling technique was employed. Two of the resistors in the bridge were heated up, and then allowed to cool down. The plots are shown in Figure 5.2.2a for **metal-film resistors** and Figure 5.2.2b for **carbon resistors**. Both plots clearly indicate (where the heating and cooling graphs are at its widest separation) that there was hysteresis of approximately 6°C for the **metal-film resistors**, and only in the region of 0.5°C for the **carbon resistors**. The reason for the hysteresis was that heating of the aluminium plate took place at a faster rate than that for cooling. There was also a temperature gradient from the heater to the temperature sensor (LM35), as well as from the heater to the resistors on the plate, even though there was every reason to believe that it was very small in both cases. The only way to decrease the apparent

hysteresis in the system was to heat the aluminium plate at a slower rate, i.e., at the same rate as that for cooling. However, this may have caused a "kink" in the data. The "problem" therefore did not lie with the hardware (circuitry) being used. Also, averaging the data readings would not alter it, since there appeared to be no significant noise. Hence, we assumed that we could not make it better, and that it was good enough for the investigation.

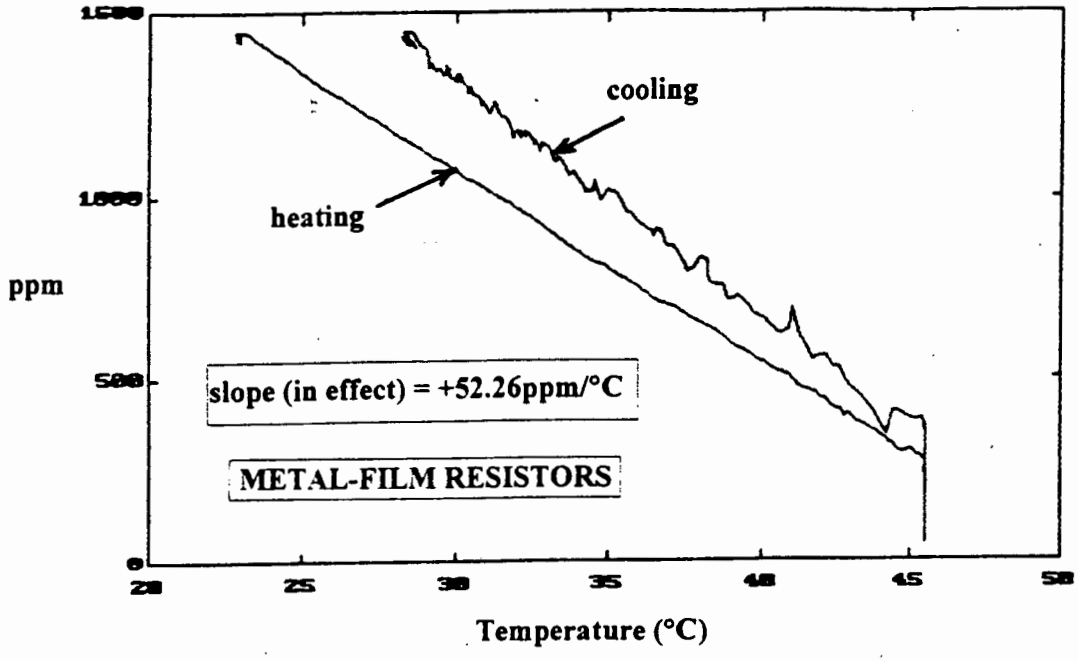

Figure 5.2.2a : The resultant plot of temperature cycling conducted on the METAL-FILM RESISTORS, where the device was heated up, and then allowed to cool down. Some hysteresis is evident in the graph. The actual slope of the graph is positive (+52.26ppm/°C), but is shown here as negative due to the polarities of the circuits used during experimentation.

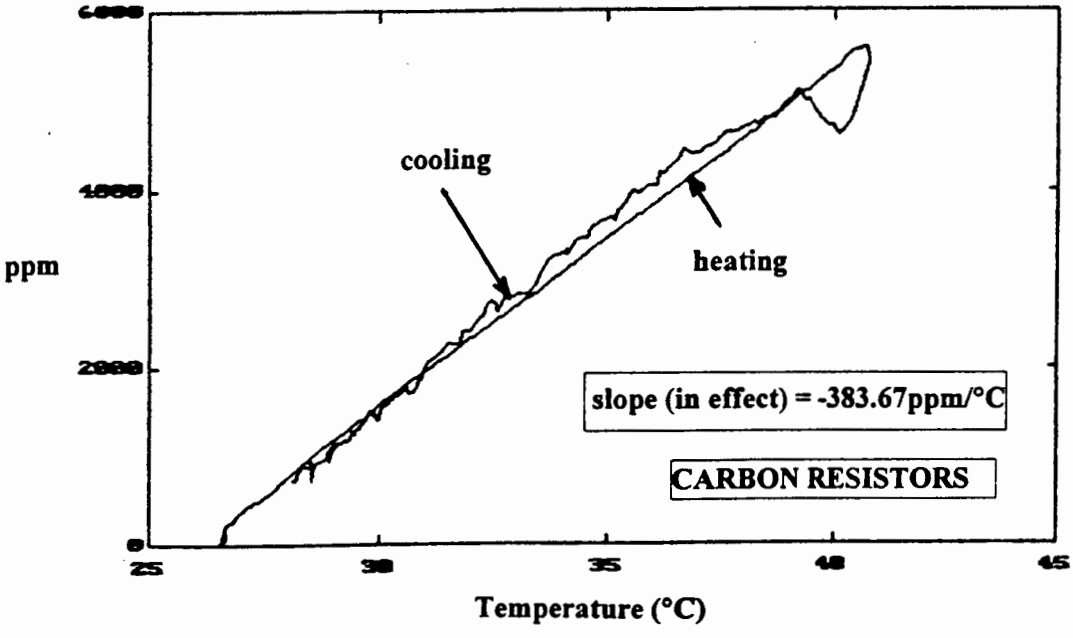

Figure 5.2.2b : A plot showing a maximum hysteresis of approximately 0.5°C for the CARBON RESISTORS, when heated up and then cooled down. The plot has a negative slope (-383.67ppm/°C), however, the graph shown is as a result of the polarities of the circuits used.

5.2.3 Resistors Temperature Coefficients

The temperature coefficients were found for both the metal-film resistors and carbon resistors. The temperature coefficients were calculated by doing linear regressions on the plots, and then fitting the regressed values onto the experimental data.

(a) Metal-Film Resistors

Figure 5.2.3a shows the plot as the metal-film resistors were heated up in the bridge to a temperature of 46°C. The plot shown has a negative slope and is linear, however, as a result of the polarities of the circuits used during measurement, **the output actually has a positive slope**. By doing a linear regression on the data, the following equation for the plot could be determined : ppm = -52.26(θ) + 2636.49. The regressed curve is shown together with the experimental data in Figure 5.2.3b. A good fit of the experimental data to that of the theoretical plot is evident in the figure. The temperature coefficient of the metal-film resistors was therefore : +52.26ppm/°C ± 0.107ppm/°C. This value compares well with values quoted in surveys on resistor types, which normally gives the temperature coefficient of standard metal-film resistors to be in the range ±50ppm/°C to 200ppm/°C.

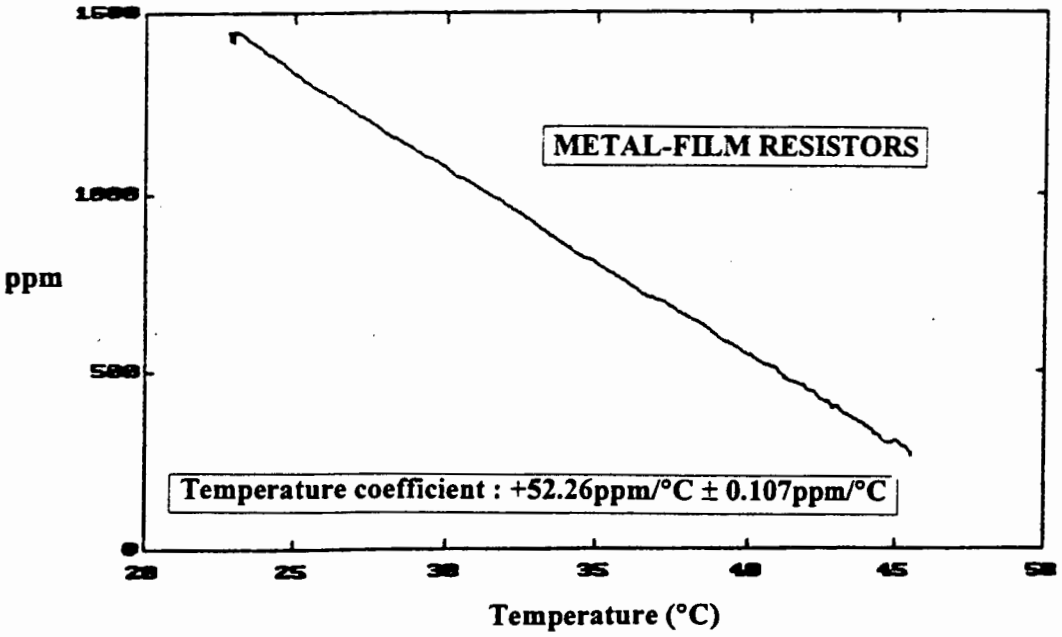

Figure 5.2.3a : Plot of the temperature characteristic of the metal-film resistors, as it was heated up to 46°C. The plot shows a linear negative slope, but in effect it is a linear positive slope of +52.26ppm/°C ± 0.107ppm/°C (as a result of circuit polarities during experimentation). There is a change in output of approximately 1200ppm for the temperature range shown.

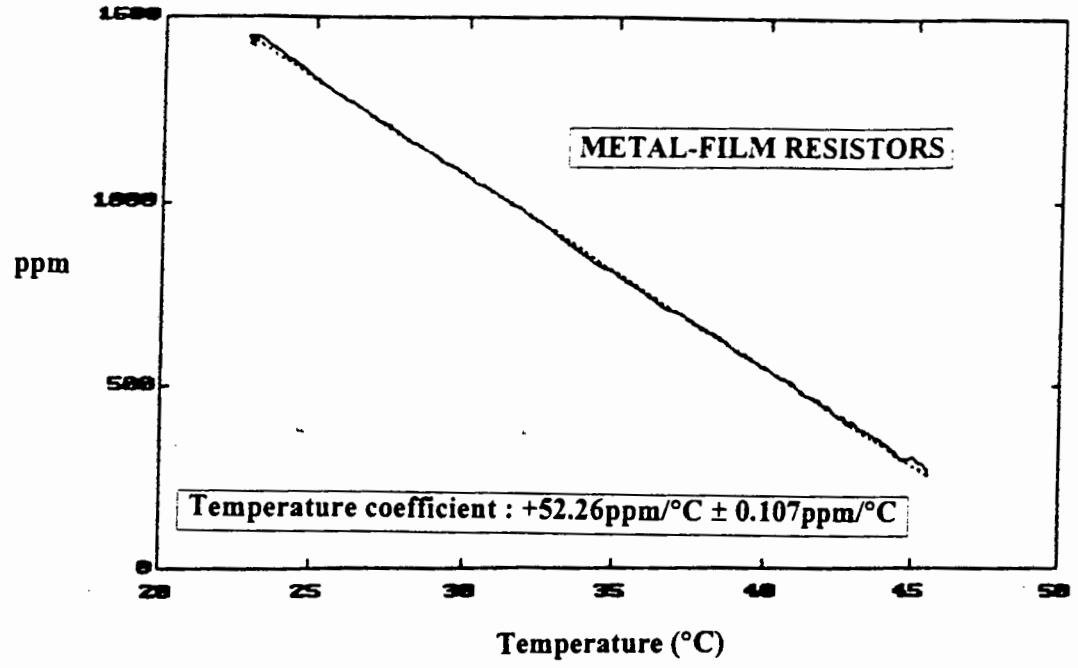

Figure 5.2.3b : The experimental values (solid line) overlaid by the regressed plot (dotted line). From this we can visually see how well the data correlates to the theoretical values. Bearing in mind the polarity change due to circuitry during measurement, the temperature coefficient for the metal-film resistors was calculated to be : +52.26ppm/°C ± 0.107ppm/°C.

A detrend graph, showing the difference between the actual experimental data and the regressed values are shown in Figure 5.2.3c. This graph gives a good indication of the variation in ppm of the metal-film resistors to that of the theoretical straight line.

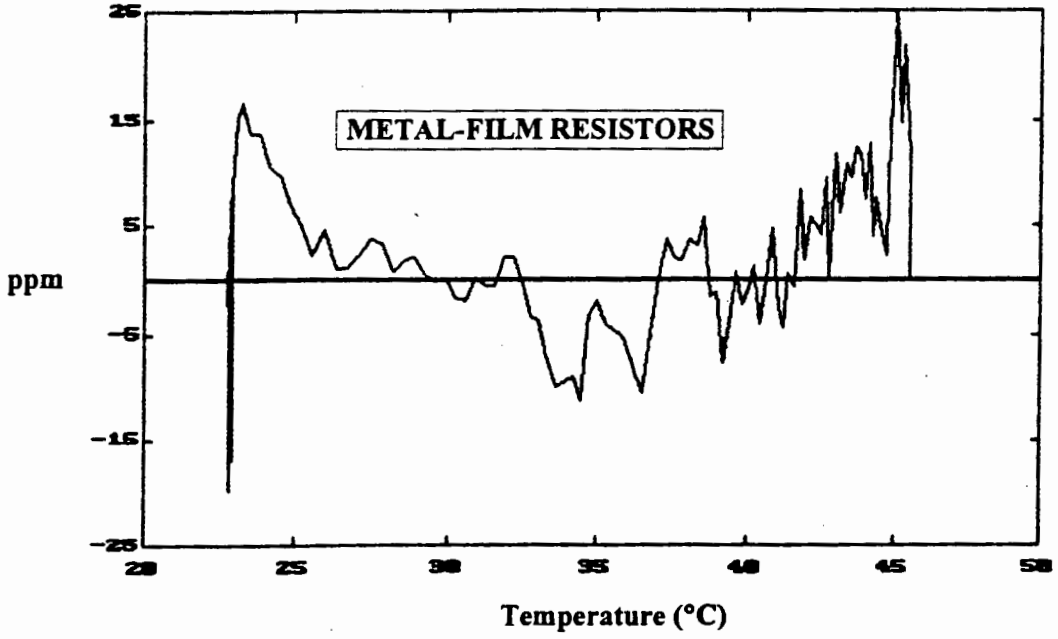

Figure 5.2.3c : Detrend graph, clearly showing how the experimental results are scattered about the general trend. The difference values, which are plotted here, is a representation of experimental readings - regressed values. These values are relatively small (-20ppm to +25ppm) in comparison with the 1200ppm change in output.

(b) Carbon Resistors

The temperature characteristic of the carbon resistors, as they were heated up to 40°C is shown in Figure 5.2.3d. The plot shown has a positive slope and is linear. However, as a result of the polarities of the circuits used during measurement, **the output actually has a negative slope.** A linear regression was done on the experimental data, and the equation of straight line was found to be : ppm = 383.6733 (θ) - 10000. Figure 5.2.3e shows the two graphs overlaid on each other, and thus clearly indicates the closeness of the experimental data to that of the theoretical regressed values. Bearing in mind that the polarity of the slope is opposite to that shown in the figure, the temperature coefficient of the carbon resistors was : -383.67ppm/°C ± 0.22ppm/°C. This value, as was the case with the metal film resistors, compares quite well with that quoted in resistor surveys (150ppm/°C to 1000ppm/°C). From the values quoted above, the carbon resistors has a far higher temperature coefficient than that of the metal-film resistors (-383.67ppm/°C compared to +52.26ppm/°C).

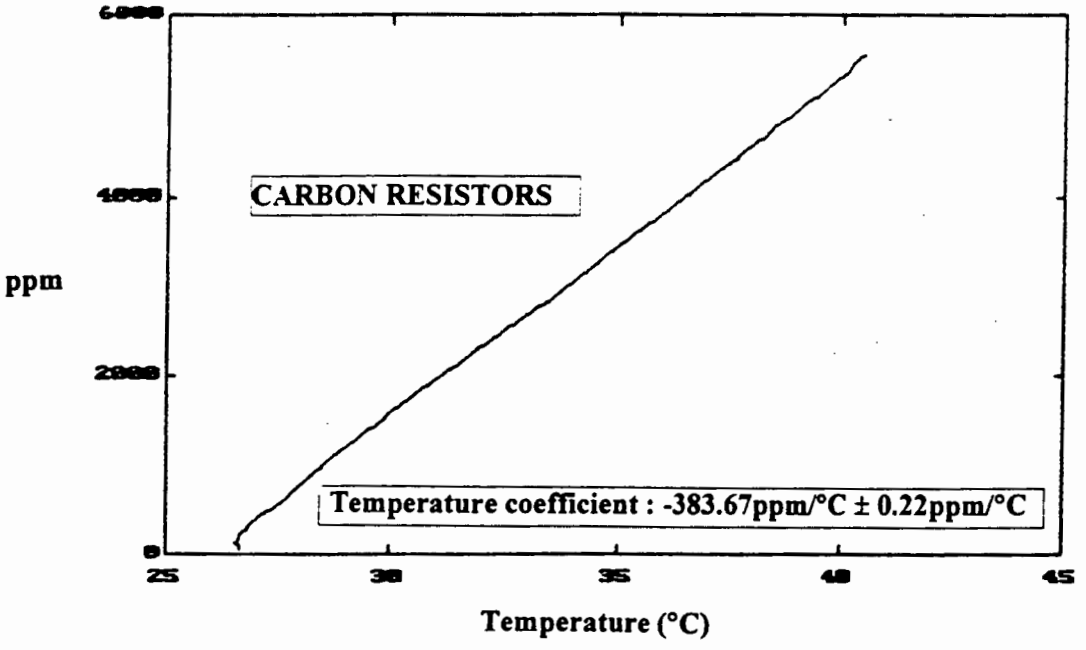

Figure 5.2.3d : The temperature characteristic of the carbon resistors, as it was heated up to 40°C. The plot shows a positive slope, however, this is due to the polarities of the circuits used during measurement. In effect, the actual slope is negative (-383.67ppm/°C) and is linear. A change in output of approximately 5500ppm is shown in the figure over the temperature range.

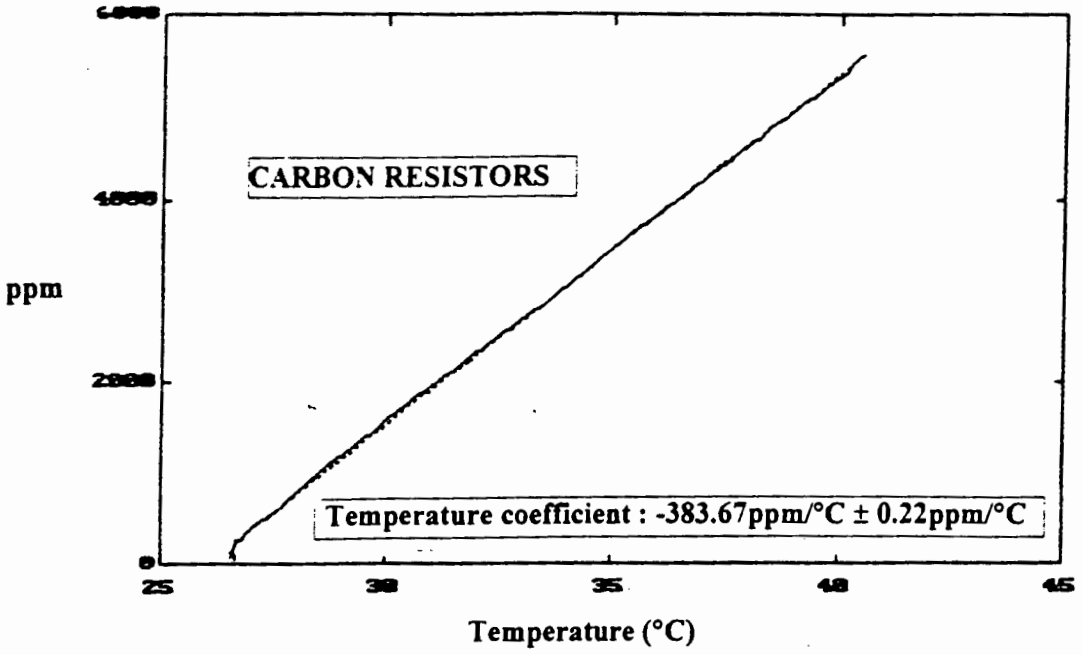

Figure 5.2.3e : The experimental values (solid line) and regressed linear plots (dotted line). There is a good correlation of the data. Remembering that the actual slope is negative (due to the polarities of the circuits used), the temperature coefficient for these resistors are : -383.67ppm/°C ± 0.22ppm/°C.

The difference values between the actual experimental data and the regressed data are shown in Figure 5.2.3f. This graph gives a good indication of the variation in ppm (-40ppm to +60ppm) of the carbon resistors to that of the linear regressed line.

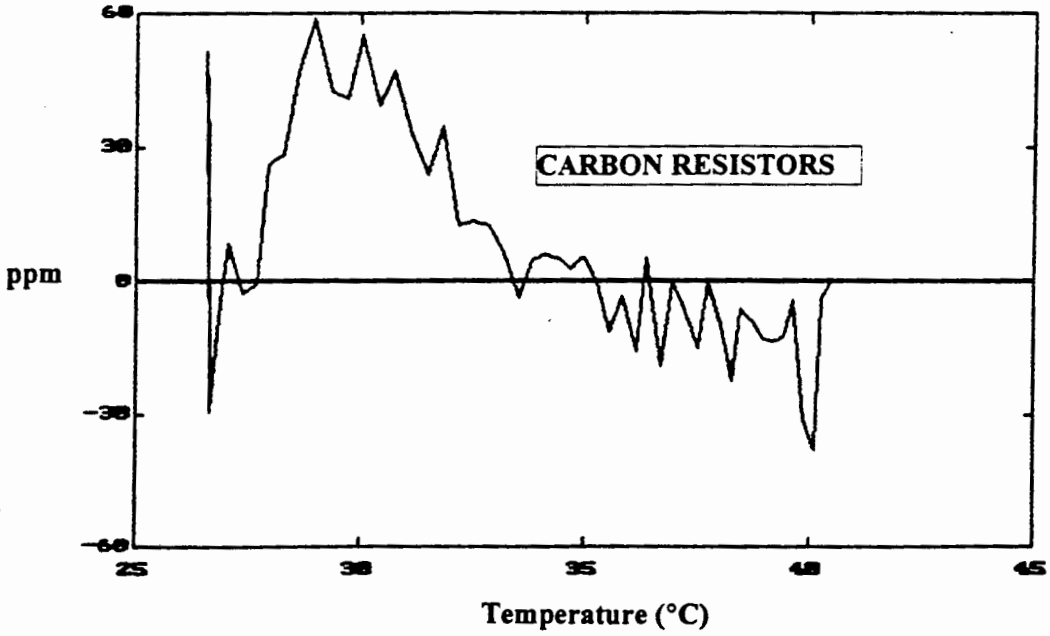

Figure 5.2.3f : The difference values which are plotted in this detrend graph, is a representation of experimental readings - regressed values. These values are relatively small (-40ppm to +60ppm) in comparison with the 5500ppm change in output.

5.2.4 In Summary

The resistance stability of a resistor is dependent on power dissipation, ambient temperature and resistance value. There are a variety of resistors used in industry today, and the different resistor types that were investigated are described below :

(a) Carbon Resistors

The carbon film resistor is the most common resistor, and the cheapest, used in commercial applications. It also has the least impressive performance and therefore is not suited to precision work, but is more than adequate for the majority of commercial uses such as television, radio, etc. Experimentation results has shown that carbon resistors with 2% to 5% tolerances has negative temperature coefficients, which means that their resistance values decrease with increasing temperature. This coefficient has been found to be : -383.67ppm/°C ± 0.22ppm/°C, and compares quite favourably to those of resistors surveys such as that found in : "The Circuit Designer's Companion", by Tim Williams. The book has quoted the temperature coefficients of carbon film- and carbon composition-resistors to be in the ranges of -150ppm/°C to -1000ppm/°C, and +400ppm/°C to -900ppm/°C respectively.

(b) Metal Film Resistors

These resistors are more expensive than carbon film, but gives superior characteristics, particularly long term stability, temperature coefficient, noise and power handling ability. The film consists of nickel-chromium alloy of various compositions for different resistance ranges. The experiments carried out has shown that these 1% tolerance resistors have positive temperature coefficients, which means that their resistances increase with increasing temperature. The coefficients was found to be : +52.26ppm/°C ± 0.107ppm/°C, which are well within the tolerance given by the quoted resistor survey values (±50ppm/°C to 200ppm/°C). Variants of the standard metal film are needed for high resistance needs.

To summarise, carbon resistors are the "better buy", but metal-film resistors are by far the most superior.

5.3 CAPACITORS

Like resistors, capacitors tend to be taken for granted. There is as much a profusion of capacitor types as there is of resistors, and it is often hard to select the optimum part for the application. The temperature coefficient for a capacitor can be an important variable when deciding on the type of capacitor for a particular use, and is defined as : "The change in capacitance C with temperature, and may be quoted in parts per million (ppm)/°C or as a percentage change of C over the operating temperature range".

5.3.1 Experimental Details

It was decided to investigate certain parameters of (a) the almost universally non-electrolytic Wima polyester capacitors, and because of the unusual properties of PZT, (b) thin film barium titanate piezoelectric transducers. It may be noted that barium titanate, a material similar to PZT, is used in strip line microwave electronics. The same layout that was used for temperature cycling (Figure 5.1a) during the resistor experiments, was once again employed here. The temperature sensing circuitry (Figure 5.1b), employing the LM35, was used without any changes. The AD620 instrumentation amplifier (together with an op-amp in its output to provide gain and an offset facility) was also used again, but additional conditioning circuitry was needed to interface the transducer (component) to the instrumentation amplifier. The conditioning circuitry, of necessity, included the high precision, wideband RMS-to-DC Converter AD637 shown below in Figure 5.3.1a.

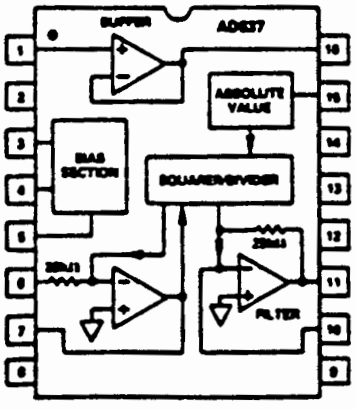

Figure 5.3.1a : Connection diagram for the AD637 Wideband RMS-to-DC Converter. Pins 1, 3 and 4 were connected to earth, whilst an ac-coupling capacitor was used on the voltage input into pin 13. The time averaging capacitor was placed between pins 8 and 9, and pins 6 and 9 were connected together.

The AD637 is a complete high accuracy RMS-to-DC Converter that computes the true root-mean-square, mean square, or absolute value of any complex ac (or ac plus dc) input waveform, and gives an equivalent dc output voltage. The actual computation performed by the AD637 follows the equation : $V_{rms} = A_{vg}\left[\frac{V_{in}^2}{V_{rms}}\right]$. The only external component required was a capacitor which set the averaging time period. The value of this capacitor also determined the low frequency accuracy, ripple level and settling time. The performance of the AD637 was tolerant of minor variations in the power supply voltages.

5.3.2 The Wima Polyester Capacitors

Once again the Wheatstone bridge set-up was used, where two of the resistors (previously in the resistors experiments) were replaced by 1.5μF Wima capacitors. The two resistors that were retained, were changed to 1KΩ resistors. The bridge was driven by a sinusoidal signal from a signal generator, and its outputs were sent via two RMS-to-DC Converters to the instrumentation amplifier. However, in this case, only one component (capacitor) was heated, whilst being in good thermal contact with the heating block. The conditioning circuitry layout is shown in Figure 5.3.2a.

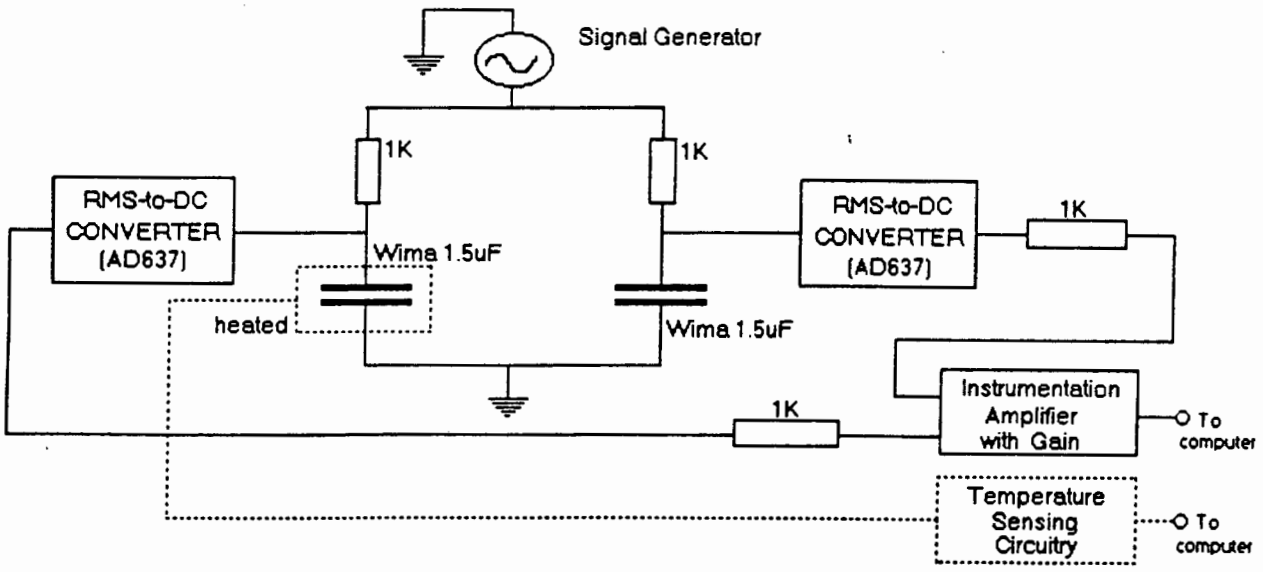

Figure 5.3.2a : Circuit used to determining the temperature coefficients of the capacitors. The use of the Wheatstone bridge is again evident, and one of the capacitors in the bridge was heated up. The out-of-balance signal was fed to the instrumentation amplifier circuitry, whilst the temperature data was sensed by the LM35 and conditioned by the temperature-sensing circuitry. The circuitry drawn with dotted lines indicate that they were in an isothermal state. The outputs of the two circuits were acquired by the computer and stored for subsequent processing.

The temperature cycling method was employed again to give insight into thermal hysteresis. The capacitor which was being heated, was in good thermal contact with the aluminium heating block. Figure 5.3.2b shows how the component was heated up to a temperature of 46°C and then allowed to cool down, whilst readings were taken at 15 second intervals. Evident from the figure is the fact that the cooling trace lagged behind the trace for when the capacitor was being heated up. The figure also shows a difference of approximately 4.6°C between the heating- and cooling-curve, at the point where the curves are widest apart.

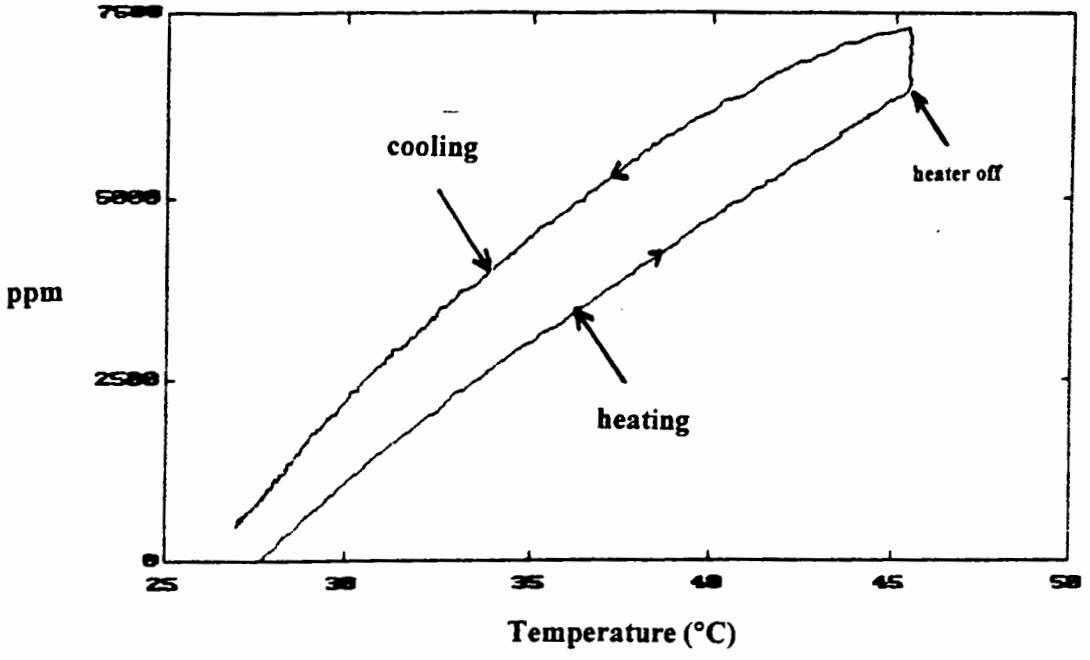

Figure 5.3.2b : The resultant plot of temperature cycling conducted on the capacitors, where the device was heated up, and then allowed to cool down. Hysteresis of 4.6°C is evident in the graph. Notice how, once the heater was switched off, the capacitor's output continued to increase. This was as a result of the bulk size of the capacitor.

The question of hysteresis arose : "Was there hysteresis present"? There could be many explanations, but one should bear in mind that the LM35 temperature sensor was bonded to the aluminium plate, and therefore sensed the cooling-down temperature of the entire plate, which just naturally took longer. Due to the fact that the capacitor was quite thick in dimension, the LM35 sensor was more likely to give an accurate reading for the bottom section (bonded directly to the plate) of the capacitor, than for the temperature of the entire component. It was thus decided to investigate this phenomenon in greater depth. The same circuitry was used as before, however, another sensor was employed. This LM35 temperature sensor was mounted on a 0.2mm aluminium disk, which was cut out to be the size of the Wima capacitor, and then bonded to the top of the capacitor. Hence, one would be able to tell

the temperature on either side of the capacitor, and therefore gain a better insight into the issue of thermal hysteresis. Figures 5.3.2c-f shows that there are remarkable differences between the temperatures at the top and bottom of the capacitor, i.e., at maximum temperature there is a difference of ±13°C. This was due to the fact that the capacitor was bulky in size, and that the top of the capacitor could cool via the air as well, which accounts for the noisier plot for the top of the capacitor than that of the bottom. By careful placing of the temperature sensor on the capacitor under test, as well as experimenting with different shaped heat sinks, it was established that there might be a case for heat-sinking or recessing capacitors when used in circuits which require precise measurement.

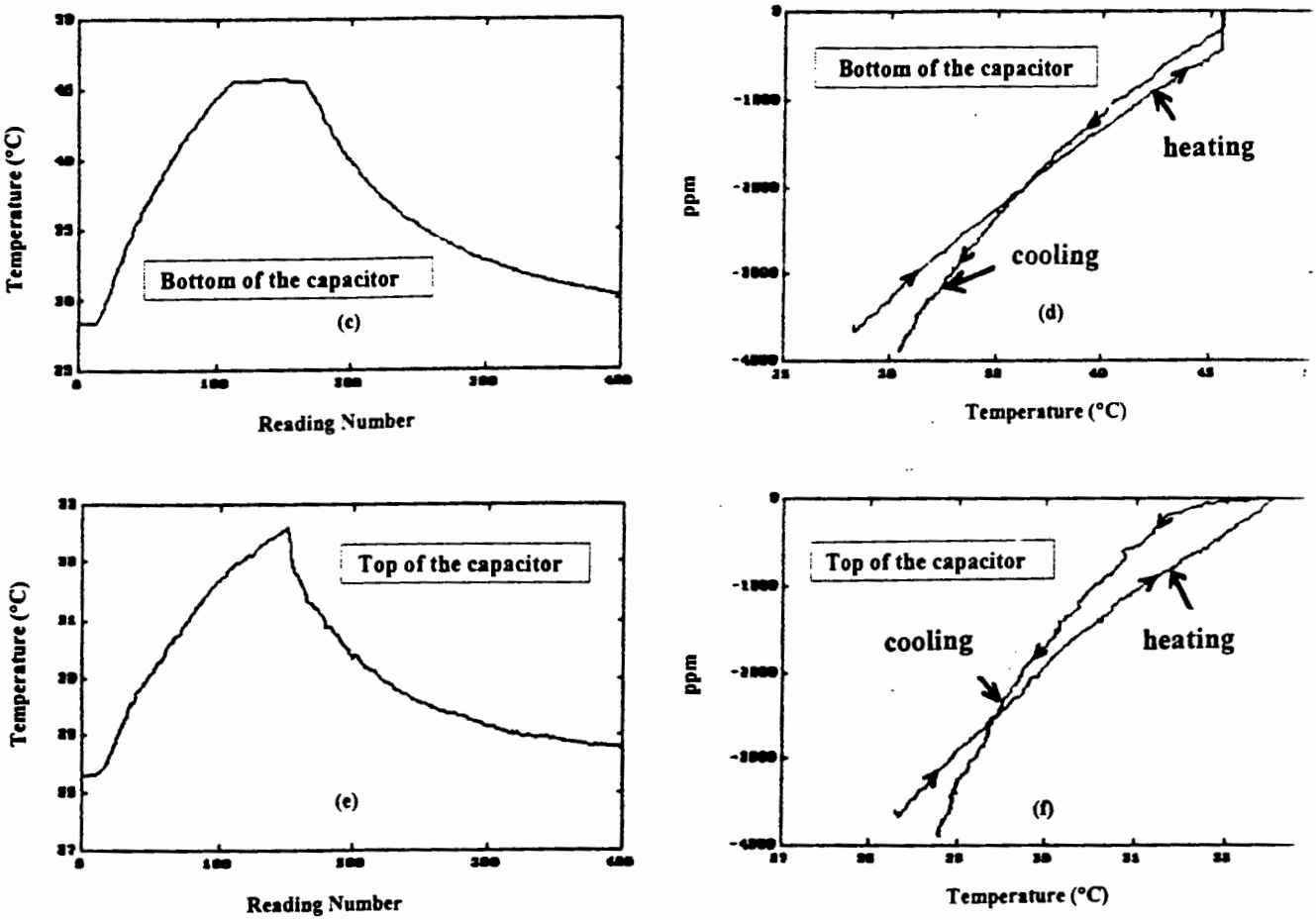

Figure 5.3.2c-f : By comparing the graphs showing the temperature change on the bottom of the capacitor (which is bonded to the plate) to the top of the capacitor, a temperature difference of almost 13°C is evident. Also, comparison of the two graphs showing how the capacitor was heated up and then allowed to cool down reveals that the plot for the temperature on the top of the capacitor is noisier than that of the bottom of the capacitor. This is due to the fact that the top section dissipates some of its heat to the air.

Figure 5.3.2g shows the plot as the capacitor was heated up in the bridge to a temperature of 46°C. The plot has a positive slope and does not appear to be too noisy.

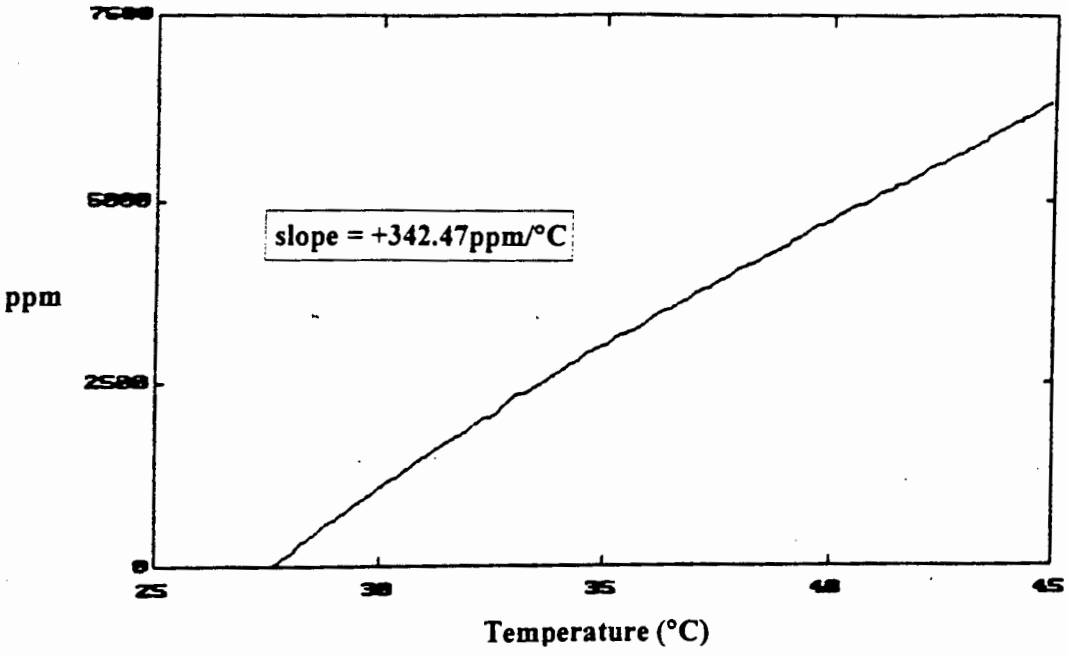

Figure 5.3.2g : Plot of the temperature characteristic for the polyester capacitor. The plot shows a positive slope of +342.47ppm/°C, and the noise (if any) is minimal.

A linear regression was done on the experimental data, and the equation was determined : ppm = 342.47 (θ) - 9000. Figure 5.3.2h shows the regressed plot (dotted line) together with the experimental data (solid line). The plot for the capacitor is not perfectly straight, however, it was possible to determine the temperature coefficient for the polyester capacitor : +342.47ppm/°C ± 10ppm/°C. Taking into account the uncertainties due to thermal effects, this value for the temperature coefficient is acceptable.

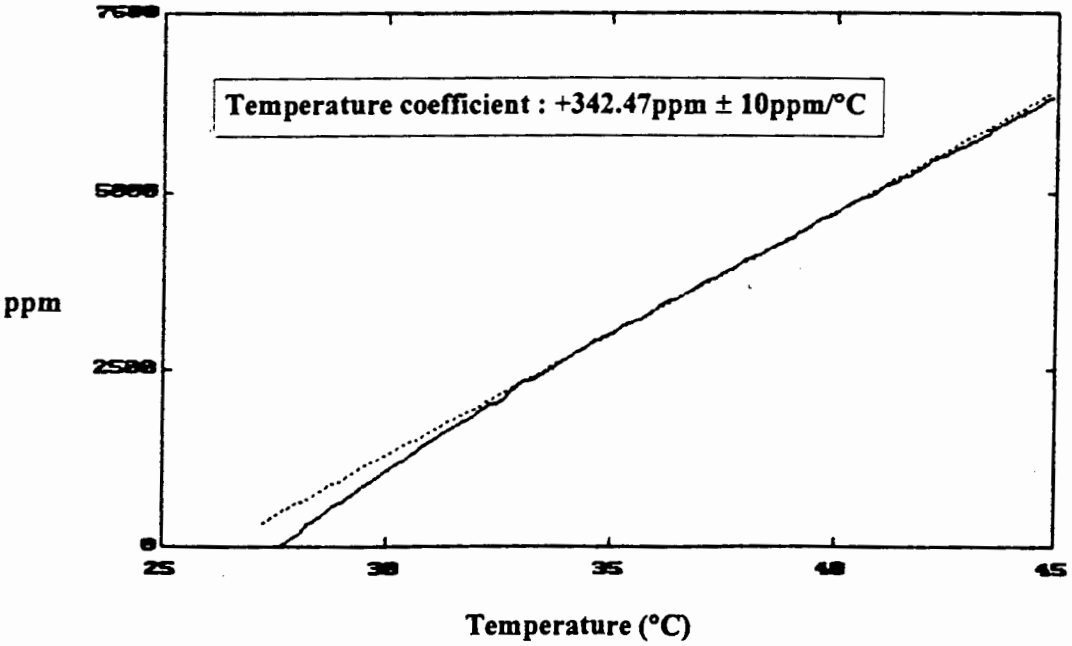

Figure 5.2.3h : The experimental values (solid line) and the regressed plot (dotted line). From this we can visually see how the data correlates to the theoretical values, clearly showing a slight curvature in the temperature characteristic of the capacitor. The temperature coefficient of the capacitor was calculated to be : +342.47ppm/°C.

The plots in Figures 5.3.2g and h shows that the capacitor has a positive temperature coefficient. As a result of this, as the temperature of the capacitor increased, the output voltage also went up. Therefore, the capacitance of the device under test was increasing and hence, the reactance was also going up in value.

A detrend graph showing the difference between the experimental data and the calculated regressed values is shown in Figure 5.3.2i. This graph clearly indicates that the plot for the heating up of the capacitor (over the 24°C range shown) is not a perfectly straight line, since the detrend graph has the most variation from the general trend around its extreme areas. Also evident from this graph is the low level of noise, i.e., approximately 25ppm.

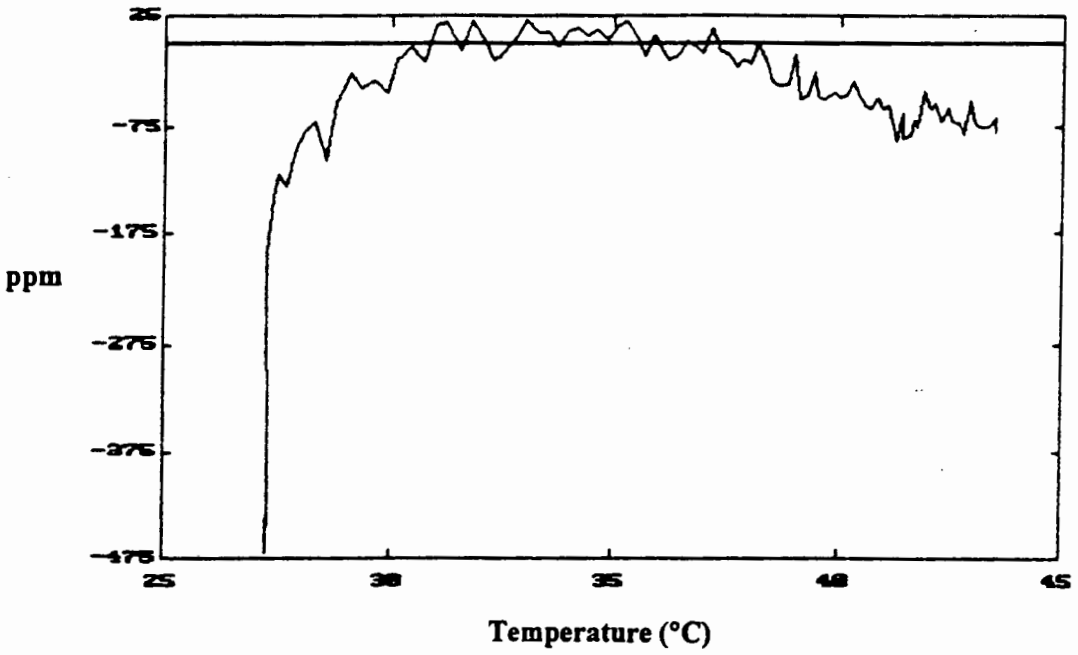

Figure 5.2.3i : Detrend graph, clearly showing how the experimental results are scattered about the general trend. The difference values, which are plotted here, is a representation of experimental readings - regressed values. The noise level is very low on this plot, i.e., approximately 25ppm for the 500ppm range shown. The graph also verifies the deviation from a perfectly linear temperature characteristic, in that the extreme parts of the graph clearly has the most variation from the general trend.

To summarise, of the film dielectrics, viz., polycarbonate, polyester, polypropylene and polystyrene, the most common is polyester. This has the highest dielectric constant, and so is capable of the highest capacitance per unit volume. Polyester has a non-linear and comparatively high temperature coefficient, i.e., experimentally it was found to be +342.47ppm/°C ± 10ppm/°C. The dissipation factor (tan δ) for a capacitor is defined as : "a measure of the lossiness of the component and is the ratio of the resistive and reactive parts of the impedance, R/X, where X = ωC." The dissipation factor for polyester capacitors are high, and varies markedly with temperature and operating frequency.

The value of capacitance, C, is also directly proportional to surface area, A, and inversely proportional to the thickness of the dielectric layer, W, i.e., $C = \varepsilon_r \varepsilon_o A/W$. We have seen during the investigation that, as a result of the Wima capacitors bulky size, there was a tremendous temperature gradient (up to 13°C) between the bottom section of the capacitor (which was bonded to the heating plate), and the top of the capacitor. This, together with the fact that these capacitors have relatively high temperature coefficients, resulted in the increase in the reactance with temperature, and thus increasing capacitance. This led to the believe that there might be a case for heat-sinking or recessing the capacitors when used in circuits which require precise measurement.

As with resistors, the actual capacitance that a component can exhibit is only mildly related to its marked value. The actual capacitance will vary with initial tolerance, temperature, applied voltage, frequency and time. The operating temperature upper and lower limits (typically -55°C to 125°C) are either dictated by expected life service or the allowable variation limits on the nominal capacitance. Most capacitors can actually be used outside their nominal temperature limits, but at reduced lifetime, hence with reduced reliability. All of the above factors make these non-electrolytic Wima polyester capacitors less useful for critical circuits where a stable, low-loss component is needed. However, it can be used for applications such as decoupling, coupling and bypass, where the stability and loss factor of the capacitor are not too important.

5.3.3 The Piezo-Ceramic Capacitors

Using the PC-interface card which I designed, as well as the experimental techniques and equipment described in previous chapters, the measurements on the piezo-ceramic capacitors and soft ferrite core inductors were done by Ziyaad Gydien, as part of an undergraduate thesis.

Certain ceramics and crystals, when mechanically strained in particular directions, become electrically polarised and this can be detected by placing metal electrodes onto opposite faces of the material, so that the change appears as a potential difference. This effect is reversible, viz., the application of an emf between the plates results in a strain directly proportional to the emf. Substances that possess this property are termed piezoelectric and the effect they exhibit is termed the piezoelectric effect. The piezo-ceramic capacitors were represented by a pair of thin-film barium titanate piezoelectric transducers, with capacitances of 23nF each. Piezoelectric materials are generally brittle and are of two kinds : naturally occurring polycrystalline materials such as quartz and materials such as barium titanate ceramic, and lead zirconium titanate ceramic (PZT).

The temperature coefficient for these materials is loosely defined as "the proportional capacitance rise per degree Celsius", and is given by $Temp.coefficient = \frac{\Delta C}{C\Delta T}$. It was decided to investigate the temperature coefficient, as well as the effects temperature has on the reactance on this material, and consequently on the capacitance. As was the case with the Wima capacitors (Figure 5.3.2a), a Wheastone Bridge set-up was used. However, the two resistors in the bridge were both changed to 10KΩ. The Wima capacitors previously used were replaced with the piezoelectric transducers, and only one of the piezoelectric transducers was heated. The signal generator and rms-to-dc converters were employed again, together with the AD620 instrumentation amplifier. The piezoelectric disk, which was to be heated, was secured on the aluminium plate with the use of a grease, since initial experiments revealed that the glue used affected the disk's performance. Also, four 100Ω "heater resistors" were now used as the heating element, since it was decided to subject the component-under-test to far higher temperatures than in previous experiments.

Figure 5.3.3a shows the familiar calibration technique, where a 1MΩ resistor was switched in- and out-of-parallel with one of the 10KΩ resistors in the Wheastone Bridge. The change in the output voltage was therefore a consequence of the 1% change in the resistance of one of the arms of the bridge, and in turn gave the sensitivity as 1.1V/ppt. Ten readings were taken at 15 second intervals with the 1MΩ resistor connected across the 10KΩ. Thereafter, the 1MΩ was removed and a further ten readings were taken at the same rate ---- this process was repeated a few times.

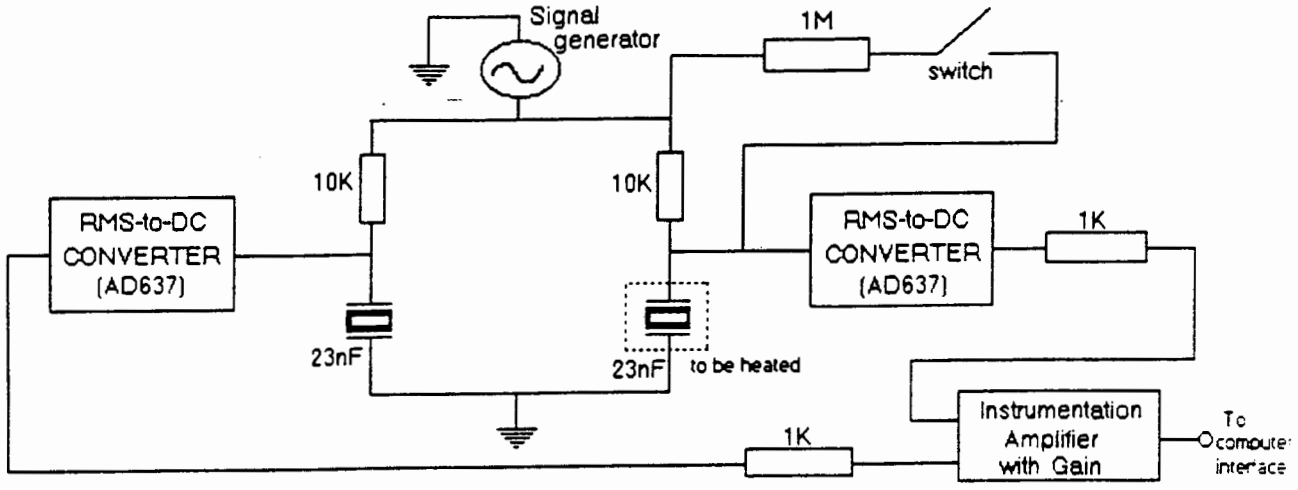

Figure 5.3.3a : The Wheatstone Bridge and accompanying circuitry used for calibrating the system before experimentation. A 1MΩ resistor was switched in- and out-of-parallel with the 10KΩ resistor, whilst readings were taken at 15 second intervals. This 1% change in the resistance caused a change in the output voltage, which gave the sensitivity as 1.1V/ppt.

As the piezoelectric transducer was heated up, the change in output voltage in effect gave a measure of the change in reactance of the component. This change in reactance was monitored as the component was subjected to temperature cycling, in order to gain insight into thermal hysteresis. The transducer was heated up to a temperature of 140°C, and then allowed to cool down. The fact that this component exhibited no thermal hysteresis is illustrated in Figure 5.3.3b below. The reason for the absence of any thermal lag was because the piezoelectric disc was extremely thin in dimension, and therefore the temperature applied to it by the heating plate was evenly spread across the component.

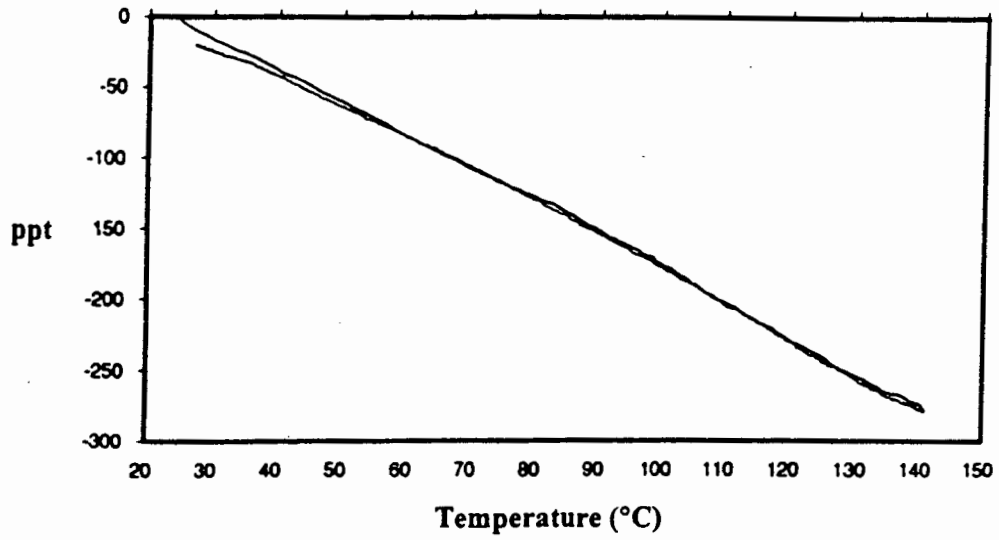

Figure 5.3.3b: The resultant plot of temperature cycling conducted on the piezoelectric transducer. The device was heated up to a temperature of 140°C, and then allowed to cool down. The plot shows that there was no thermal hysteresis exhibited by this component. The lack of hysteresis was due to the fact that the transducer was very thin in dimension (a disk), and therefore the heat applied to it was evenly distributed throughout the component.

As can be seen from figure 5.3.3b above, the piezoelectric transducer showed a linear decrease in reactance with increasing temperature. This change in reactance of the component was extrapolated to a temperature of 440°C, and is shown in Figure 5.3.3c. The equation used for extrapolating the line was : ppt = -2.4157 (θ) + 56.3, which gave the slope as -2.4157ppt/°C.

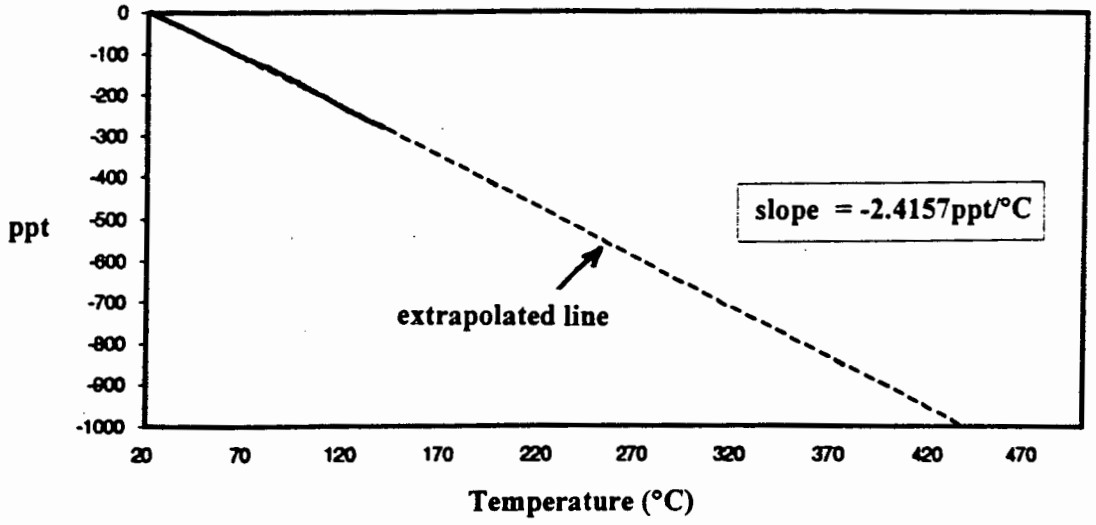

Figure 5.3.3c : Extrapolated plot of the change in reactance (in ppt) for the piezoelectric transducer, as it was heated up. The plot was extrapolated to a temperature of 440°C using the equation ppt = -2.4157 (θ) + 56.3, and shows a change of 1000ppt for that temperature range. The negative linear slope for this plot was therefore -2.4157ppt/°C.

In order to determine the temperature coefficient for the component-under-test, the following equations were used to convert the change in reactance to changes in capacitance with changing temperature. We know that $X_c = \frac{-1}{\omega C}$, therefore

$\frac{1}{X_c}\frac{dX_c}{dt} = \frac{1}{C}\frac{dC}{dt}$, which can be rewritten as $\frac{dC}{dt} = \frac{C}{X_c}\frac{dX_c}{dt}$, or as $\frac{dC}{dt} = \omega C^2 \frac{dX_c}{dt}$.

Hence, from the final equation above, the changes in reactance could be converted to changes in capacitance for the piezoelectric transducer. Figure 5.3.3d shows the plot for the change in capacitance as the temperature was increased to 55°C. A change of 7ppt is evident for the temperature range shown, and a linear regression was done on the plot since it was reasonably linear over that range. The thick, darker line in the plot represents the regressed line. This best-fit straight line was found to be : ppt = 0.2129 (θ) - 4.782, which gave the positive temperature coefficient for the piezoelectric transducer as +0.2129ppt/°C or +212.9ppm/°C.

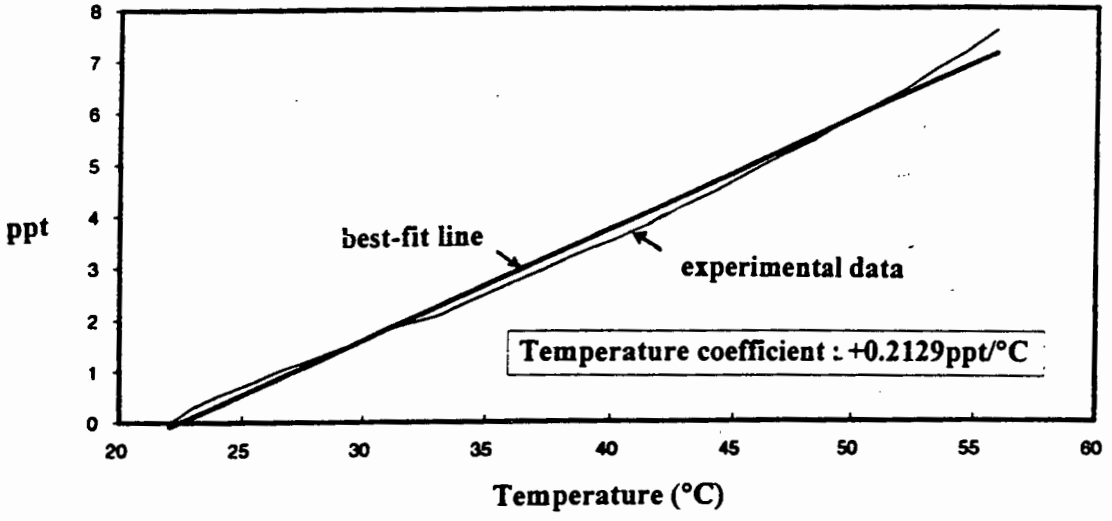

Figure 5.3.3d : Graphs showing the change in capacitance of the piezoelectric transducer with temperature, as well as a best-fit straight line. The experimental plot is fairly linear over the 7ppt range shown, and therefore the equation : ppt = 0.2129 (θ) - 4.782 was used to best fit this straight line. The equation gave the positive temperature coefficient as +0.2129ppt/°C or +212.9ppm/°C.

The orientation of the crystal axis results in a permanent polarisation of the ceramic, analogous to the magnetisation of a ferromagnetic material. At high temperatures, the orientated crystal axis loses its polarity and the ceramic is no longer piezoelectric. The temperature of this transformation is called the Curie temperature. It was decided to investigate what the Curie temperature would be in the case of the component-under-test. Hence, the component was heated up to a temperature of 140°C and it was noticed that the capacitance increased exponentially with temperature. An exponential extrapolation, with equation : ppt = $0.3943\ e^{0.0421\ (\theta)}$, was done on the data until, theoretically, the Curie temperature was reached. The extrapolated curve, as seen in Figure 5.3.3e, shows that the capacitance approaches a coefficient of infinity as the temperature approaches 200°C.

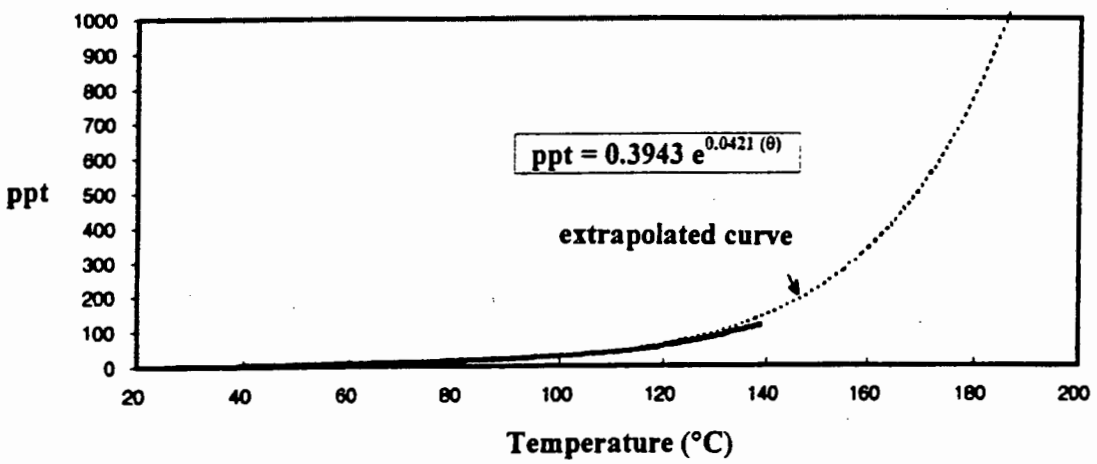

Figure 5.3.3e : Plot of the change in capacitance as the component was heated up to 140°C. Using the equation : $0.3943\ e^{0.0421\ (\theta)}$, the curve was extrapolated to 200°C exponentially and shows a change in capacitance of 1000ppt. The capacitance approaches infinity as the temperature approaches infinity.

To summarise, the expected temperature dependence of the piezo-ceramic was evident, and the temperature coefficient was found to be 212.9ppm/°C. However, the exponential increase in capacitance with temperature was alarming, viz., as the temperature increases, the change in capacitance increases to nearly infinity, until the Curie point is reached.

5.4 SOFT FERRITE CORES

The properties of permeable cores are reminiscent of the dielectric characteristics (variability with voltage, temperature and frequency) of the hi-K (permittivity) ceramics. The most common core material, ferrite, is in fact a type of ceramic. Ferrites are metal-oxide ceramics, made of a mixture of Fe_2O_3 and either manganese-zinc or nickel-zinc oxides pressed or extruded into a range of core shapes.

Soft ferrites are semi-conducting polycrystalline oxides, most of which have spinal lattice crystalline structures, and exhibit the property of ferromagnetism. In a ferromagnetic material, magnetism occurs under the influence of an externally applied field. On removal of this field, the material returns to its non-magnetised state and is termed "magnetically soft". Ferromagnetic materials are subdivided by internal energies into a great number of discrete regions called magnetic domains, in which the magnetic moments of adjacent atoms are aligned. In the normal state, i.e., no external magnetic field, these fields are randomly orientated and it is not possible to detect any magnetisation by measurement. When an external field is applied, domains tend to align themselves in the direction of the field. Because of internal energies acting on domains, some of the changes in orientation will lag behind the external field. This, and the irreversible nature of some changes, contribute to the characteristic shape and hysteresis of a B-H curve (magnetic flux versus applied magnetic field).

In metals, ferromagnetism is due to atomic forces aligning adjacent electron 'spins' in parallel, creating very strong magnetic fields within a body. The magnetic moments of atoms are additive over the relatively large area of a single domain. Ferrites differ from metals, since their structures contain two magnetically opposing systems and can be represented as successive lattice planes of metals separated by oxygen atoms. Exchange interactions between metal and oxygen neighbours result in a reduction in electron conductivity, giving ferrites their high resistivity and low eddy-current losses at high frequencies.

Two different pairs of soft ferrite manganese-zinc cores were used in the experiments. The one pair was the large low-frequency pot core type, used in power transformers and with an inductance of 38.1mH, whilst the other pair was of the smaller high-frequency E-core type, used in telecommunications circuits and with an inductance of 468μH. The pairs of specimens were chosen to give very little difference at room temperature. The circuitry set-up used to investigate the capacitors (see Figure 5.3.2a), i.e., Wheastone bridge, RMS-to-DC Converters, instrumentation amplifier, signal generator, LM35 temperature sensor, and their accompanying circuitry, was employed again during these experiments, but with the cores replacing the capacitors in the Wheastone bridge. The circuitry was insulated from the environment to ensure that air flow and drafts did not affect the readings when temperature runs were done. The cores were glued onto the aluminium plate. To achieve thermal stability, it was decided to use a strip of aluminium heatsink to clamp the cores to the plate, and thus include a larger surface area of the core. It was found that the cores were very sensitive to applied pressure, and therefore, once the cores were secured onto the plate, their inductances were measured again.

In industry, cores are generally used with their Q values as high as possible. Hence, the experiments were aimed at using the cores at a frequency where their Q factors were approximately a maximum. The quality of an inductor in a resonant circuit is commonly described by the Q factor, the ratio of the reactance and resistance at a given frequency. Q (the magnification or quality factor) is given by : $Q_o = \frac{\omega_o L}{R}$ for a series resonant circuit, and $Q_o = \frac{R}{\omega_o L}$ for a parallel resonant circuit. The tuned circuit used to obtain a set of Q values for the inductors is shown in Figure 5.4a below. At resonance, the collector part of the circuit was equivalent to a parallel RLC circuit. R_d was the resistance of the inductor at a specific frequency. The variable capacitance had a range of 11pF to 231pF, and was set to a specific value after which the signal generator was adjusted to a resonant frequency. At resonance, the amplitudes of the sinusoids at the collector and emitter were measured. From transistor theory, we know that $\frac{V_c}{V_e} = \frac{R_c}{R_e}$,

therefore $R_c = \frac{V_c}{V_e} R_e$, where V_c and V_e are the amplitudes of the signals at the collector and emitter respectively. Also, $Q = \frac{R_d}{\omega_o L}$, and since $R_d = R_c$ = resistance of the inductor in the collector arm, different values of Q could be calculated by varying the capacitance value. In this way, the Q values were obtained for the inductors so that the driving frequency of the signal generator could be determined.

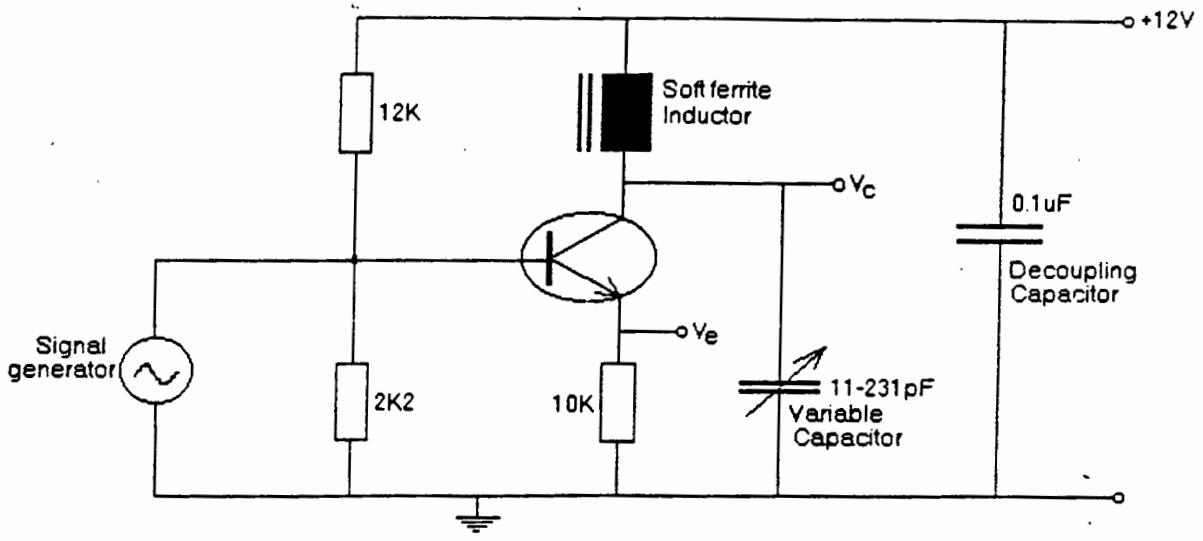

Figure 5.4a : The circuit used to obtain Q values for the inductors, so that the driving frequency of the signal generator could be determined. At resonance, the collector part of this circuit was equivalent to a parallel RLC circuit. The variable capacitance was set to a specific value after which the signal generator was adjusted to a resonant frequency.

Calibration was achieved in exactly the same way as that used for the piezoelectric transducers, i.e., by periodically switching a 1MΩ resistor in- and out-of-parallel with the 10KΩ resistor in one of the arms of the bridge. Readings were taken at 15 second intervals. This 1% change in the resistance in the bridge circuit, resulted in a change in output voltage of 0.433V, giving the sensitivity as 4.33V/ppt. Figure 5.4b below shows the graph used for calibration. The changes in output voltage were then calibrated to get dX_L in parts per thousand. We know that $X_L = \omega L$, and using the fact that $\frac{dX_L}{X_L} = \frac{dL}{L}$, then $\frac{1}{X_L}\frac{dX_L}{dt} = \frac{1}{L}\frac{dL}{dt}$ and $\frac{dL}{dt} = \frac{L}{X_L}\frac{dX_L}{dt}$, or $\frac{dL}{dt} = \frac{1}{\omega}\frac{dX_L}{dt}$. This equation was used to convert changes in reactance to changes in inductance, where $\omega = 2\pi f$ and the operating frequencies were 40kHz and 400kHz for the pot- and E-core respectively.

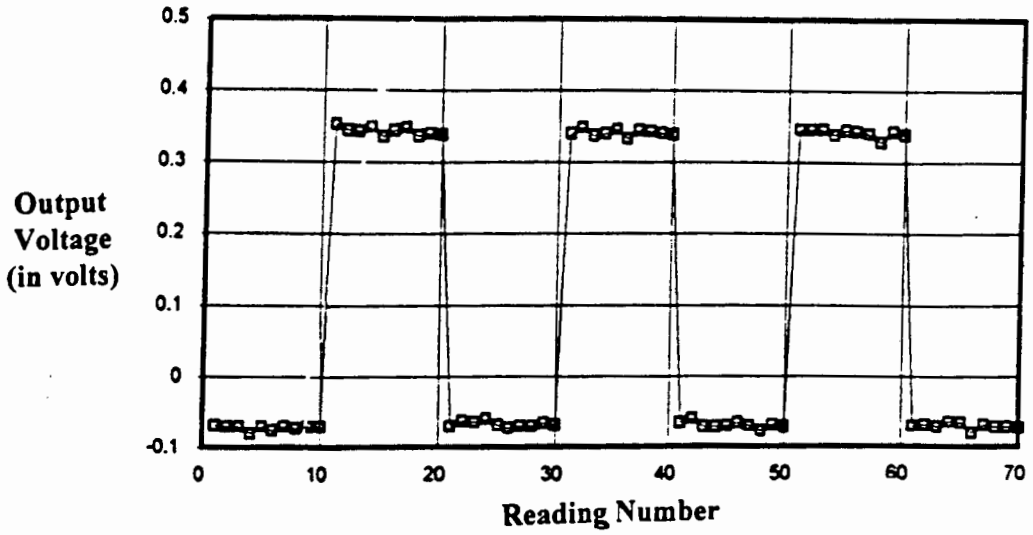

Figure 5.4b : The Wheatstone bridge and accompanying circuitry was used again during calibration of the system before experimentation. A 1MΩ resistor was switched in- and out-of-parallel with the 10KΩ resistor, and this 1% change in the resistance caused a change in output voltage of 0.433V, giving the sensitivity as 4.33V/ppt.

The main factor affecting the accuracy of the results was the phenomenon of thermal lag. During "temperature runs", the heat was not evenly distributed throughout the components bodies since large parts of their surface area were not in contact with the aluminium heating plate. The centres of the components were therefore not at the same temperature as their heated surfaces, resulting in temperature gradients across individual components. The pot core was heated up to a temperature of 57°C, as illustrated in Figure 5.4c, and then allowed to cool down.

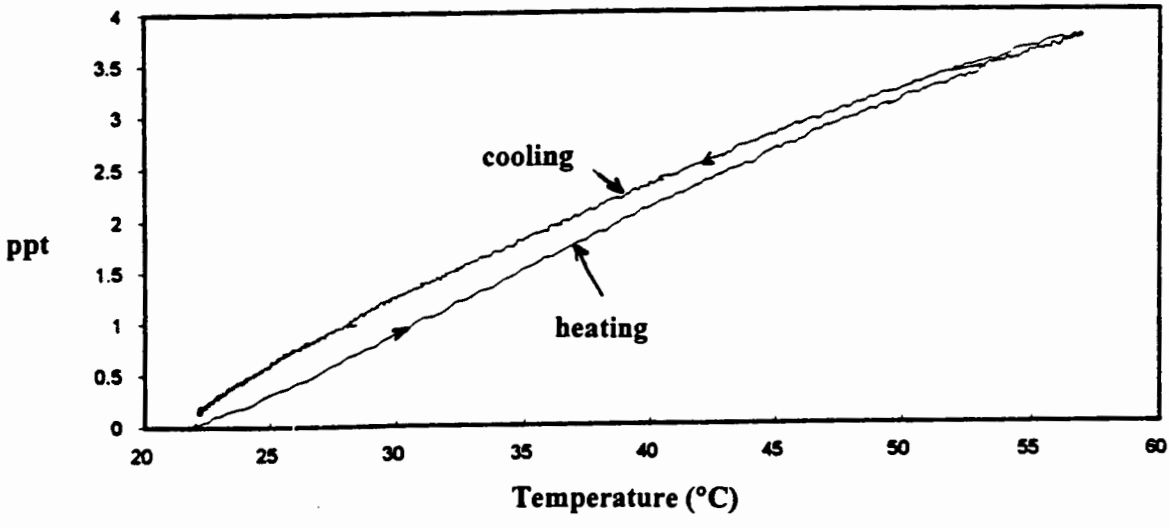

Figure 5.4c : Temperature cycling resulted in this plot, where the change in inductance was monitored as the pot core was heated up to a temperature of 57°C, and then allowed to cool down. Thermal hysteresis, of 2.6°C, is evident in this plot. This was as a result of the rate of temperature increase at which the surface in contact with the heating plate was being heated up, and the resulting thermal lag in the rest of the component because the heat was not evenly distributed throughout the component.

As the specimen was heated up, the rate of temperature increase was so high that the core surface temperature matched that of the plate, but the temperature throughout the rest of its body lagged behind. This meant that an accurate change in inductance versus temperature could not be attained. One way of minimising the error due to thermal hysteresis was by reducing the rate of temperature change. This is illustrated by observing the hysteresis the hysteresis loops ABC in Figures 5.4d and e.

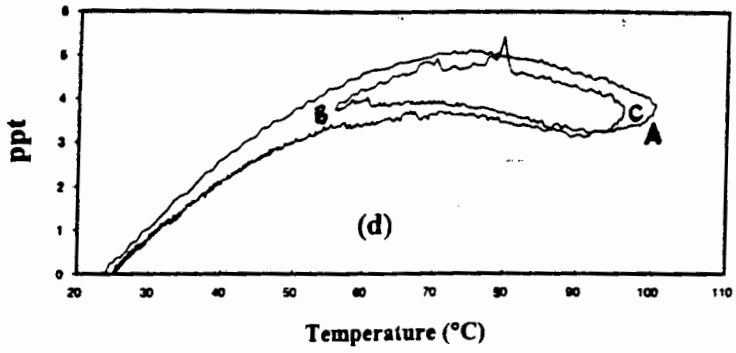

Figure 5.4d : The pot core was heated up to poi with the "heater voltage" set to a maximum ini The heater was then turned off, and the core w allowed to cool down to point B. Thereafter, w maximum "heater voltage" applied, it was heat again until point C and then allowed to cool to temperature, generating the hysteresis loop AB

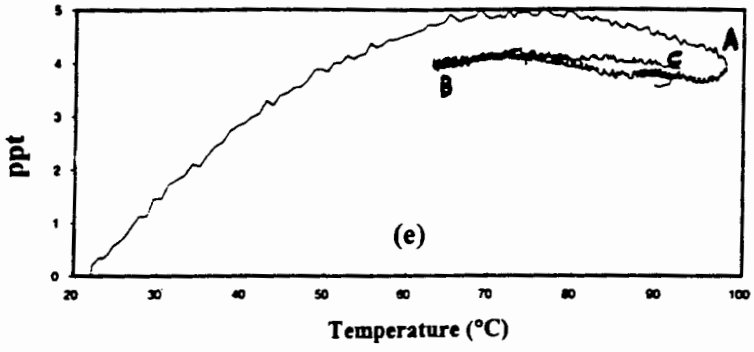

Figure 5.4e : The pot core was heated up, with maximum "heater voltage", to point A. Then, t voltage was turned down to 25V, and later 20V then 15V until point B. At point B, the voltage turned up again in steps of 5V until point C. Tl compromise for reducing the thermal hysteresis the introduction of a higher level of noise comp to the plot in Figure 5.4d.

The hysteresis loop ABC in Figure 5.4d was obtained by rapid heating and subsequent cooling, i.e., by turning the "heater voltage" up to a maximum initially, and then switching the heater off and allowing the specimen to cool down to room temperature over a long period. Figure 5.4e shows a reduced hysteresis curve ABC, obtained by a slow and gradual heating and cooling process. The "heater voltage" was adjusted gradually in steps, compared to the process used in Figure 5.4d. The reduced hysteresis loop proves that more accurate data can be obtained by subjecting components-under-test, with large surface areas, to slower temperature changes. However, coupled to the slow temperature change is the increased level of noise evident on the hysteresis curve.

The temperature coefficient for an inductor is defined as : "the proportional inductance rise per degree Celsius", and is given by $\frac{\Delta L}{L\Delta T} = \frac{\Delta \mu}{\mu \Delta T}$, where ΔT is the temperature rise (°C) causing the ΔL in inductance, or Δμ (permeability). Figures 5.4f and g show the plots for the change in inductances as the temperature was increased to 57°C for the pot- and E-core respectively. In either case, the thick, dark lines represent the best-fit straight lines used to determine the temperature coefficients of the two core types. In the case of the pot core, the temperature coefficient was found to be +0.1174ppt/°C or +117.4ppm/°C, and +0.1037ppt/°C or +103.7ppm/°C for the E core.

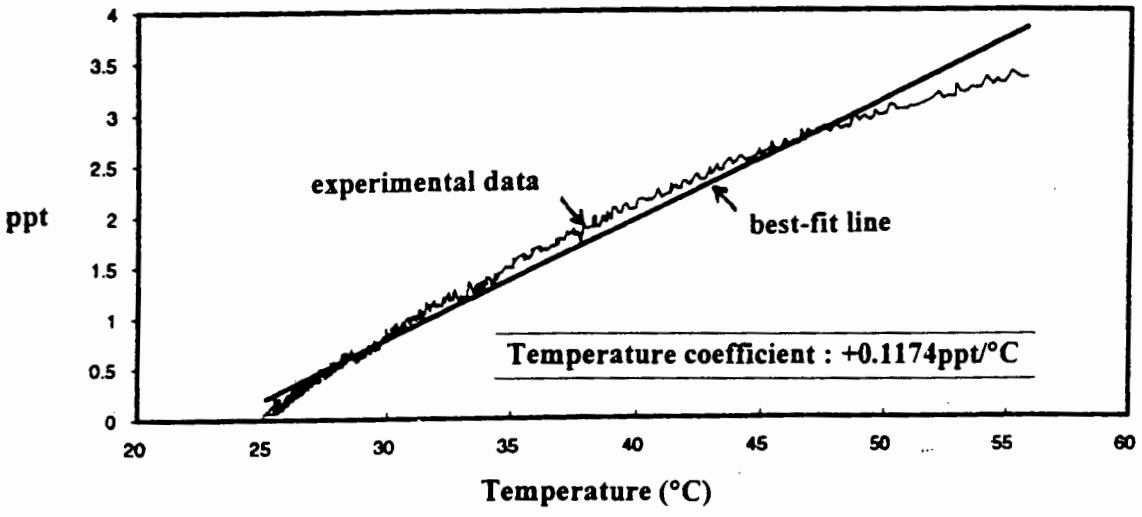

Figure 5.4f : Graph showing the change in inductance of the pot core ferrite with temperature, as well as a best-fit straight line. The equation : ppt = 0.1174 (θ) - 2.741 was used to fit the experimental data. The equation gave the positive temperature coefficient for the pot core as +0.1174ppt/°C or +117.4ppm/°C.

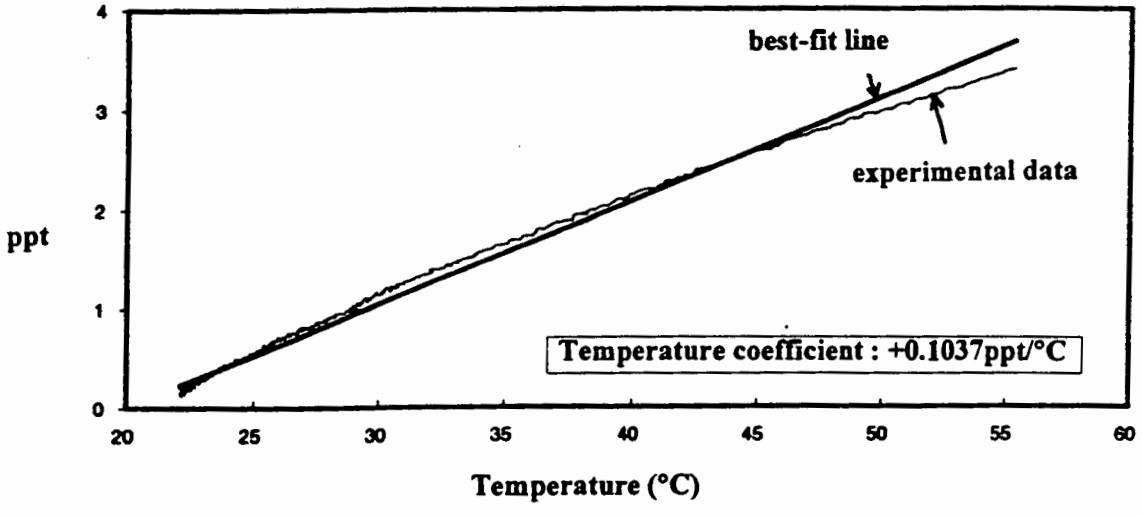

Figure 5.4g : Graph showing the change in inductance of the E core ferrite with temperature, as well as a best-fit straight line. The equation : ppt = 0.1037 (θ) - 2.0685 was used to fit the experimental data. The equation gave the positive temperature coefficient for the pot core as +0.1037ppt/°C or +103.7ppm/°C.

The Curie temperature for a ferrite core is that temperature above which the disruption of magnetic ordering in the crystal lattice, by increasing thermal motion, causes the material to lose its ferromagnetic character, and the permeability falls to near unity. Once the temperature drops below the Curie temperature, the material regains its ferromagnetic character again. It was decided to investigate whether or not it was possible to determine the Curie temperatures of these cores. The cores were heated up to 100°C, and it was noted that the inductance of both cores increased in a quadratic manner. Polynomial regressions were done for both curves, and then these graphs were extrapolated. The polynomial regressions determined the equations for :

the pot core as : $ppt = -0.0019\,(\theta)^2 + 0.2828\,(\theta) - 5.7189$,

and for the E core as : $ppt = -0.0017\,(\theta)^2 + 0.2596\,(\theta) - 4.7889$.

This parabolic characteristic was very similar for each of the cores, as both of them reached a maximum of approximately 5ppt around 75°C and returned to zero at about 130°C. A change of 5ppt represents a 0.5% change in inductance over a temperature range of 50°C. The similarity in performance was to be expected because, although the ferrites were not the same size, they were both manganese-zinc ferrites. Also, the graphs give the change in inductance in parts per thousand, and not in Henrys. Figures h and i are the plots of the change in inductance with temperature for the pot- and E-core respectively.

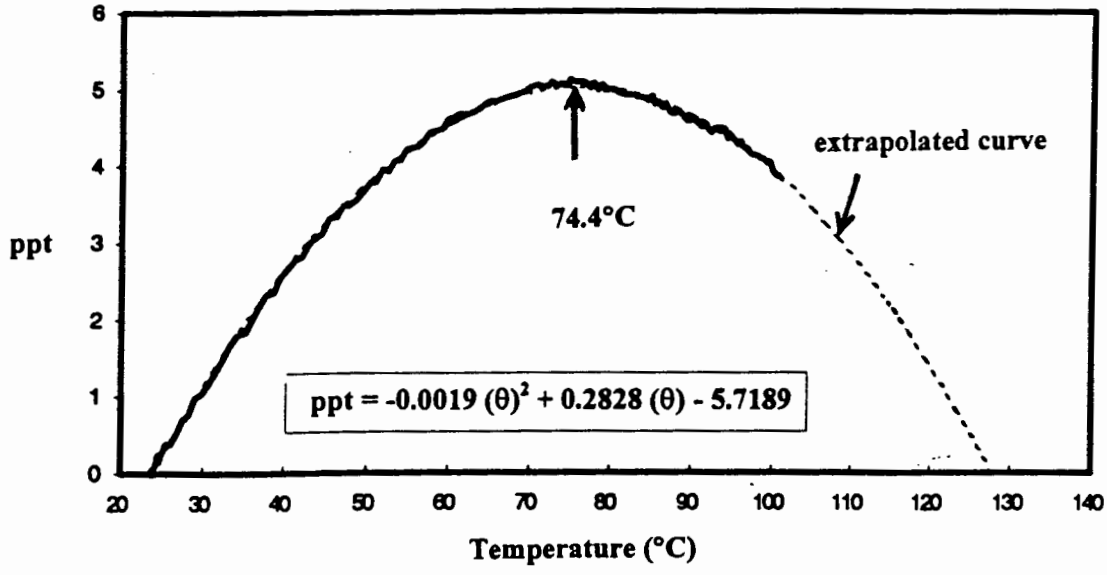

Figure 5.4h : Plot of the parabolic change in inductance as the pot core was heated up to 100°C. Using the regressed equation : $ppt = -0.0019\,(\theta)^2 + 0.2828\,(\theta) - 5.7189$, the curve was extrapolated to 130°C. The parabolic plot illustrates a change in inductance of about 5ppt, reaching a maximum at 74.4°C.

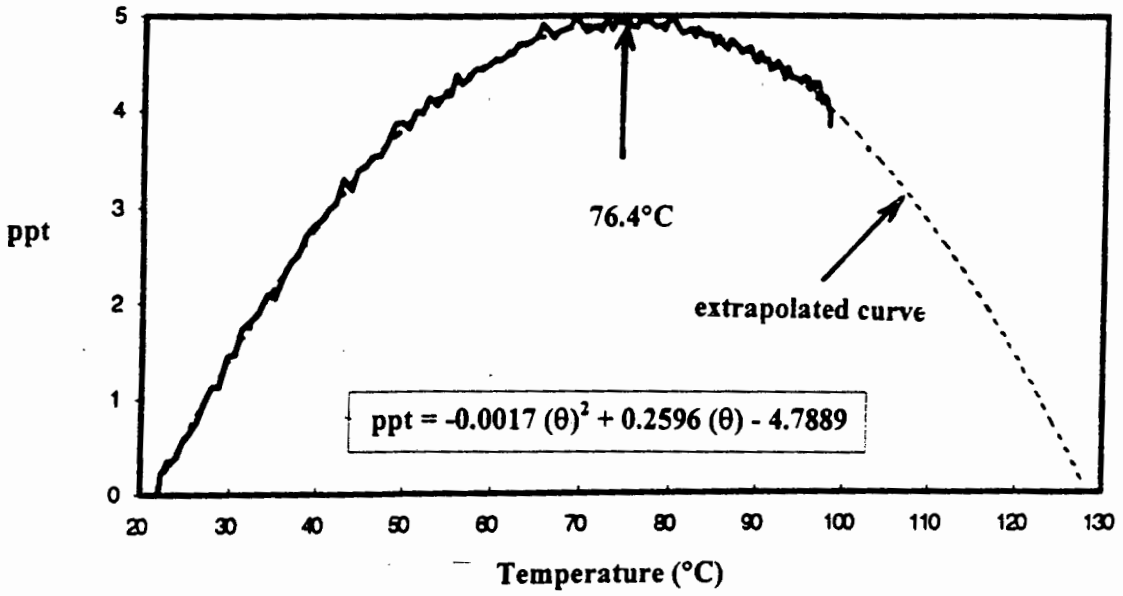

Figure 5.4i : Plot of the parabolic change in inductance as the E core was heated up to 100°C. Using the regressed equation : ppt = -0.0017 (θ)² + 0.2596 (θ) - 4.7889, the curve was extrapolated to 130°C, and shows a change in inductance of about 5ppt over the range. The parabolic maximum is reached at a temperature of 76.4°C.

To summarise, the pot- and E-cores has very similar temperature coefficients, i.e., +0.1174ppt/°C for the pot core and +0.1037ppt/°C for the E core. Both these cores are extremely temperature dependent, which was expected, even though a maximum change of 5ppt was exhibited over a 100°C temperature range. It is interesting to note that the barium titanate piezoelectric transducers has temperature coefficients which were double that of the cores, viz., +0.2129ppt/°C.

5.5 ZENER DIODES

By suitable selection of dimensions and impurities within the silicon diode, it is possible to control the voltage at which reverse breakdown occurs. The slope of the diode V/I curve becomes quite flat in this region and the device can be used as a voltage regulator or clamp, and devices characterised for this purpose are called zener diodes. Just as with other components, the zener is not perfect. Its slope resistance is not zero, its "breakdown knee" is not sharply defined, it has a leakage current below breakdown, and its breakdown voltage has tolerance and temperature coefficient. Unlike other components, the temperature coefficient of the zener's breakdown voltage is quite subtle. It was therefore decided to investigate the temperature coefficients of the commonly-used zener diodes.

The aluminium plate, "heater resistors", LM35 sensor, and temperature-sensing circuitry were all retained from previous experiments. Only one zener diode was heated up in these experiments, and its changing output was fed (see Figure 5.5a below) to the instrumentation amplifier. This zener diode was placed in close proximity to the LM35 temperature sensor on the heating plate, in order to avoid any discrepancies in temperature between the two components. The instrumentation amplifier was followed by an op-amp with appropriate offset, and the total gain of the circuitry was 1480.

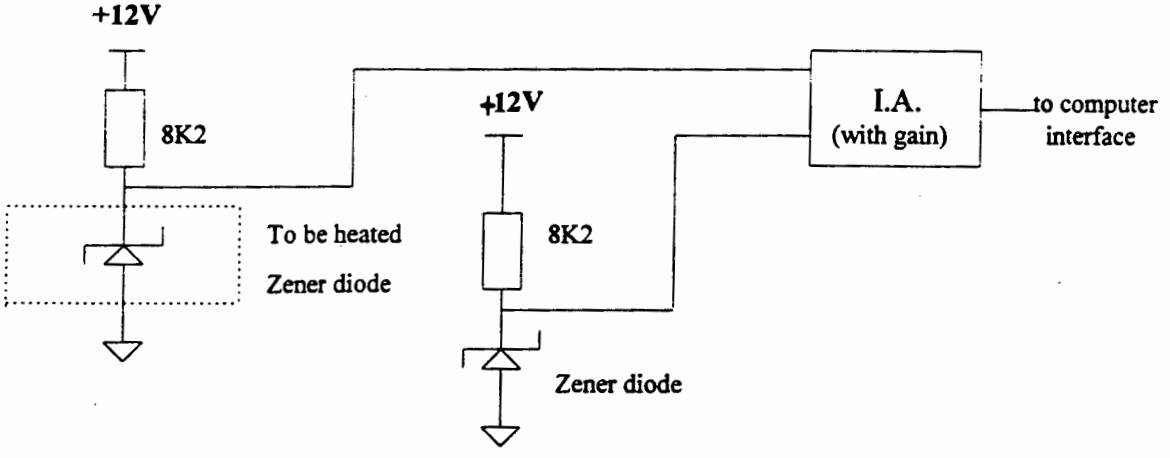

Figure 5.5a : The circuit used to determine the temperature characteristics of the zener diodes. The output from the "heated component", which underwent parameter changes, was inputted to pin 2 (negative input) of the instrumentation amplifier, whilst the other output, acting as a reference, was inputted to pin 3 (positive input).

Temperature cycling for all of the zener diodes illustrated the absence of thermal hysteresis for each of the diodes studied. This was expected since the zener diodes were placed in good thermal contact with the heating plate, were not bulky in dimension, and the circuit techniques employed would have reduced any occurrence of hysteresis to virtually zero.

Figures 5.5a-e below show how the various diodes were heated up, and the relative change in their outputs as a result of this temperature change. Evident from these graphs is the fact that the 3.9V and 4.7V zener diodes have negative-going slopes, whilst the 6.8V, 8.2V and 9.1V diodes have positive-going slopes. All the slopes tend to be linear in character, and with minimal noise. Looking at the graph for the 6.8V diode in (c), one sees that it deviates most from the linear trend. However, the 6.8V zener diode shows the smallest change in output, i.e., approximately 6ppm, over the temperature range shown. In fact, the voltage change in this zener diode is almost independent of temperature, with noise of about 2ppm. This was expected from the 6.8V zener diode, which exhibits the best temperature characteristic out of the batch studied. The 3.9V and 9.1V zener diodes show the largest change in output over their respective temperature changes, whilst the 4.7V zener diode has a slight curvature to its temperature characteristic. Linear regressions were done on all the experimental data, and the following equations and temperature coefficients (in parts per thousand and million) were calculated for the various zener diodes :

- 3.9V => ppt = -0.771 (θ) + 16.21; temperature coeff. = -0.771ppt/°C ± 0.0014ppt/°C,
- 4.7V => ppt = -0.0415 (θ) + 1.02; temperature coeff. = -0.0415ppt/°C ± 0.0003ppt/°C,
- 6.8V => ppm = +0.86 (θ) - 39.16; temperature coeff. = +0.86ppm/°C ± 0.05ppm/°C,
- 8.2V => ppt = +0.464 (θ) - 19.228; temperature coeff. = +0.464ppt/°C ± 0.001ppt/°C,
- 9.1V => ppt = +0.636 (θ) - 20.93; temperature coeff. = +0.636ppt/°C ± 0.007ppt/°C.

Immediately obvious, from the calculated temperature coefficients above, is the fact that the 6.8V zener diode has the smallest coefficient, and therefore represents the best choice in diodes for practical use (out of the batch studied), where temperature dependence is important. There appears to be a "crossover" between temperature coefficients from positive to negative between 4.7V and 6.8V. Figures 5.5f-i are plots of the theoretical straight lines, superimposed onto the experimental data.

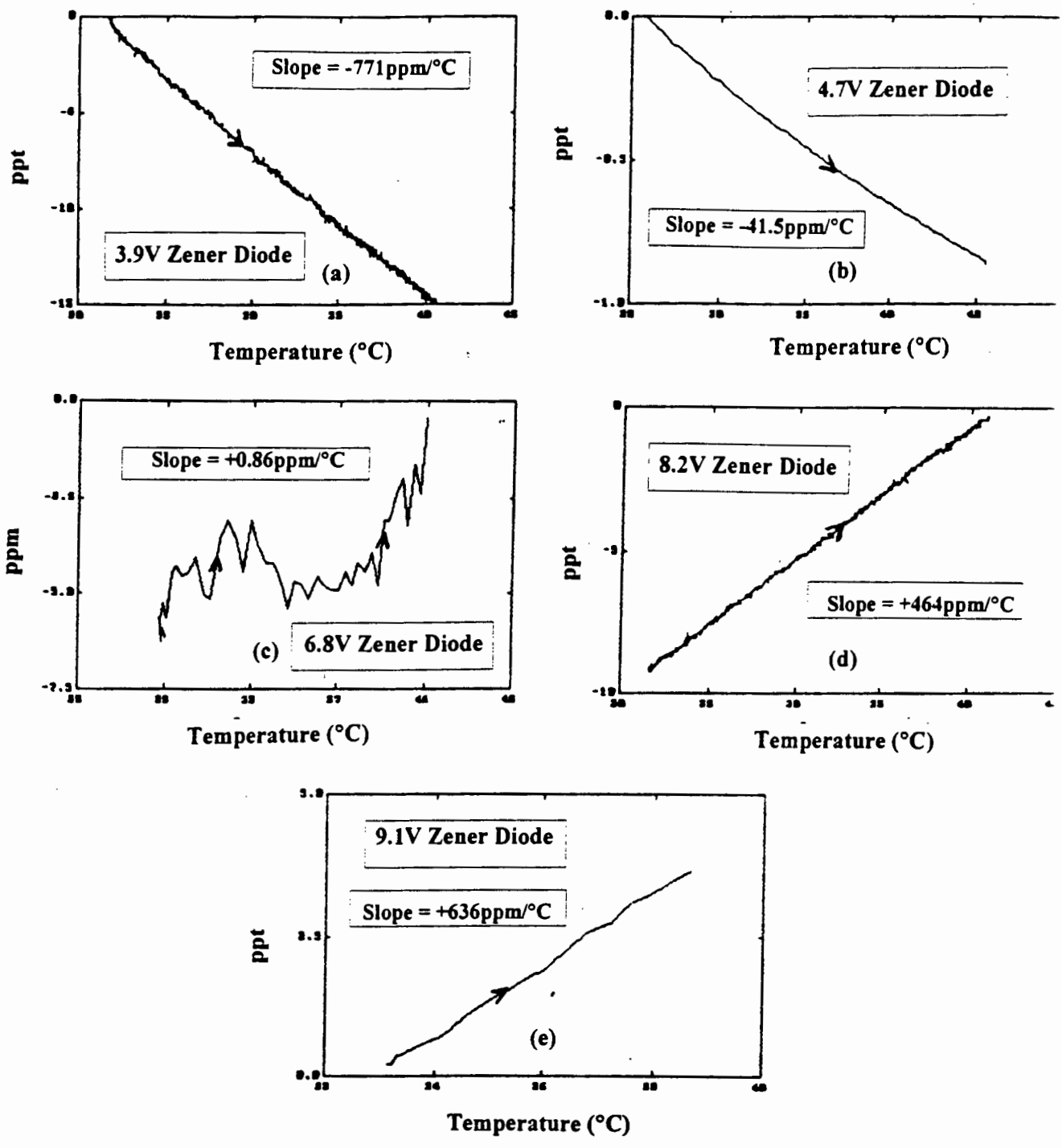

Figures 5.5a-e : The figures above show that the 3.9V and 4.7V zener diodes (a and b respectively) have negative slopes, whilst the 6.8V, 8.2V and 9.1V zener diodes (c, d and e) have positive slopes. All of the slopes have linear trends, with the 6.8V diode deviating the most from this trend. However, the 6.8V zener diode shows the smallest change over the temperature range, i.e., only about 6ppm. The voltage change in this zener diode is almost independent of temperature, with noise of about 2ppm. This was expected of the 6.8V zener diode. The 3.9V and 9.1V diodes show the largest change in output over their respective temperature ranges. The 4.7V zener diode has a slight curvature to its temperature characteristic.

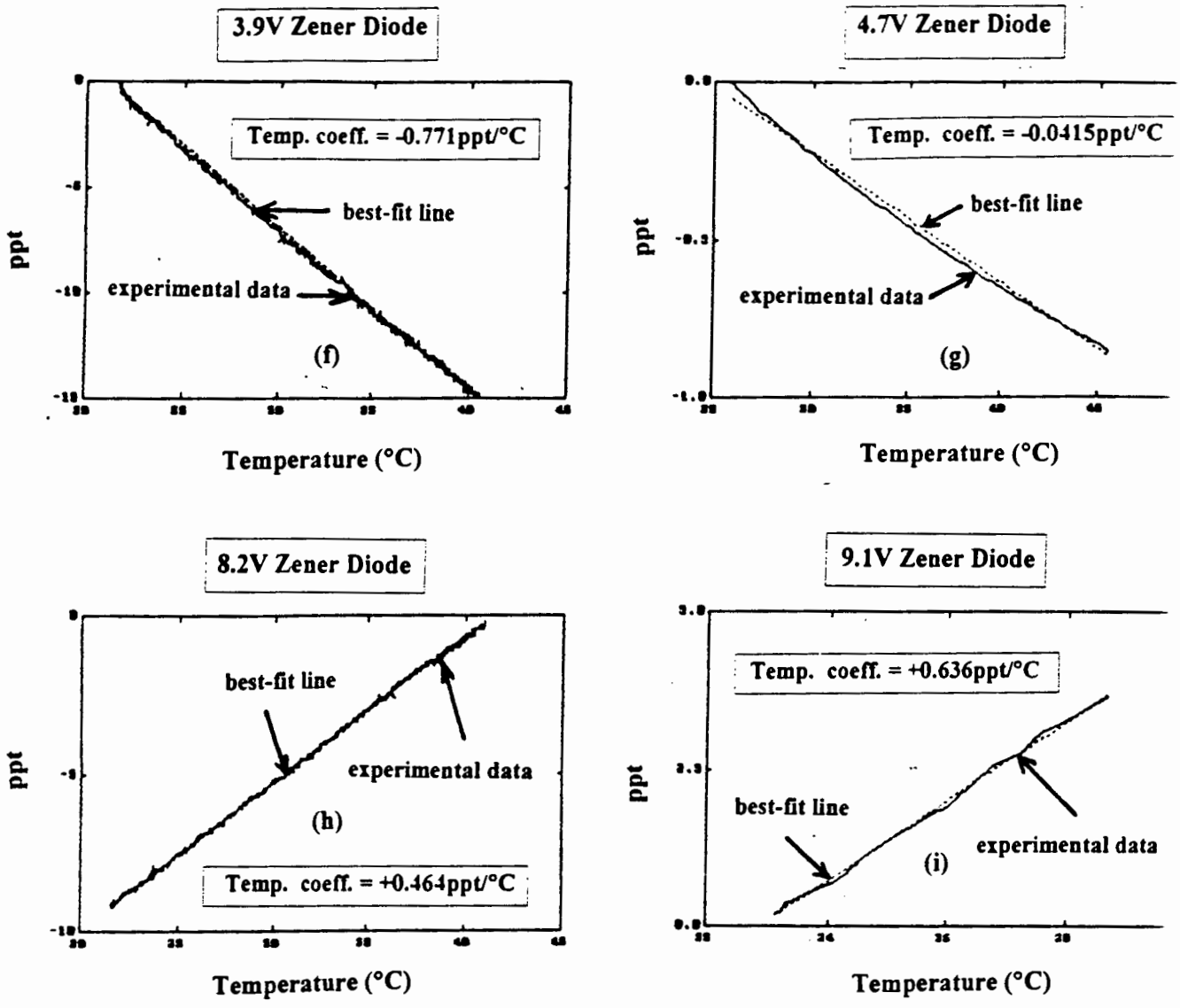

Figures 5.5f-i : Plots of the linearly-regressed theoretical straight lines, superimposed onto the experimental data. The dotted lines represent the theoretical lines, and the solid lines the experimental data for each zener diode. There appears to be a "voltage crossover" between the negative temperature coefficients (for the lower voltage zener diodes) and the positive temperature coefficients (for the higher voltage zener diodes), and this "optimum" zener voltage appears to be in-between 4.7V and 6.8V. If one had the choice of regulation voltage, and temperature coefficient was important, then it would be best to choose a zener voltage in that region. The plot for the 3.9V and 8.2V zener diodes show changes in their output voltages of approximately 15ppt and 9ppt respectively, over the 20°C temperature range shown. The slight curve in the temperature characteristic of the 4.7V zener diode is clearly seen by comparing it to the regressed straight line, and it exhibited an output voltage change of 0.9ppt over the 20°C range shown. The 9.1V diode, however, displayed an output change of approximately 4ppt over the 6°C temperature range shown.

Detrend graphs, illustrating the difference between the experimental data and the regressed values, were drawn (Figures 5.5j-m below) for the 3.9V, 4.7V, 8.2V and 9.1V zener diodes. These graphs are good indicators of the variation in parts per thousand of the diodes to that of the theoretical straight lines. The difference values are relatively small : about 1ppt, 0.075ppt, 0.3ppt, and 0.2ppt for the 3.9V, 4.7V, 8.2V, and 9.1V zener diodes respectively.

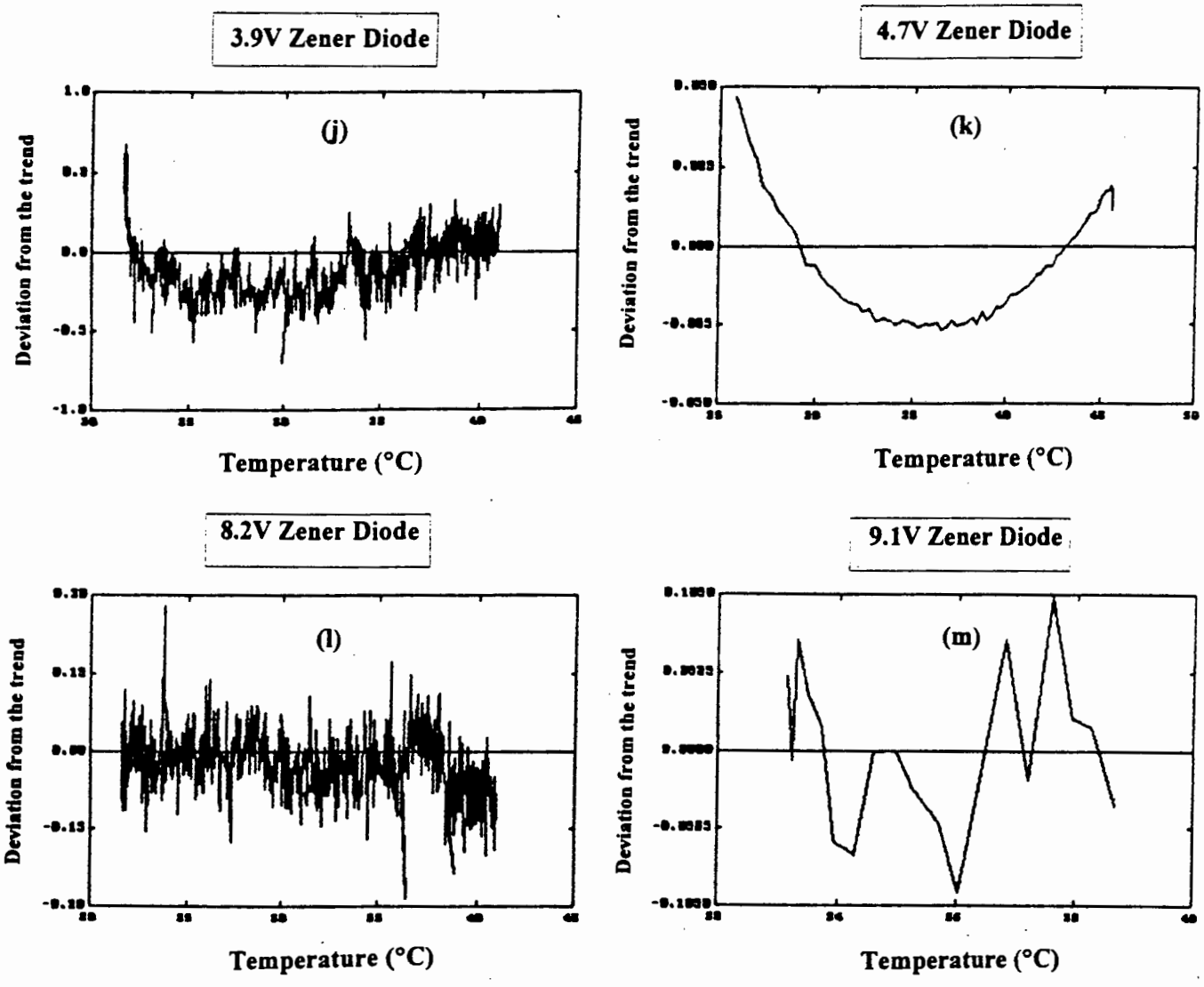

Figures 5.5j-m : Detrend graphs, clearly showing the difference values between the experimental data and the theoretical regressed values. These graphs gives good indications of how the experimental results are scattered about the general trend. These difference values are all small, viz., in the case of the 3.9V diode : 1ppt for the 15ppt change in output, in the 4.7V diode's case : 0.075ppt for the 0.9ppt change in output, in the 8.2v diode's case : 0.3ppt for the 9ppt change in output, and in the case of the 9.1V diode : 0.2ppt for the 4ppt change in output.

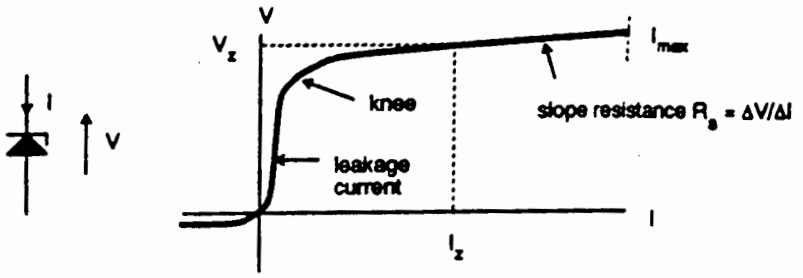

Figure 5.5n : Zener reverse breakdown voltage-current characteristic.

Figure 5.5n above shows the zener reverse breakdown voltage-current characteristic. Zener diodes are supplied for a quoted voltage, which is always defined at a given reverse current I_z. At this current, it will be within the specified tolerance, but at other currents it will differ, the difference being a function of the zener slope resistance R_s. The actual range of working voltage can be calculated by adding $(I - I_z) \times R_s$ to the quoted voltage range, where I is the working current and I_z is the current at which the zener voltage is quoted. Over some range of I_z, which one can determine from published curves, R_s can be assumed to be fairly linear. As the current decreases, the characteristic approaches the "knee" of the curve and R_s increases sharply. There is very little point in operating the zener diode intentionally on the "knee".

Below the "knee", when the reverse voltage is not sufficient to begin the breakdown, there is still some current flow. This is due to leakage in the same way, and with the same temperature dependence , as a conventional diode. Leakage is usually specified for a zener diode at some voltage below the breakdown voltage, of the order of 20-30% less. According to R. Smith in "Circuits, Devices and Systems", there are in fact two mechanisms for reverse breakdown in silicon. Electron tunnelling is the dominant mechanism at low voltages and very thin junction barriers, while avalanche breakdown is dominant for higher voltages and thicker barriers. Depending on the required voltage, one mechanism or the other will predominate, and the crossover is at 5V. The practical significance is that the two mechanisms have opposite temperature coefficients, evidenced in the experimental results. They are also the reason for the dramatic variations in slope resistance, as shown in the temperature coefficient and slope resistance variability for the

Philips BZX79 range of zener diodes (Figures 5.5o and p below). Because these characteristics depend on the basic physics of the zener effect, other manufacturers' ranges will show similar performance. This, in fact, can be substantiated by comparing the calculated experimental temperature coefficients with that illustrated in the graphs below.

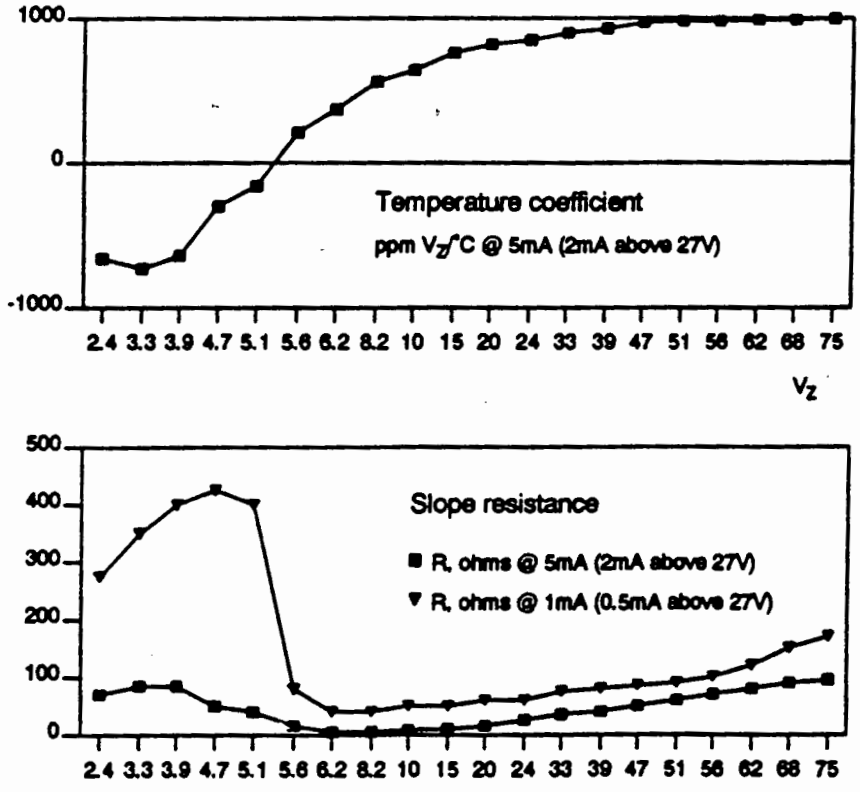

Figure 5.5o-p : Zener slope resistances and temperature coefficients versus zener voltage for the Philips BZX79 series of zener diodes. (*Source : Philips Components published data)* Notice how closely the temperature coefficients determined during experimentation relates to those in these graphs. Also, the opposite temperature coefficients (positive and negative) are evident in these graphs, with the "crossover" between 5V and 6V.

Zeners are not normally characterised for noise output and noise is not usually a problem in voltage regulator applications, since it is many orders of magnitude below the dc zener voltage and can be virtually removed by the addition of a parallel decoupling capacitor. If the capacitor is omitted, then noise can be significant for precision references. A device with a breakdown voltage of about 5.6 - 5.9V has a temperature coefficient of roughly +2mV/°C, which balances the temperature coefficient of a conventional forward-biased silicon junction. By putting the two in series, a virtually-zero-temperature-coefficient zener can be created, with an effective breakdown voltage of between 6.2V and 6.4V.

These are available off-the-shelf as "precision reference diodes", with a closely adjusted temperature coefficient and tolerance for use as voltage references.

To summarise, a full range of zener diodes were studied, from the 3.9V (with a -771ppm/°C temperature coefficient) to one of the 9.1V zener diodes, with a very high positive temperature coefficient. The 6.8V zener diode, as is well known, was virtually independent of temperature (+0.86ppm/°C temperature coefficient) and, in addition, had only 2ppm of noise. A crossover voltage between the negative temperature coefficient of the 4.7V zener and the positive temperature coefficient of the 6.8V zener diode was confirmed experimentally. Also, the temperature coefficients that were determined by experimentation compares favourably with the values quoted for the BZX79 series of zener diodes in the Philips Component published data.

6. VOLTAGE REGULATORS

For most non-critical applications, the best choice for a voltage regulator is the simple 3-terminal type. It has only three connections, i.e., input, output and ground, and is factory-trimmed too provide a fixed output. Typical of this type is the 78xx and 79xx series, for positive and negative voltages respectively. These are available with several output voltages making them useful in a wide range of applications. The voltages available allow these regulators to be used in logic systems, instrumentation, hi-fi, and other solid-state electronic equipment. The voltage is specified by the last two digits of the part number and those investigated were the 5V regulators of both polarities, and the +12V regulator. The currents chosen were about half the maximum recommended values. The regulators, being on aluminium heatsink, were taken to be the temperature of the sink. Current limiting was included to limit the peak output current to a safe value.

6.1 EXPERIMENTAL DETAILS

Figure 6.1a shows how the components were arranged so as to facilitate the experiment.

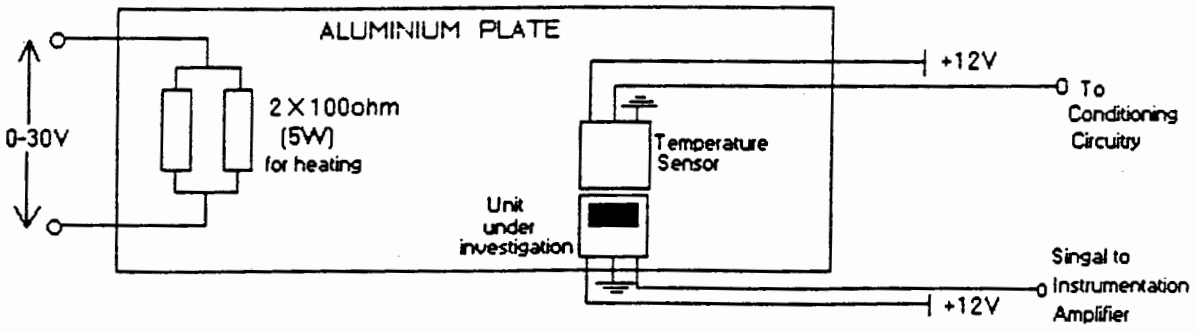

Figure 6.1a : This layout was used for temperature cycling. The heater was remotely placed so as to minimise temperature gradients, whilst the LM35 temperature sensor and the voltage regulator were located in close proximity. The LM35's output was fed to the input of the temperature sensing circuit. The regulator's voltage was fed to an instrumentation amplifier. Suitable loads, not shown here, were selected.

The circuit used to condition the "temperature signal" is shown in Figure 6.1b. The output of the first op-amp gave a useful indication of the volts/degree change, hence, the second op-amp's output was adjusted to the range required for the computer.

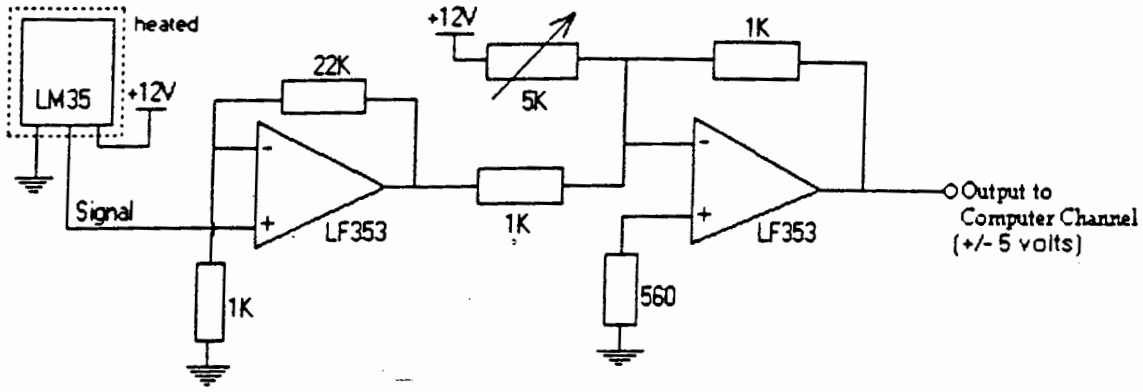

Figure 6.1b : The temperature sensing circuitry used to convert temperature changes in degrees, to signal changes in volts. Typically, a sensitivity of 0.1 volts per degree was used. Its output was fed to one of the computer channels.

The circuit used (in this case, the LM7805 +5V regulator) is shown in Figure 6.1c.

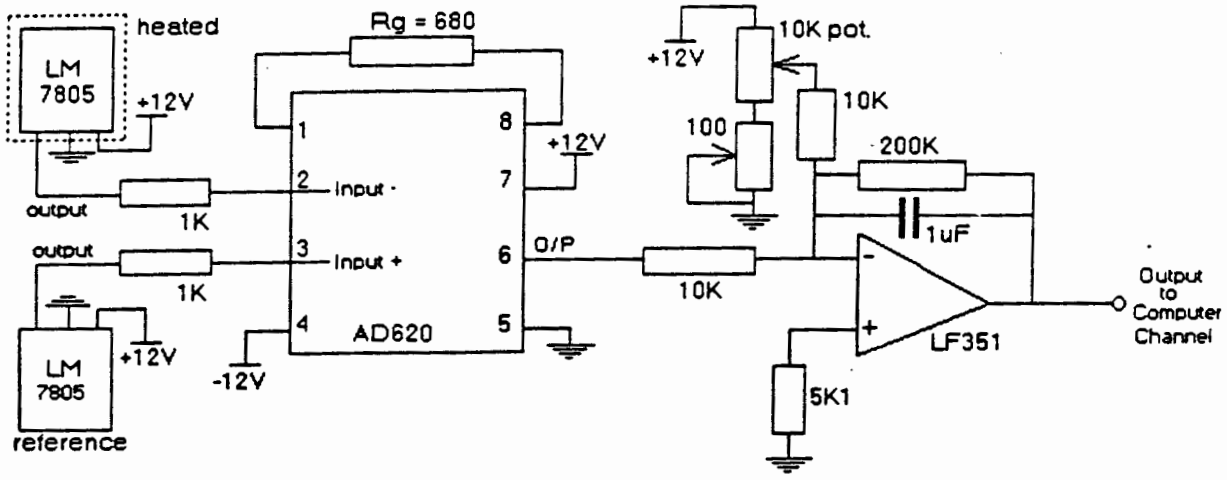

Figure 6.1c : The circuit used to determine the temperature characteristics of the regulators. One of the regulators acted as a reference, whilst the other was heated up. The overall differential gain was about 1480. The two potentiometers were necessary for course and fine adjustment during set-up.

The instrumentation amplifier amplified the difference in inputs, and was set up with a gain of 74. The gain of the amplifier was determined using the formula : Gain = 1 + (49.4KΩ/Rg) and was set by the one resistor, Rg. The gain of the filter circuitry, following the instrumentation amplifier, was set to 20, thus giving a total gain of 74 * 20 = 1480.

6.2 EXPERIMENTAL RESULTS

The precise calibration was obtained in situ by putting a current through a low-value resistor in the earth lead of the regulator. This was done on the reference device, as shown in Figure 6.2a.

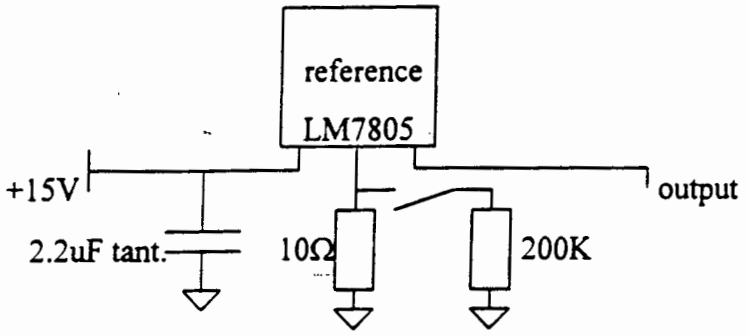

Figure 6.2a : A 200KΩ resistor (twenty thousand times larger than the resistor in the earth leg of the regulator) was placed in parallel across the 10Ω resistor. This changed the value of the resistor – and hence the voltage by 0.05%. The 1.06V change in output voltage gave the calibration as 0.0212 volts per ppm.

The computer was configured to take 120 readings at 1 second intervals. Initially 20 readings were taken without the 200KΩ resistor connected in parallel to the 10Ω resistor, then 20 more readings with the 200KΩ connected. This process was repeated a few times until 120 readings were taken in total. From Figure 6.2b an output voltage of 1.06V was obtained from a voltage change of 50ppm in the earth lead of the regulator.

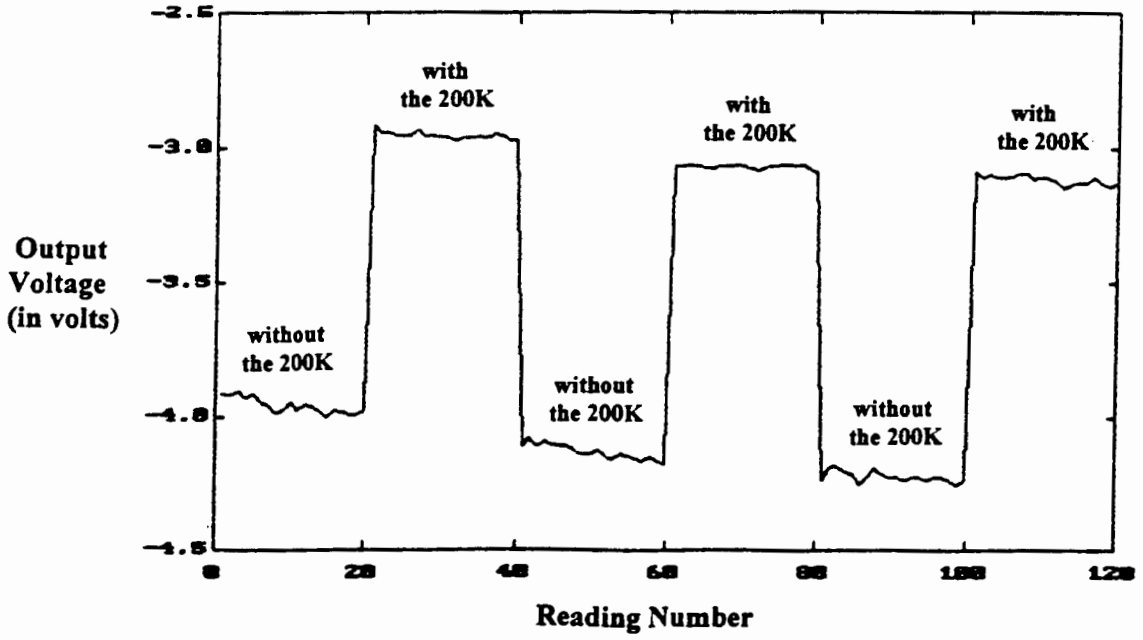

Figure 6.2b : Plot of output voltage change as the resistance in the earth leg of the regulator was increased and decreased during calibration. A very slow drift in voltage with time is evident.

Temperature cycling gives a good insight into thermal hysteresis, which is due to reversal of heat flow on heating and cooling. The body of the reference regulator was placed in good thermal contact with the aluminium surface. However, the actual integrated circuit, which is situated in the centre of the "regulator's package", was not in direct contact with the aluminium surface. This resulted in a slight temperature difference between the centre of the device and its casing. Figure 6.2c shows how the device was heated up to a temperature of 45°C, and then allowed to cool down. The figure also demonstrates that the heating and cooling curves differ by just over one degree at the point where the curves are at its widest separation.

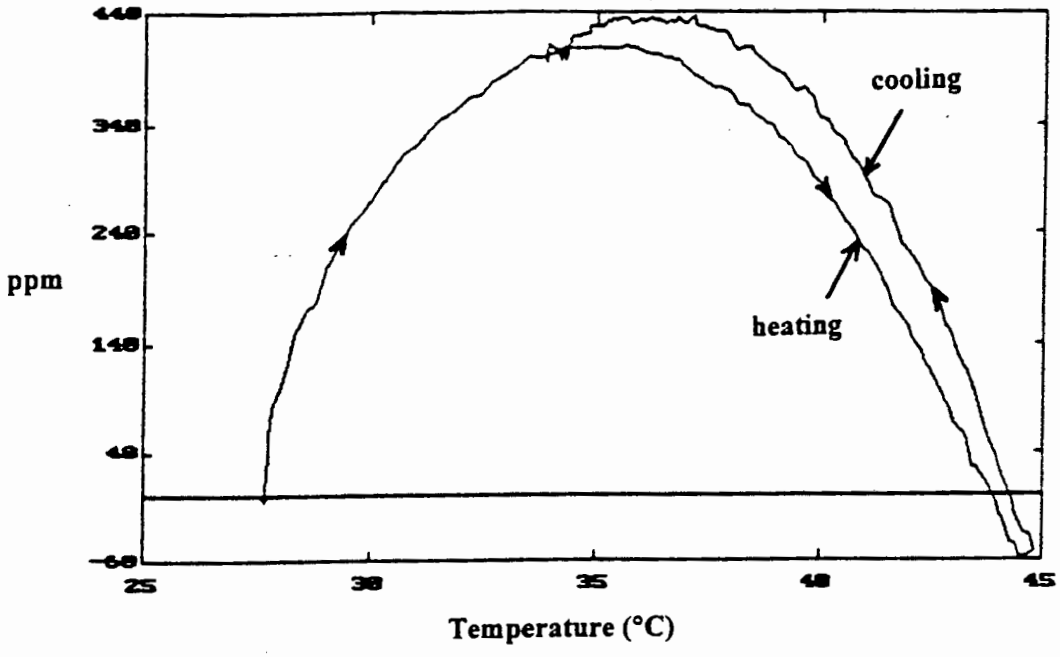

Figure 6.2c : Plot of the temperature characteristic of the LM7805 (+5V) regulator. The device was heated up, and then allowed to cool down. The graph shows hysteresis of just over one degree at the point on the curve where the heating and cooling are at its widest separation.

It was found that the LM7805 (+5V regulator), when heated, exhibited a parabolic output response with the axis at approximately 36°C. The plot shown in Figure 6.2d below is over a 20°C span, and the output approximates a perfect parabola very closely.

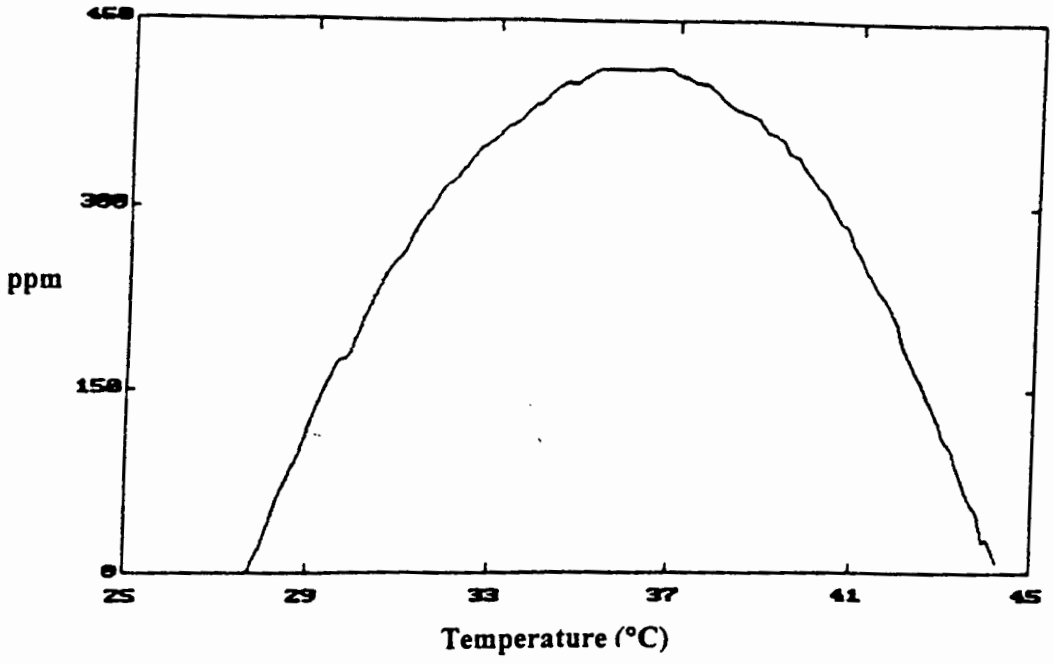

Figure 6.2d : Plot of the temperature characteristic of the LM7805 (+5V) regulator, as it is heated up. The plot approximates a perfect parabola very closely, and has a maximum in the region of 36°C.

The maximum of the temperature characteristic, shown in Figure 6.2d above, is shown in Figure 6.2e. The curve has been expanded in this region for this regulator, and only require 35ppm to cover the 4 volts near the peak. The readings taken are indicated by the "crosses" on the figure. The peak of the curve is reasonably adjacent to temperatures encountered in practice. Inherent noise has been superimposed on the parabolic curve, and shows the low noise level of the LM7805.

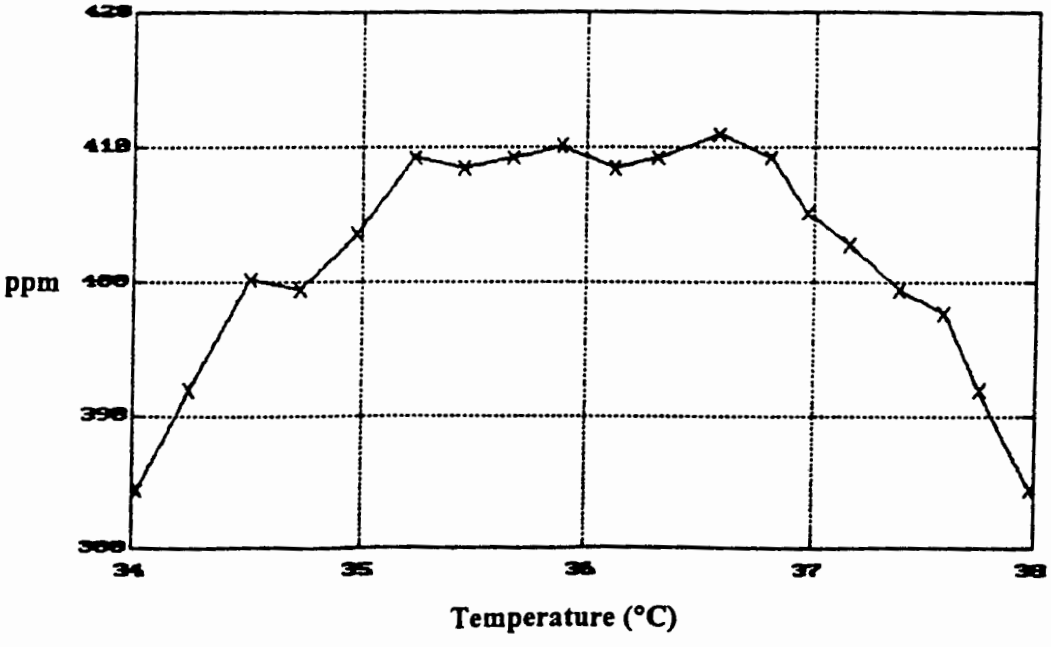

Figure 6.2e : An expanded view of the upper portion of the parabolic plot. The four degrees shown cover the maximum output for the LM7805 regulator, and is only 35ppm. Inherent noise has been superimposed on the parabolic curve.

A polynomial regression was done on the data of the parabolic response of the regulator. This was carried out to see how well the experimental data compared to a perfect parabola. In Figure 6.2f, the solid line represents the experimental data, whilst the dotted line represents the regressed curve. The equation obtained from the regression results is : ppm = $-5.99262\theta^2 + 431.795\theta - 7366.87$. This gives the axis of the parabola as 36°C, and is also evident from the graph. From this equation, the regressed (theoretical) values were calculated.

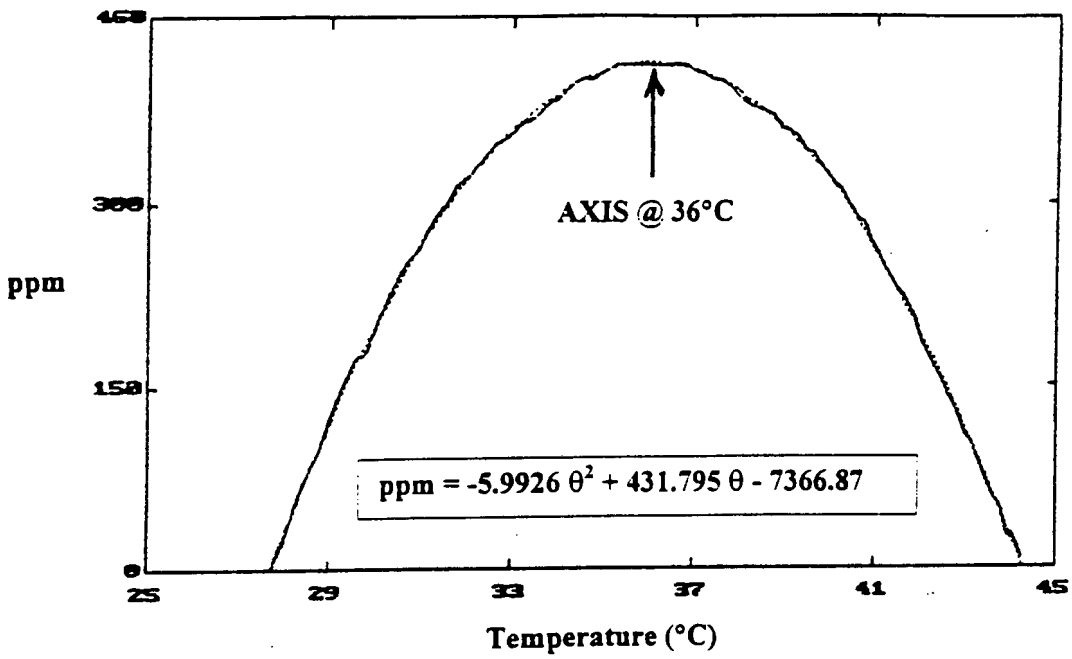

Figure 6.2f : The actual experimental values overlaid by the regressed polynomial. From this we can visually see how well the data correlates to the theoretical curve.

The regressed values were compared to the actual experimental readings, and their differences calculated. Thus, a significant relationship was established between the two variables by correlation. In effect, this tells us how the data points are scattered about the general trend. Figure 6.2g illustrates this concept in a Detrend Graph. Notice that the differences between the data points and the general trend are quite small, even though it appears to be large as a result of the expanded scale. As can be seen from the figure, a maximum deviation of approximately 15ppm is seen over the 18°C temperature range. Also, the graph in the figure clearly shows that the most deviation occurred around the extremities of the temperature range, whilst around the maximum part of the curve the deviation was in the region of 3ppm.

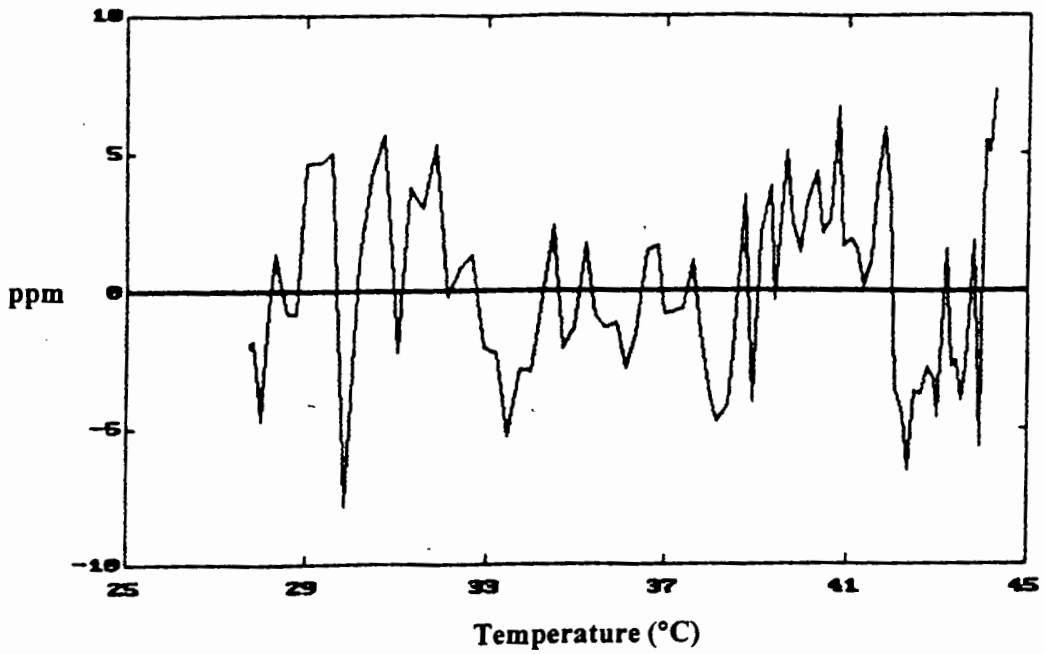

Figure 6.2g : Detrend graph, clearly showing how the experimental results are quite closely scattered about the general trend. The difference values, which are plotted here, is a representation of experimental readings - regressed values. These values are very small (15ppm max.), even though it appears to be large as a result of the expanded scale.

6.3 THE LM7905 (-5V) REGULATOR

It was decided to investigate the LM7905 (-5V) regulator. The same parabolic feature was expected. The circuitry and devices used for temperature cycling and sensing, described in Section 6.1, was used again. However, the conditioning circuitry was changed to accommodate the LM7905. This now included low-pass filters on each input to the instrumentation amplifier, as well as a voltage follower circuit to act as an offset-adjust for the final stage op-amp, which adjusted the output required for the computer. A 33Ω resistor was placed in the earth leg of both the regulators. The gain resistor of the instrumentation amplifier was 680Ω. Using the formula : Gain = 1 + (49.4KΩ / Rg), this resulted in a gain of 74. The gain of the second op-amp was set to 20, thus giving a total gain of 74 * 20 = 1480.

Dynamic calibration was performed using the LM7905 (-5V) regulator, and this was done using a similar technique that was employed for the +5V regulator. A 33Ω resistor was placed in the earth leg of the regulator. A 330KΩ resistor, also connected to the earth input of the regulator, had one of its legs switched between +15V and -15V. This had the effect of changing the voltage by [30 X (0.033/330)] = 3mV. The process was repeated a few times while the output was monitored and recorded. The dynamic calibration technique was conducted on the reference regulator. Figure 6.3a shows the procedure :

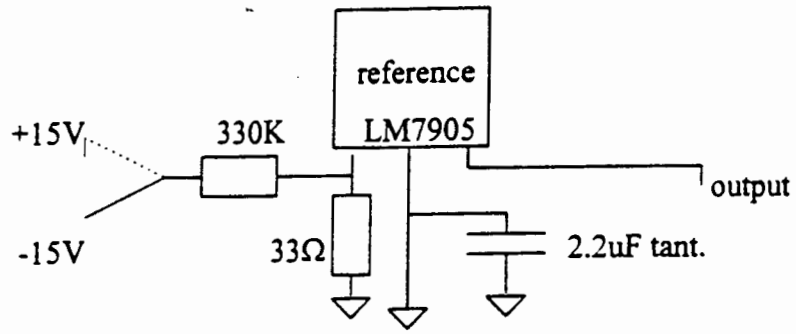

Figure 6.3a : A 330KΩ resistor is placed in the earth leg of the -5V regulator. This changed the value of the resistance -- and hence, caused an output voltage change of 2.4V. The free end of the 330KΩ resistor was switched between +15V and -15V.

The resulting calibration plot is shown in Figure 6.3b below :

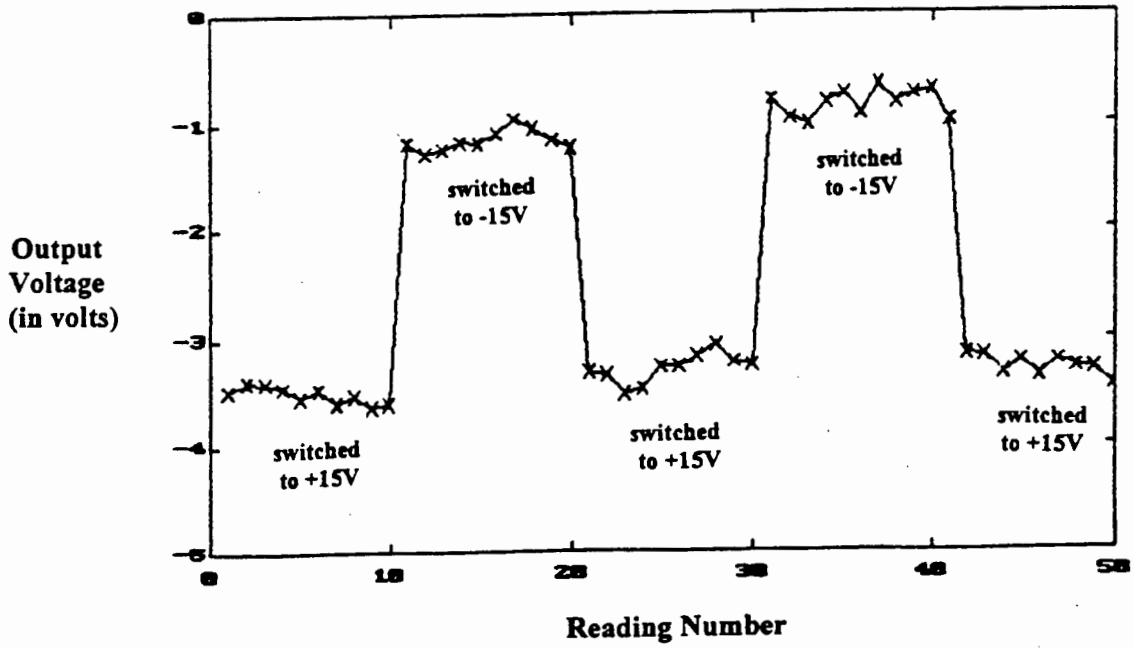

Figure 6.3b : Calibration plot of output voltage change for the 3mV steps. The average change in output voltage was 2.4V. The sensitivity is now 0.8 parts per thousand (800ppm). The noise present in these readings is at once evident.

The calibration factor was determined in the following manner :

The average change in voltage, during calibration, was ΔVout = 2.4V.

Since the entire voltage swing was 30V, $\Delta i = \frac{30V}{330K\Omega} = 0.091mA.$

Therefore, Δv in the 33Ω resistor : $\Delta v = ir = 0.091mA \times 33\Omega = 0.003mV.$

Thus, ΔVout = 2.4V if ΔVin = 3mV, or $\Delta V = 0.8V$ if ΔVin = 1mV.

Restated, ΔVout = 0.8V per mV ..... which can be rewritten as : $\frac{\Delta Vout}{\Delta v} = 0.8$

Hence, in 5V : $\frac{\Delta Vout}{\Delta v/5} = 0.8 \Rightarrow \frac{\Delta Vout}{\Delta v} = 0.8 \times 5 = 4V/ppt$

Finally, $\frac{\Delta Vout}{\Delta v} = 4V/ppt = 4mV/ppm$ (calibration factor).

In effect, this means that 1V = 250ppm, 2V = 500ppm, etc.

In order to gain insight into thermal hysteresis regarding the LM7905, the circuitry was subjected to temperature cycling. Figure 6.3c shows a plot of ppm versus temperature for the LM7905 during a hysteresis test. From the plot it is evident that there is a definite thermal hysteresis as regards the LM7905, which at its widest point of separation for the plot on the way up and down appears to be approximately 220ppm.

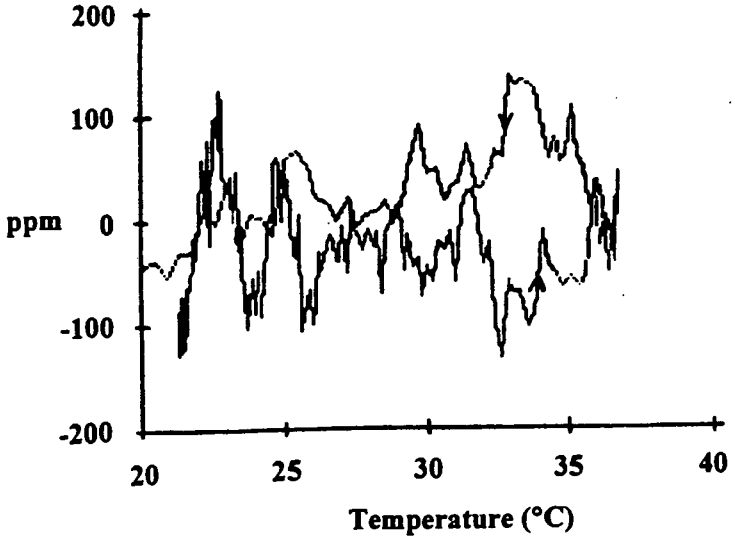

Figure 6.3c : Temperature cycling is shown in the plot above. The LM7905 was heated up to a temperature of approximately 37°C, and then allowed to cool down. Thermal hysteresis is quite evident in the plot going up in temperature compared to the plot coming down. At its widest point of separation, the hysteresis is approximately 220ppm. This is almost lost in the "noise" which was about ±100ppm.

It was decided to investigate the noise levels associated with the LM7905 (-5V) regulator. The circuitry used was not changed, however, the temperature was kept constant at room temperature and the circuit output was monitored. Readings were taken at 15 second intervals, for a maximum of 100 readings. The resulting output is shown in Figure 6.3d :

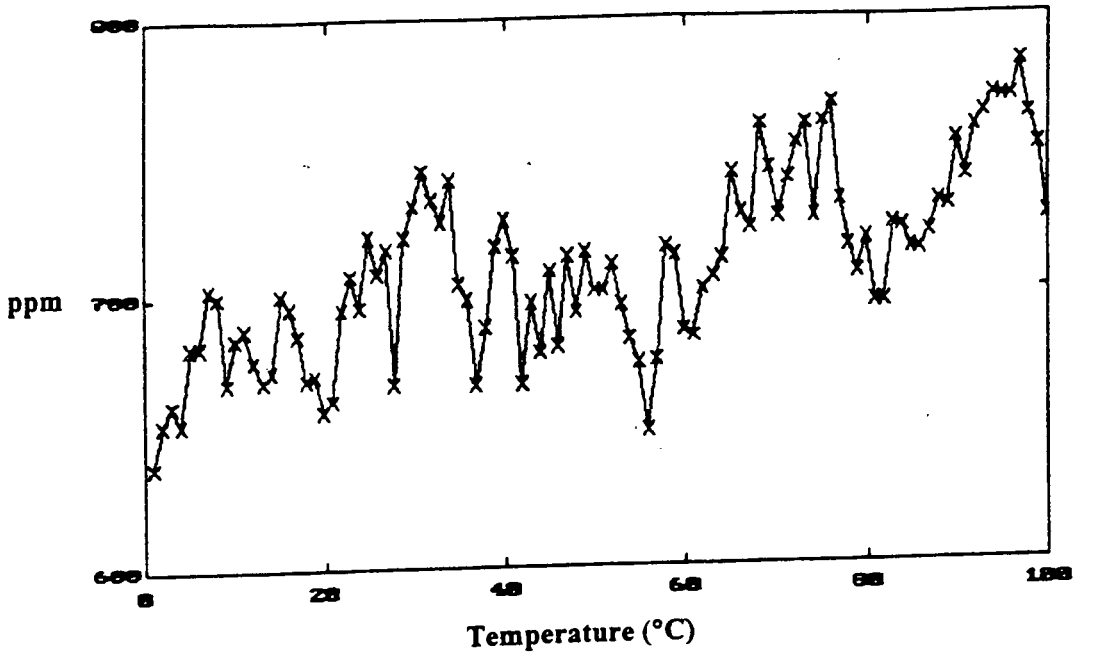

Figure 6.3d : Graph showing the noise levels associated with the output of the LM7905 when kept at constant room temperature. Readings were taken at 15 second intervals, and the response indicates noise of 100ppm.

The LM7905 also exhibited a parabolic response when heated to approximately 33°C.

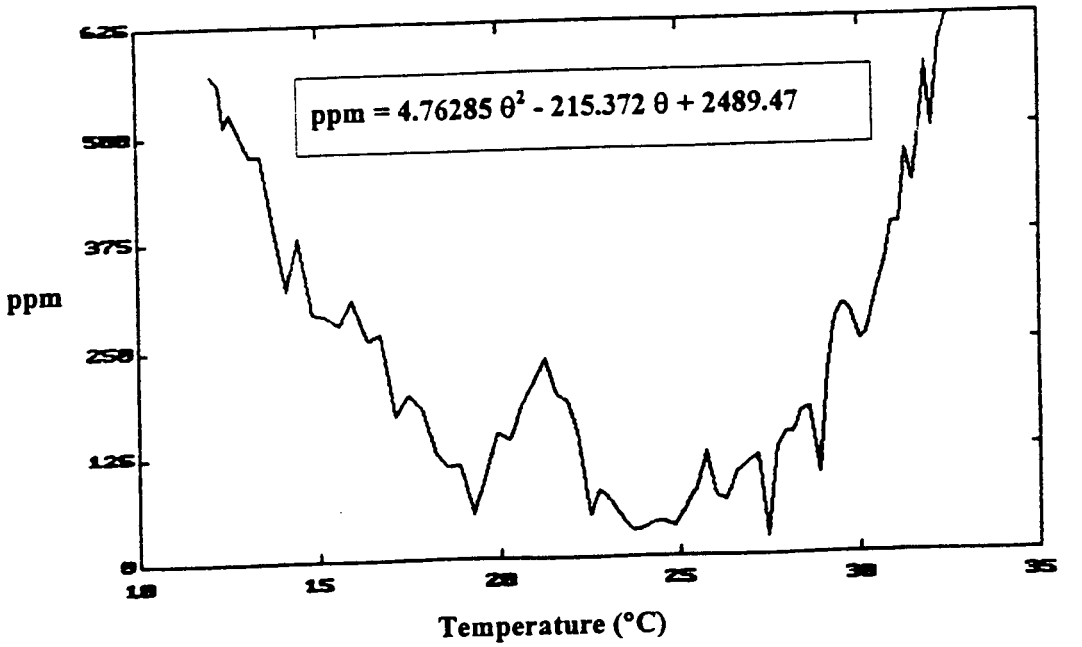

Figure 6.3e : Plot of the temperature characteristic of the LM7905 (-5V) regulator, as it is heated up. The parabola characteristic is still evident, and has a minimum value of 22.6°C. The plot, shown over a 22°C span, is not a smooth curve as a result of noise.

The plot shown in Figure 6.3e above is over a 22°C span. As expected, the slope of the parabola has the opposite sense to that of the positive regulator. Also evident from the plot is the fact that the response of the negative regulator is much more noisy than that of the positive regulator.

A polynomial regression was done on the data used in Figure 6.3e in order to ascertain how well the parabolic response of the regulator compared to a theoretical parabola. In Figure 6.3f below, the solid line represents the experimental data whilst the dotted line represents the regressed curve. The equation : $ppm = 4.762850^2 - 215.372\theta + 2489.47$ was obtained from the regression results, and the theoretical values were calculated from this. The minimum value of the quadratic was found, from the equation, to be 22.6°C, and this is evident in the graph. The minimum value of the curve is approximately adjacent to room temperature, and therefore is commonly encountered in industry. Also evident from Figure 6.3f is the fact that the response of the negative 5V regulator does not match the theoretical curve as closely as that of the positive 5V regulator.

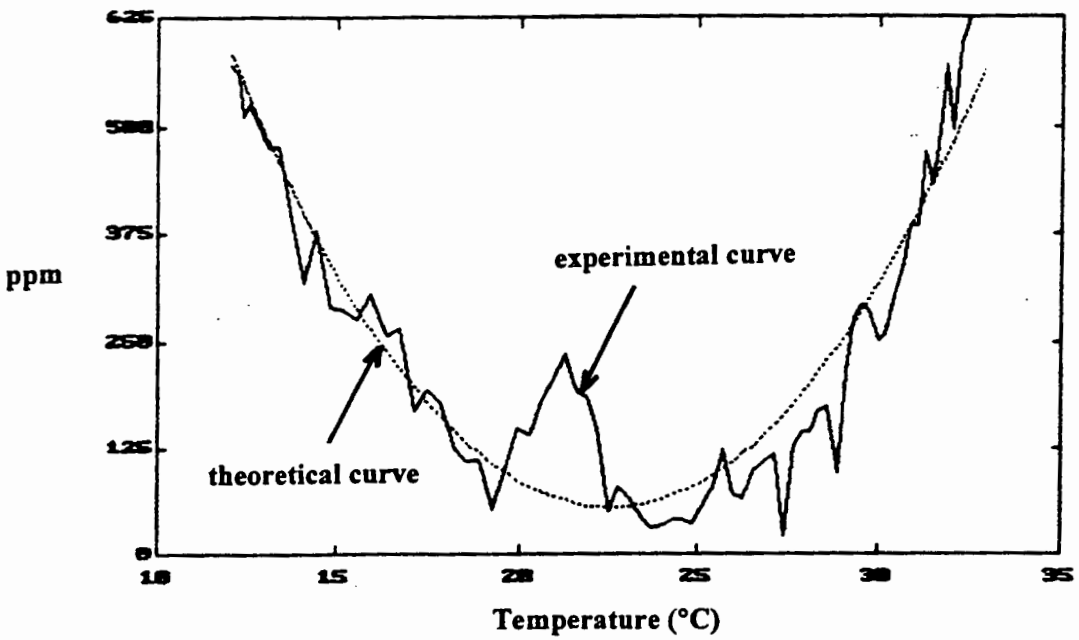

Figure 6.3f : A graphical comparison of the experimental data and the theoretical parabola. The response of the -5V regulator does not fit the regressed curve as closely as does the response of the +5V regulator. The deviation from the regressed curve appears to be greatest in the area around the minimum (axis) of the parabola, whilst not as pronounced at the extreme ends of the plot.

The output response of the negative regulator trends very closely to the theoretical curve around the extreme ends of the plot. This is very different around the area close to the axis of the parabola, where the difference appears to be at its largest. The LM7805 (+5V) regulator had exactly the opposite characteristic, i.e., the output response approximated the theoretical parabola quite closely in the vicinity of its axis, and less closely at the extreme ends of the plot (see Figure 6.2g). The experiment involving the LM7905 was repeated many times to validate the accuracy of the measurements. Also, the experiment was conducted using many different LM7905 regulators, as well as other laboratory equipment by another user. Each time similar results were obtained, confirming that the -5V regulators are inherently much noisier than their positive counterparts.

The difference between the regressed values and the experimental data was calculated and graphed. This is shown in Figure 6.3g, and serves as a good indicator of the correlation between the two variables. The differences appears to be enormous as a result of the expanded scale. A maximum deviation of approximately 310ppm is evident from the graph, over the 22°C temperature range shown.

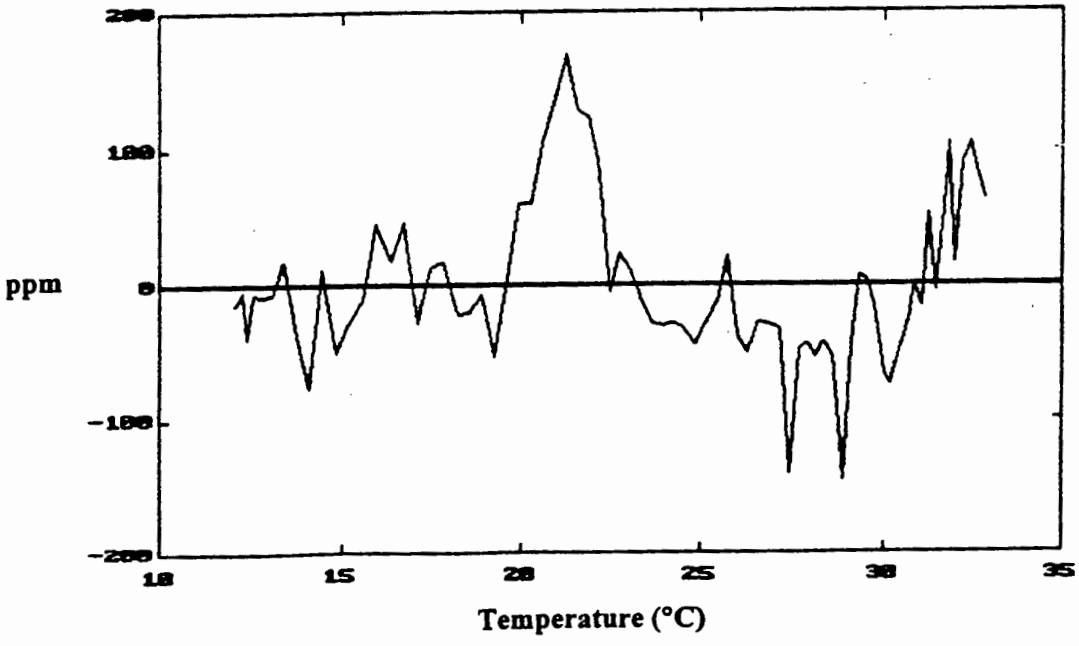

Figure 6.3g : Detrend graph showing how the experimental results are scattered about the general trend. The difference values, which are plotted here, is a representation of experimental readings - regressed values. These values are large in comparison to that of the positive regulator, and range from approximately -140ppm to +170ppm.

6.4 THE 12V REGULATOR

In order to verify whether other commonly used regulators also exhibited the parabolic temperature characteristic, it was decided to investigate the +12V regulator.

Once again, precise calibration was achieved by conducting measurements whilst putting a current through a low-value resistor in the earth lead of the regulator. This was done on the reference device, and the same technique was used as before (illustrated in Figure 6.4a) :

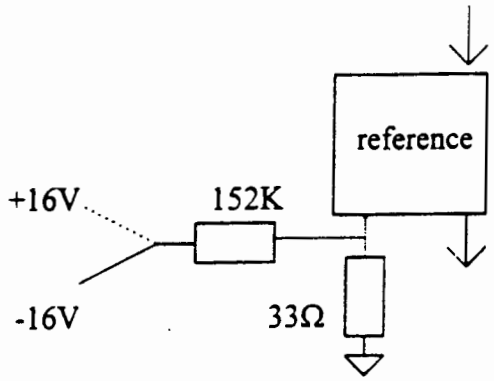

Figure 6.4a : A 152KΩ resistor is placed in the earth leg of the regulator, together with a 33Ω. The free end of the 152KΩ resistor was switched between +16V and -16V. This caused a change of [(32 X 33)/152] = 6.9mV, which ultimately resulted in a change of output voltage of 1.89V.

The resulting calibration plot is shown in Figure 6.4b below :

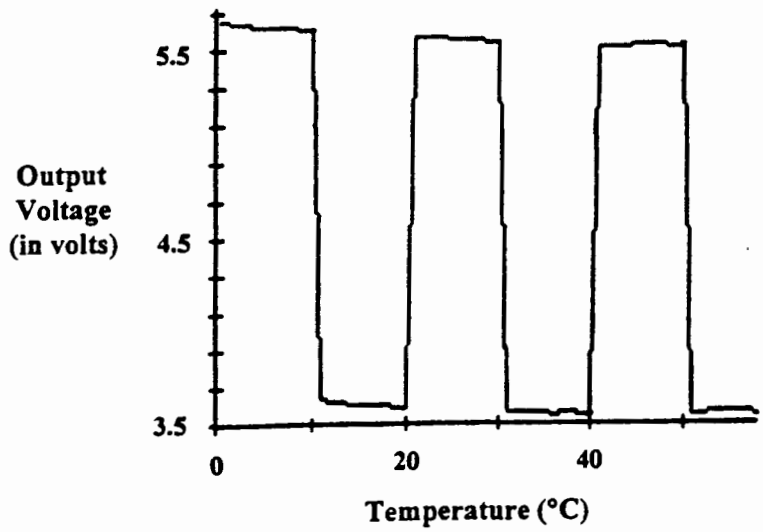

Figure 6.4b : Calibration plot of output voltage change as one end of the 152KΩ resistor was switched between +16V and -16V. The average change in output voltage was 1.89V, for the 6.9mV change in the earth leg of the regulator.

The calibration factor was determined in the following way :

The total change in voltage was $\Delta V = 32V$ (16V either way).

The average change in voltage, during calibration, was $\Delta V_A = 1.89V$.

Therefore, $\Delta v = \frac{32 \times 33}{152}$mV = 6.9mV. Hence, $\frac{\Delta V_A}{\Delta v} = \frac{1.89V}{6.9mV} = 0.274$V/mV.

And, 1mV in 12V is $\frac{\delta v}{V} = \frac{10^{-3}}{12} = 83$ppm.

Therefore, $\Delta V_A = 0.274$V/mV = 83ppm..... hence, 1ppm = $\frac{274}{83}$mV = 3.3mV.

The calibration factor was therefore 3.3mV/ppm.

The +12V regulator was heated up to approximately 40°C in order to establish whether it too had a parabolic temperature characteristic. Due to the output polarity of the circuit used, the parabola plot shown is inverted in Figures 6.4c and d. This regulator has a high, almost linear, increase with temperature. The quadratic term is present, but is small. By extrapolating back in temperature, the axis of the parabola arising from the quadratic term must be at a very low temperature. To show the noise, a line (the linear regression line) was taken as a reference. Figure 6.4c shows the data relative to the line and it has a "bow" arising from the curvature.

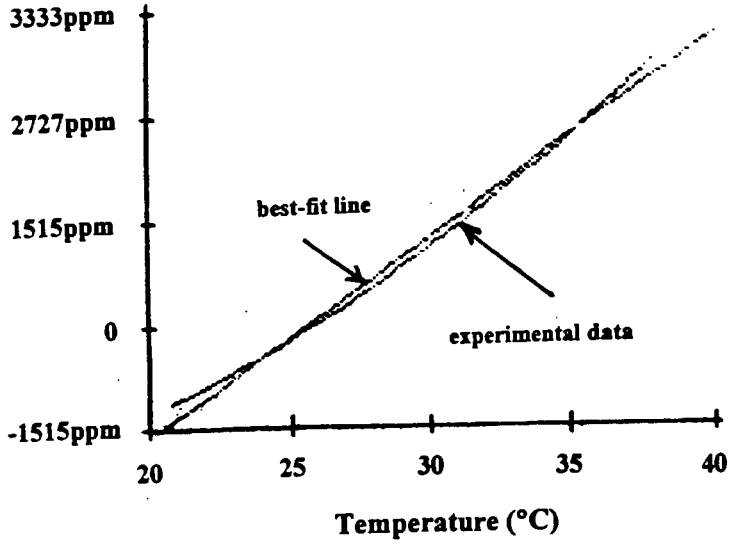

Figure 6.4c : Plot of the temperature characteristic of the +12V regulator, as it is heated up. The curved plot is shown relative to a linear regressed line, and it has a "bow" arising from the curvature. The quadratic term is present but is small. By extrapolating backward, the axis was found to be 11°C.

The departure from linearity is shown in Figure 6.4d. The parabolic feature is an artefact of the quadratic term. It was in fact possible, from the data, to extrapolate backward and find the axis of the true parabola, where $\frac{d(ppm)}{d\theta} = 0$. The axis was calculated to be 11°C.

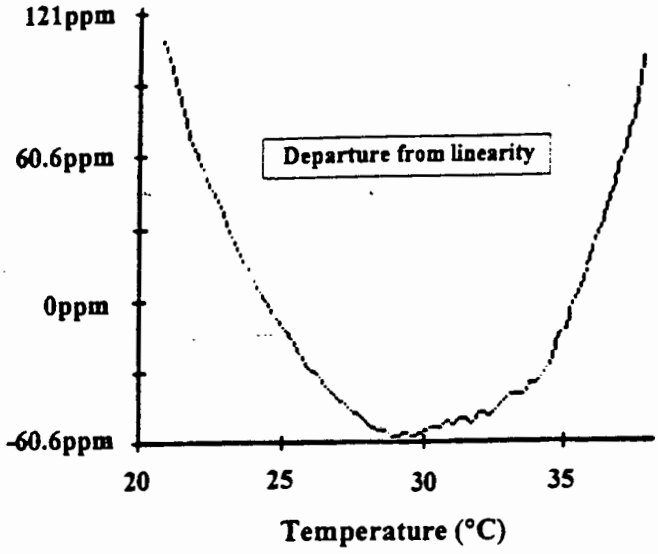

Figure 6.4d : The parabolic characteristic is evident from this plot, which represents the departure from linearity for the +12V regulator.

With the aid of numerical methods and the equation of the curve, a polynomial regression was done on the extrapolated plot of the regulator. The difference was calculated between the experimental values and the regressed values, and as a result a detrend graph was plotted for the +12V regulator. This graph shows how well the output response of the regulator correlates to the theoretical variables, and is shown in Figure 6.4e.

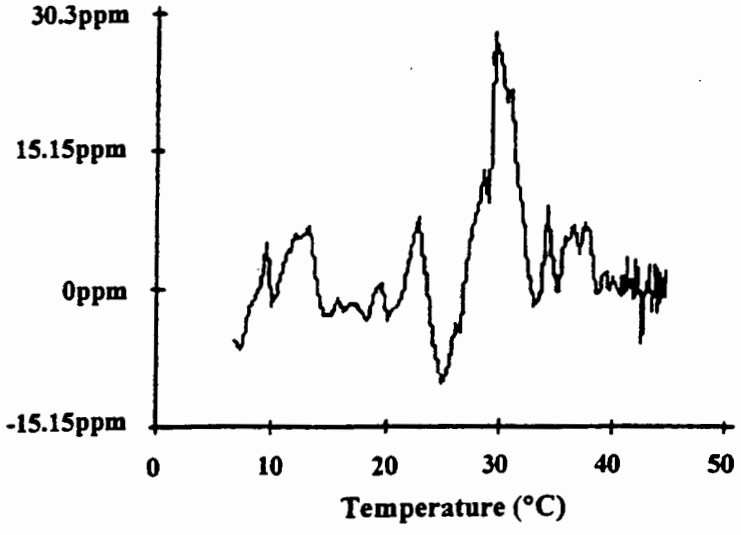

Figure 6.4e : Detrend graph showing how the experimental results are scattered about the general trend. The difference values, which are plotted here, is a representation of experimental readings - regressed values.

6.5 THE GENERAL TEMPERATURE CHARACTERISTICS

It was decided to provide some practical, output response values, which could be expected by a user when making use of "off-the-shelf" voltage regulators. These "typical" values, for each of the types studied, represent the expected regulator output responses at given temperatures, and can be taken into account when designing circuitry employing these devices.

- The +5V regulator :

Table 6.5I, for a +5V regulator, shows the actual deviation about +5 volts near the axis of its output response. The temperatures of the axes of regulators, can be expected to be near 36°C. The table can be used (with some circumspection) to obtain a very good +5V voltage reference.

θ (temperature)	mV above arbitrary +5V
θ = 29°C	+5.47
θ = 33°C	+1.10
θ = 36°C	+0.1
θ = 37°C	+0.19
θ = 41°C	+2.80

Table 6.5I : Table showing the actual deviation from +5V, for a LM7805 (+5V) voltage regulator, near the axis of its output response. The values are provided at ceratin given temperatures, and can be used as guidelines for any user of these devices.

- The -5V and +12V regulators :

Tables 6.5II and III below shows some of the -5V- and +12V regulators output results, in voltage, at given temperatures. These have been provided, and can be used, to be of assistance in the same manner as the results given for the +5V regulators, in Table 6.5I.

Table 6.5II : -5V Voltage Regulator

θ (temperature)	mV below arbitrary -5V
θ = 13°C	-2.5
θ = 16.3°C	-1.25
θ = 22.6°C	-0.27
θ = 29.3°C	-1.25
θ = 32.5°C	-2.5

Table 6.5III : +12V Voltage Regulator

θ (temperature)	mV above arbitrary +12V
θ = 27.7°C	+4.39
θ = 32.2°C	+20.33
θ = 36.1°C	+32.74
θ = 39.5°C	+40

Tables 6.5II and III : Tables showing the actual deviation from -5V and +12V, for a LM7905 (-5V) and LM7812 (+12V) voltage regulators respectively, near the axes of their output responses. The values are provided at ceratin temperatures, and can be used as guidelines for any user of these devices. The axes for LM7905 regulators can be expected to be near 22.6°C, and 11°C for the LM7812 voltage regulators.

6.6 TEMPERATURE COMPENSATION

Since the LM7805 (+5V) regulator had a nearly perfect quadratic output response, it was decided to pursue the matter by attempting to build a circuit that would be able to do the necessary temperature correction as the regulator heats up. The idea was to emulate the quadratic response of the regulator exactly, but in the opposite sense, so as to nullify the variation and thus get the final resultant output to be as close to a constant as possible.

It was decided to use a multiplier, the AD633JN, to satisfy the requirements for a quadratic response. This integrated circuit had high impedance, differential X and Y inputs, and a 20V/μs slew rate. The low impedance output voltage of the device is a nominal 10V full-scale provided by a buried zener, and no external components or expensive user calibration is required when using this chip. High (10MΩ) input resistances make signal source loading negligible. Also, the internal scaling voltage is generated by a stable zener diode, and the multiplier accuracy is essentially supply insensitive. This multiplier integrated circuit is shown in Figure 6.5a below :

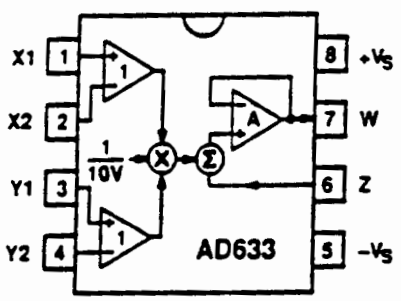

Figure 6.5a : A connection diagram for the AD633JN Multiplier Integrated Circuit. Pins 5 and 8 were connected to the supply voltages of -15V and +15V respectively. Pins 2 and 4 were connected together and also to earth, whilst pin 6 was connected directly to earth. Input pins 1 and 3 were connected together, as well to the output from the inverting circuitry preceding it. Pin 7 provided the quadratic output defined by the equation :

$$W = \frac{(X_1 - X_2)(Y_1 - Y_2)}{10V} + z.$$

This circuit would incorporate the temperature sensing circuitry, so as to be responsive to any temperature changes. A block diagram of the circuitry is shown in Figure 6.5b.

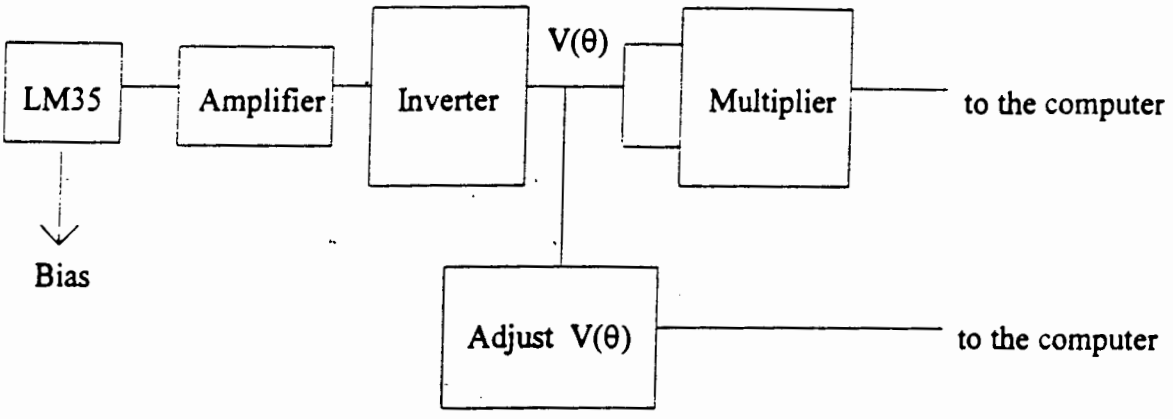

Figure 6.5b : A block diagram of the temperature-compensating circuit which was used in conjunction with the temperature-sensing circuitry, employing the LM35. This circuit was used to nullify the quadratic temperature characteristic of the LM7805 (+5V) regulator.

One of the initial problems was to determine where to set the offset, so that the multiplier would have its axis at the same temperature as that of the regulator. Since the maximum value of the parabola for the LM7805 was in the region of 36°C, it was calculated that the offset had to be -1.64V. Figure 6.5c shows the multiplier output, which also exhibits the parabolic characteristic, but in the opposite sense to that of the regulator.

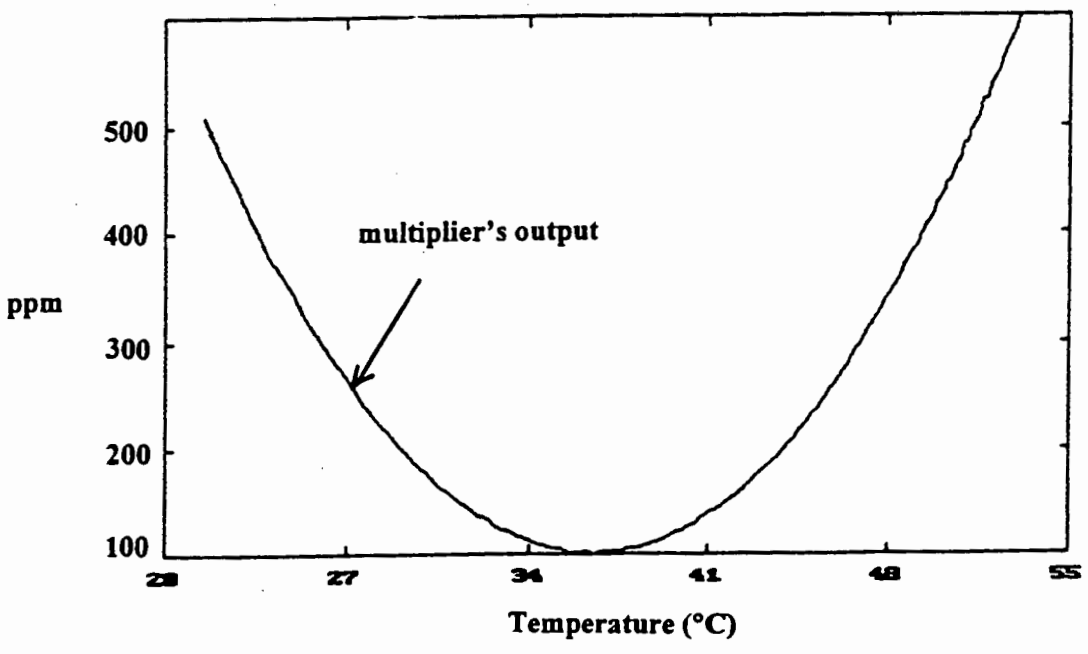

Figure 6.5c : Plot of the output of the temperature-compensating circuitry. The parabolic curve has its axis in the region of 36°C, which coincides with that of the regulator.

The completed circuit used to get the final resultant output of the +5V regulator to be as close to a constant as possible, is shown in Figure 6.5d below :

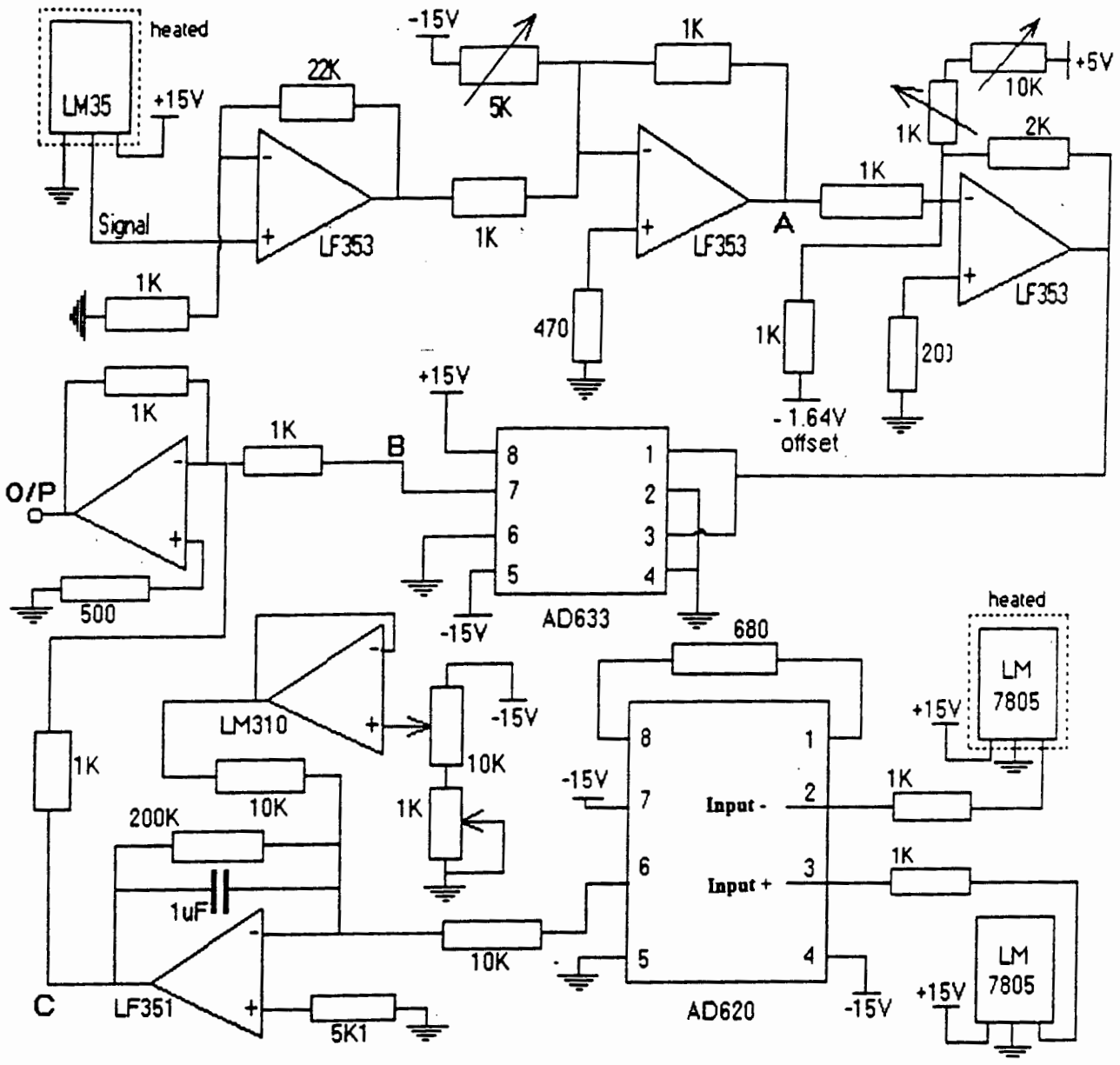

Figure 6.5d : Circuit diagram of the complete circuitry used in order to get the final resultant output of the LM7805 (+5V) regulator to be as close to a constant as possible. The following letters represent outputs of sub-circuits, i.e., A : output of the temperature sensing circuitry, B : output of the multiplier circuit, and C : output from the conditioning circuitry, employing the instrumentation amplifier. The final output of the summing circuitry is denoted by : O/P. Repeated calibration and fine tuning of all these components were necessary to achieve the desired results.

Figure 6.5e shows the output plots for both the multiplier (dotted line) and the regulator (solid line). With repeated fine tuning of the circuitry, the results shown were achieved.

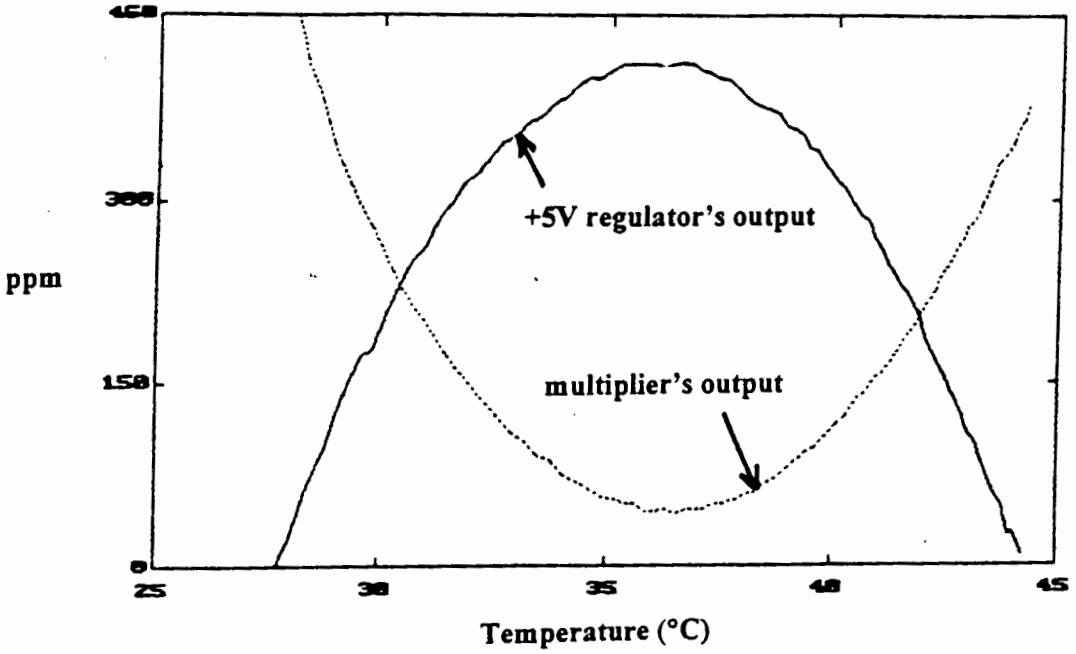

Figure 6.5e : Output plots for both the multiplier (dotted line) and the regulator (solid line). The multiplier's axis was set so as to coincide with that of the regulator at 36°C.

With lots more fine adjustments, the output plot shown in Figure 6.5f was attained. This represents the final summed output of the circuitry shown in Figure 6.5d. As can be seen, a change of only 20ppm was achieved for the regulator output, compared to approximately 400ppm without the temperature-compensating circuit over the same temperature range as before. At this point, it was decided not to pursue the matter any further.

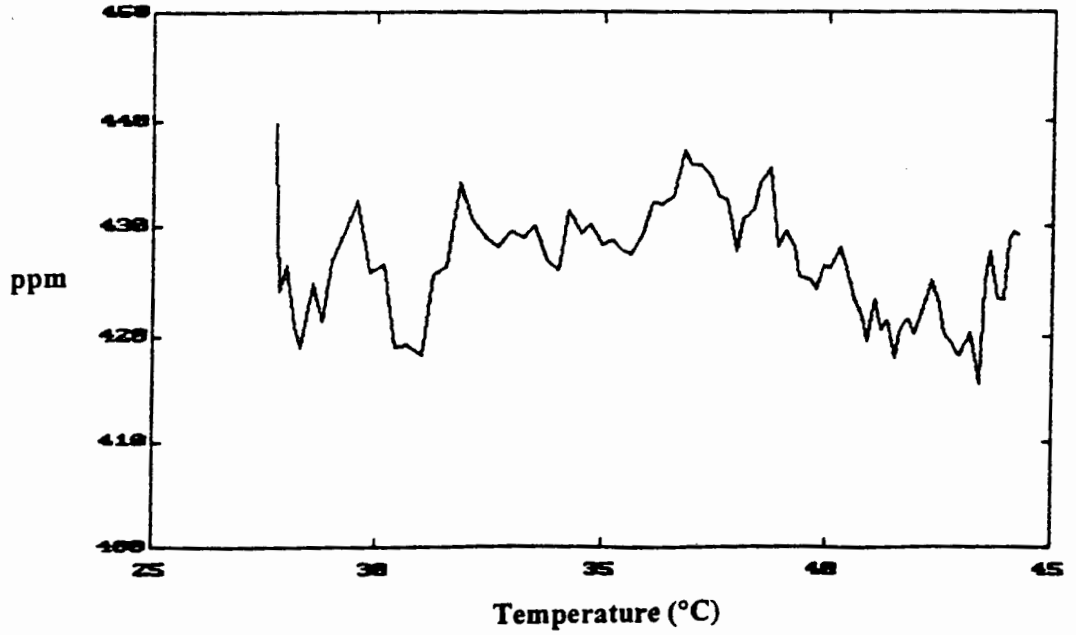

Figure 6.5f : A plot of the summed output response. Over the temperature range shown, the output only varies by 20ppm (compared to the variation of approximately 400ppm without the temperature-compensating circuit).

6.6 In Summary

The temperatures, at which the axes of minimum and maximum for each quadratic response were situated, were found to be 36°C, 22.6°C and 11°C for the +5V, -5V and +12V regulators respectively. There was a small degree of hysteresis displayed during "thermal runs", e.g., hysteresis of just over one degree Celsius for the +5V regulator. This was due to the fact that the actual integrated circuits of the regulators are situated in the centre of the device-packages, hence, there existed a slight thermal gradient between the bodies, which was in thermal contact with the heating plate, and the centres of the devices. For the -5V regulators, the hysteresis was almost lost in the inherent noise of the measurement. Practically this means that even if one thinks that one could keep the temperature constant, within an application, and have a good -5V regulator, one still has to contend with this amount of noise. Repeated experiments (repeatability) showed that negative regulators are significantly more noisy in its output response than positive ones. Perhaps when one needs a stable negatively regulated voltage, one could use a positive regulator and then invert its output.

Common to the regulators are the following :

- The peaks of the individual parabolic characteristics were reasonably adjacent to temperatures encountered in practice.
- The parabolic characteristic : $V = V_o + a\theta + b\theta^2$, encountered with all the regulators studied, is evident when the linear term vanishes to zero, and the quadratic term dominates the function. To be as good a parabola as was being obtained during the experiments, the θ^3-term has to be very small or next to nothing, since a strong third-order term would of course distort the parabola. Therefore the suggestion is that the third order is not present. The theoretical interpretation of these results is challenging.

Also, proven during experimentation, the parabolic characteristic of the +5V regulator was independent of load, i.e., with different currents drawn from it. To summarise, other regulators of the same series were also tested, but the +5V regulators had by far the most stable characteristics.

7. CONCLUSIONS

Based on the findings of this report, the following conclusions may be drawn :

(a) An accurate, versatile and inexpensive measurement-card, which plugs directly into the bus of a personal computer, was successfully designed and developed onto a 135mm × 110mm double-sided printed circuit board. The unit employs a 12-bit analogue-to-digital converter, with a measured maximum conversion rate of 13.97μs (max. conversion frequency of 71.6kHz). This compares well with the quoted conversion rate of 13.8μs (72.46kHz), given in the data sheets by National Semiconductor. Established experimentally, was the fact that the converter exhibited no hysteresis or deadspace over its specified input range. The LSB step of the converter was accurate, and the steps in the output were unambiguous. To achieve an accuracy of one least significant bit (approximately 0.02%), the final accuracy of the unit, the issue of computer power supply noise first needed to be addressed. It was found that all computers have excessive noise on its power rails. With the aid of a spectrum analyser, the main noise sources and their frequencies were identified : the switching action of the computer's switched-mode power supply (20kHz), the computer clock (8MHz), and mains power supply interference (50Hz). A resistor-inductor-capacitor (RLC) network was developed to filter out the unwanted frequencies that corrupted the computer supply lines, and proved successful in 'cleaning up' the supply rails. This filter can be used, with advantage, in any I/O device which makes use of a computer's bus. A four channel analogue multiplexer was added to the circuitry of the 12-bit ADC unit, to enable four independent data lines to be accommodated. Trials at once established that zero signals on each channel's input converted to zero output voltage. Maximum signal (for 12-bit conversion) on one the channels resulted in a clean 12-bit output, revealing 4096 levels in equal steps of one least significant bit, and the crosstalk to the other three channels was zero.

Software was developed, using Pascal and TurboVision, to facilitate the real-time interface between the "analogue world" and the computer. Various features were added to the software, to make it user-friendly, e.g., pull-down menus, colour, use of a mouse, etc. As a practical test, two channels of the interface card were connected to a measuring unit consisting of a pressure sensor (MPX100AP) and temperature sensor (LM35). Skilful software techniques enabled the card to function as a 'weather station' for both short periods (minutes, hours) and long periods (days, weeks). Typical results were obtained and these proved to be highly satisfactory.

The practical 12-bit Measurement PC-Interface Card has thus reached the excellent performance of many boards presently employed in laboratories and industry. In fact, because of the extreme care that was taken in designing and building the board, the card attained an accuracy of 0.02%, which is remarkably better than most A/D cards available on the market at present. The card was employed successfully during the investigative experiments, and is presently being used for data acquisition by the Process Computing Department at Koeberg Nuclear Power Station in Melkbosstrand (Cape).

(b) The operational amplifier (op-amp) is the basic building block for analogue circuits, and performs functions such as buffering, isolation, gain, level translation, current-to-voltage conversion, and voltage-to-current conversion. The op-amp is a high-gain amplifier, designed for use in feedback circuits to perform stable, predictable operations, which are inherently determined by the external components and configuration. The negative feedback of op-amp circuits results in the output resistance being negligibly low. The voltage follower, with 100% feedback, was chosen as being the most challengingly low value available, and was therefore investigated. The experiment was conducted at the limit of measurement, and the final output resistance of the LF351 operational amplifier was found to be 3.83mΩ. The influence of the gain resistors, and power supplies on the response of an op-amp was also investigated. By lowering the power supply voltages from ±12V to ±8V, and with the op-amp configured as a unity-gain inverting amplifier, the error/deviation from unity increased from 0.345 parts per thousand to 1.255 parts per thousand. This 3.5 times increase in error, substantiates the fact that power supply fluctuations do influence the operation of operational amplifiers. However,

experimentation established that, in general, as long as the input signal voltage is not more than 70% of the supply voltage, the error is a minimum.

(c) The change in the performance of components, as a function of temperature, supply voltage, and other parameters was measured :

• The resistance stability of a resistor is dependent on power dissipation, ambient temperature and resistance value. Two of the resistor types were studied, and experimentation results showed that carbon resistors with 2-5% tolerances has negative temperature coefficients. This coefficient was found to be : -383.67ppm/°C ± 0.22ppm/°C. This means that their resistance values decrease with increasing temperature. The carbon film resistor is the most common resistor, and the cheapest, used in commercial applications. It also has the least impressive performance and therefore is not suited to precision work, but is more than adequate for the majority of commercial uses such as television, radio, etc. The 1% tolerance metal-film resistors exhibited a positive temperature coefficient, i.e., their resistances increases with increasing temperature, and it was established experimentally as : +52.26ppm/°C ± 0.107ppm/°C. The metal-film resistors exhibited a change in output of 1200ppm over a 25°C temperature range, whilst the carbon film resistors displayed a 5500ppm change in output over the same temperature range. The metal-film resistors are more expensive than carbon film, but gives superior characteristics, particularly long term stability, temperature coefficient, noise, and power handling capability.

• As with resistors, the actual capacitance that a component can exhibit is only mildly related to its marked value. The actual capacitance will vary with initial tolerance, temperature, applied voltage, frequency and time. The Wima polyester capacitors studied, showed a non-linear and comparatively high temperature coefficient, viz., +342.47ppm/°C ± 10ppm/°C. The value of capacitance C, is also directly proportional to surface area A, and inversely proportional to the thickness of the dielectric layer W, i.e., $C = \varepsilon_i \varepsilon_o A/W$. As a result of the Wima capacitor's bulky size, there was a tremendous temperature gradient

(up to 13°C), during experimentation, between the bottom section of the capacitor (which was bonded to the plate), and the top of the capacitor. This, together with its relatively high temperature coefficient, resulted in an increase in the reactance with temperature, thus increasing the capacitance. These capacitors exhibited a change in output, over a 18°C temperature range, of approximately 6300 ppm. This led to the belief that there might be a case for heat-sinking or recessing the capacitors when used in circuits which require precise measurement. The Wima polyester capacitors are therefore less useful for critical circuits where a stable, low-loss component is needed, however, it can be used for applications such as decoupling, coupling and bypass.

- Piezo-ceramic capacitors were also investigated, and these were represented by a pair of thin-film barium titanate piezoelectric transducers, with capacitances of 23nF each. When heated, these components exhibited no thermal hysteresis. This was due to the fact that the piezoelectric discs were extremely thin, and thus the heat was evenly spread across the component. It was established that these components had positive temperature coefficients, i.e., +212.9ppm/°C. An investigation into the Curie temperature, i.e., the temperature where the crystal axis loses its polarity and the ceramic is no longer piezoelectric, was done, and the component was heated to 140°C. The capacitance increased exponentially with temperature, according to the equation : $ppt = 0.3943\ e^{0.0421\,(\theta)}$. This exponential curve was extrapolated until it approached a coefficient of infinity around 200°C, theoretically, the Curie temperature. The component exhibited a change in output of approximately 1000ppt, over the 200°C temperature range.

- The thermal properties of two pairs of soft ferrite manganese-zinc cores were investigated. The one pair was the large, low-frequency pot core type, used in power transformers and with an inductance of 38.1mH, whilst the other pair was of the smaller, high-frequency E-core type, used in telecommunications circuits and with an inductance of 468μH. The main factor affecting the accuracy of the results was the phenomenon of thermal lag. As the specimen was heated up, the rate of temperature increase was so high that the core surface temperature matched that of the heating plate, but the temperature throughout the rest of its

body lagged behind. This meant that accurate change in inductance versus temperature could not be obtained. One successful method of minimising the error due to thermal hysteresis was by reducing the rate at which the specimen was heated up, however, coupled to the slow temperature change was the increased level of noise. In the case of the pot core, the temperature coefficient was found to be +117.4ppm/°C, and +103.7ppm/°C for the E-core. In an attempt to determine the Curie temperature of these cores, they were heated up to 100°C, and it was noted that the inductance of both core types increased in a quadratic manner. Polynomial regressions determined the equations for,

the pot core as : $ppt = -0.0019\,(\theta)^2 + 0.2828\,(\theta) - 5.7189$,

and for the E-core as : $ppt = -0.0017\,(\theta)^2 + 0.2596\,(\theta) - 4.7889$.

This parabolic characteristic was very similar for each of the cores, as both reached a maximum of approximately 5ppt around 75°C, and returned to zero at about 130°C. The similarity in performance was to be expected because, although the ferrites were not the same size, they were both manganese-zinc ferrites. It is interesting to note that the barium titanate piezoelectric transducers has temperature coefficients which are double that of the cores, viz., +212.9ppm/°C.

• Unlike other components, the temperature coefficient of a zener diode's breakdown voltage is quite subtle. It was therefore decided to investigate the temperature coefficients of the commonly-used zener diodes. The various diodes were heated up, and the relative changes in their outputs, as a result of this temperature change, was monitored and logged. Linear regressions were done on all the experimental data, and the following temperature coefficients were calculated :

=> 3.9V zener diode : temperature coefficient = -0.771ppt/°C ± 0.0014ppt/°C,

=> 4.7V zener diode : temperature coefficient = -0.0415ppt/°C ± 0.0003ppt/°C,

=> 6.8V zener diode : temperature coefficient = +0.86ppm/°C ± 0.05ppm/°C,

=> 8.2V zener diode : temperature coefficient = +0.464ppt/°C ± 0.001ppt/°C

=> 9.1V zener diode : temperature coefficient = +0.636ppt/°C ± 0.007ppt/°C.

The 6.8V zener diode thus has the smallest temperature coefficient, and showed the smallest change in output, i.e., approximately 6ppm over a 20°C temperature range. The 6.8V zener diode therefore represents the best choice in diodes for practical use (out of the batch studied), where temperature dependence is important. There appears to be a "crossover" between temperature coefficients from positive to negative between 4.7V and 6.8V. In fact, there are two mechanisms responsible for reverse breakdown in silicon, i.e., electron tunnelling is the dominant mechanism at low voltages and very thin junction barriers, while avalanche breakdown is dominant for higher voltages and thicker barriers. Depending on the required voltage, one mechanism will predominate, and the "crossover" is at 5V. The practical significance is that the two mechanisms have opposite temperature coefficients, as seen in the experimental results. Because these characteristics depend on the basic physics of the zener effect, other manufacturers' ranges will show similar performance.

(d) Voltage regulators, of the 78xx and 79xx series and normally used in logic systems, instrumentation, hi-fi, etc., were studied. All the regulators investigated, showed a parabolic output response with increased temperature. The temperatures, at which the axis of minimum and maximum for each quadratic response were situated, were found to be 36°C, 22.6°C and 11°C for the +5V, -5V and +12V regulators respectively. The peaks of the individual characteristics were reasonably adjacent to temperatures encountered in practice. The parabolic characteristic : $V = V_o + a\theta + b\theta^2$, is evident when the linear term vanishes to zero, and the quadratic term dominates the function. To be as good a parabola as was being obtained during the experiments, the θ^3-term had to be very small or next to nothing, since a strong third-order term would of course distort the parabola. There was a small degree of thermal hysteresis displayed, by all the regulators, during "temperature runs", e.g., hysteresis of just over one degree Celsius for the +5V regulator. For the -5V regulators, the hysteresis was almost lost in the inherent noise of the measurement. Practically this means that if one thinks that one could keep the temperature constant, within an application, and have a good -5V regulator, one still has to contend with this amount of noise. Repeated experiments showed that negative regulators are significantly more noisy than positive ones. Perhaps

when one needs a stable negatively regulated voltage, one could use a positive regulator and then invert its output. Since the +5V regulator had a nearly perfect quadratic output response, it was decided to pursue the matter further. A temperature compensating circuit was built to do the necessary temperature correction as the regulator heated up, i.e., this circuitry emulated the quadratic response of the regulator exactly, but in the opposite sense, so as to nullify the variation and thus get the final resultant output to be as close to a constant as possible. An output change of only 20ppm was achieved for the regulated output, compared to 400ppm without the temperature compensating circuitry over the same temperature range as before.

The experiments and measurements described, were all accomplished by making use of a PC-based data acquisition system. The adherence to universal testing procedures, the accurate data acquisition system, careful and skilful circuit design, all contributed to the high resolution techniques required to measure component and device performance.

"I often say that when you can measure what you are speaking about and can express it in numbers, you know something about it; but when you cannot measure it, when you cannot express it in numbers, your knowledge is of a meagre and unsatisfactory kind; it may be the beginning of knowledge, but you have scarcely in your thoughts advanced to the stage of science whatever the matter may be"

Lord Kelvin

APPENDICES

APPENDIX A :

1. Software Code
2. Software Graphics

APPENDIX B :

Photographs

APPENDIX C :

Circuit Diagrams

APPENDIX A

1. SOFTWARE CODE

This is the Pascal and TurboVision code, necessary for the proper operation of the 12-bit PC-interface card. The software has been provided as an executable "package" for the user, thus eliminating the need to run the software on a Pascal platform. However, the necessary modular code which is linked to make the software executable are separate Pascal files, and has been provided here. It includes :

- Kurt. Pas
- Initvars. Inc
- Menu. Pas
- About. Pas
- Output. Pas
- Test. Pas

KURT. PAS

```
Unit Kurt; {Measurement_module;}

Interface

USES   crt,dos,totfast,totmisc,totio1,totinput;

VAR    adc_decoder,loop,decoder,n,x,y,z,data_ready,temp      : integer;
       NoReadings                                  : Integer;
       i,j,period_countA,period_countB,mask_var,freq_decoder : integer;
       sum,total_count,frequency,period_count,temp1        : real;
       datacount,sign_bit,kDelay                   : integer;
       A_to_Dcount_total,volts                     : real;
       counter,EOC,A_to_DcountA,A_to_DcountB,decod          : integer;
       channel_1,channel_2,channel_3,channel_4             : real;
       f1                                          : text;
       filename                                    : string;
       done,ToScreen1,TestCycle                    : boolean;
       chr                                         : char;
       ch                                          : char;
       Reading1                                    : array[1..1000] of real ;
       Reading2                                    : array[1..1000] of real ;
       Reading3                                    : array[1..1000] of real ;
       Reading4                                    : array[1..1000] of real ;


Procedure
DoKurt(Channel1,Channel2,Channel3,Channel4:boolean;VarLength,KDelay:LongInt;iobase:integ
er;
            ToScreen1:boolean);
Procedure TestCycle1;
IMPLEMENTATION

PROCEDURE initialisation(iobase:integer);
  BEGIN
    n:=iobase ;
    port[n+3]:=$92;  { Base address }
  END;

PROCEDURE select_A_to_D;
  BEGIN
    decoder:=0;
  END;

PROCEDURE select_ADC1;
  BEGIN
    adc_decoder:=0;
  END;
```

```
PROCEDURE select_ADC2;
  BEGIN
    adc_decoder:=16;
  END;

PROCEDURE select_ADC3;
  BEGIN
    adc_decoder:=32;
  END;

PROCEDURE select_ADC4;
  BEGIN
    adc_decoder:=48;
  END;

PROCEDURE adc_calibration;
  BEGIN
    port[n+2]:=15+decoder+adc_decoder;
    port[n+2]:=7+decoder+adc_decoder; { set /CAL to '0' and /CS,/WR,/RD to '1' }
    port[n+2]:=15+decoder+adc_decoder;
    delay(10);                  { allow CAL to end }
  END;

PROCEDURE get_ADC_input;
  BEGIN
    port[n+2]:=decoder;           { ADC module selected }
    decod:=decoder+adc_decoder;
    port[n+2]:=decod;             { 1 of 4 inputs selected }
    delay(10);
    port[n+2]:=15+decod;    { all 3 signals high }
    delay(0);
    port[n+2]:=10+decod;    { /CS and /WR go low }
    delay(0);
    port[n+2]:=11+decod;    { /WR goes high, conversion complete }
    delay(0);

    REPEAT
      EOC:= ((port[n+1] AND 32) SHR (5)); {check if conversion complete}
    UNTIL EOC=1;

    delay(0);
    port[n+2]:=9+decod;       { /RD goes low }
    delay(0);
    A_to_DcountA:=port[n];     { read port A }
    A_to_dcountB:=port[n+1];   { read port B }
    sum:=0;
    mask_var:=1;
    z:=0;
    sign_bit:= A_to_DcountB SHR 4;   { Check the sign bit +ve or -ve }
    sign_bit:=sign_bit and 1;
```

```
    FOR loop:= 1 to 4 do
      BEGIN
       temp:=A_to_DcountB AND mask_var;
       mask_var:=mask_var*2;
       temp:=temp SHR z;
       temp1:=temp * EXP((z+8)*LN(2));
       sum:=sum+temp1;
       z:=z+1;
      END;

    A_to_Dcount_total:=sum + A_to_DcountA;  { total counts }

    IF sign_bit = 0 THEN   { Implies that number positive }
      BEGIN
       volts:=(A_to_Dcount_total/4095)*5;
       port[n+2]:=11+decod;          { /RD goes high }
      END

    ELSE
      BEGIN
       A_to_Dcount_total:=(4095-A_to_Dcount_total)+1;
       volts:=-(A_to_Dcount_total/4096)*5;
       port[n+2]:=11+decod;          { /RD goes high }
      END;
  END;

Procedure initialise_arrays;
  BEGIN
       channel_1:=0;
  END;

PROCEDURE get_filename;
  BEGIN
   Screen.writeln('');
   Screen.write('Please  Enter filename ...  ');
   readln(filename);

   IF exist(filename)=true THEN
     BEGIN
      beep;
      Screen.write('Filename already exists, enter another(y/n)?');
      chr:=readkey;

      IF (chr = 'y') or (chr = 'Y') THEN
        BEGIN
         Screen.write('Please  Enter filename ...  ');
         readln(filename);
         clrscr;
        END
```

```
        ELSE
          BEGIN
           Screen.write('Rewriting file ');
           Screen.writeln(filename);
          END;
       END;
   END;


procedure CheckForInput;
begin
      Key.delaykey(1);
   CASE Key.LastKey of

      100 : begin  {D}
            done:=true;
            Writeln('Program stopped press any key.');
            Key.GetInput;
           end;
      68  : begin
            done:=true;
            Writeln('Program stopped press any key.');
            Key.GetInput;
           end;

      112 : BEGIN  {P}
            Writeln('Program Paused. .... Press any key to continue.');
            Key.GetInput;
           end;
      80  : begin
            Writeln('Program Paused. ....Press any key to continue.');
            Key.GetInput;
           END ;
   END;
end;


    { ═══════════ MAIN PROGRAM ═══════════ }


Procedure
DoKurt(Channel1,Channel2,Channel3,Channel4:boolean;VarLength,KDelay:LongInt;iobase:integ
er;
           ToScreen1:boolean);
var  h, m, s, hund , q : word;
   Endtime  : real ;
   a , b , c , d , checkti : longint ;
```

```
Procedure WriteOutput;
begin

    if not ToScreen1 THEN BEGIN

        if Channel1 Then Begin
         select_ADC1;
         select_A_to_D;
         get_ADC_input;
         channel_1 :=volts;
        End;

        If Channel2 Then begin
          select_ADC2;
          select_A_to_D;
          get_ADC_input;
          channel_2 :=volts;
        End;
        If Channel3 Then Begin
          select_ADC3;
          select_A_to_D;
          get_ADC_input;
          channel_3 :=volts;
        End;
        If Channel4 Then Begin
          select_ADC4;
          select_A_to_D;
          get_ADC_input;
          channel_4 :=volts;
        End;

        write(datacount:4);
        IF channel1 THEN
        write(channel_1:17:3);
        IF channel2 THEN
        write(channel_2:17:3);
        IF channel3 THEN
        write(channel_3:17:3);
        IF channel4 THEN
        write(channel_4:17:3);
        writeln;


      {write to disk}
      writeln(f1,datacount:4,channel_1:15:3,channel_2:15:3,
            channel_3:15:3,channel_4:15:3);

    END
    else begin
      j := j + 1 ;
```

```
            if Channel1 Then Begin
               select_ADC1; select_A_to_D; get_ADC_input; reading1[j] := volts ;
            end;

            if Channel2 Then Begin
               select_ADC1; select_A_to_D; get_ADC_input; reading2[j] := volts ;
            end;

            if Channel3 Then Begin
               select_ADC1; select_A_to_D; get_ADC_input; reading3[j] := volts ;
            end;

            if Channel4 Then Begin
               select_ADC1; select_A_to_D; get_ADC_input; reading4[j] := volts ;
            end;

         end;
   end;

   Procedure CheckOutputTime ;
   var  TimeCheck ,
        StartTime : real ;
   begin

        {Get End Time}
        GetTime(h,m,s,Q);
        a := h ; a :=  a * 10000000 ;
        b := m ; b :=  b *   100000 ;
        c := s ; c :=  c *     1000 ;
        d := q ; d :=  d *       10 ;
        StartTime := a + b + c + d   ;

        writeoutput ;

        GetTime(h,m,s,q);
        a := h ; a :=  a * 10000000 ;
        b := m ; b :=  b *   100000 ;
        c := s ; c :=  c *     1000 ;
        d := q ; d :=  d *       10 ;
        CHECKTI := a + b + c + d   ;

        TimeCheck :=  CHECKTI - StartTime ;
        clrscr ;
        writeln('Time per cycle', TimeCHeck ) ;
        key.readkey;

   end;
```

```
BEGIN

screen.box     (3,3,78,5 ,white,1);
screen.cleartext(4,4,77,4);

screen.ShadFillBox(3,21,78,23,Yellow,2);
screen.writeAt(24,22,Black,' [P] Pause  [D] Done  [R] Resume ');
screen.box     (3,7,78,18,white,1);

screen.setwindow(4,4,77,17);    (* set open window cords *)
screen.cursreset;
write('  No');
IF channel1 THEN
screen.write('       CHANNEL 1');
IF channel2 THEN
screen.write('       CHANNEL 2');
IF channel3 THEN
screen.write('       CHANNEL 3');
IF channel4 THEN
screen.write('       CHANNEL 4');

screen.setwindow(4,8,77,17);    (* set open window cords *)

screen.cursreset;
clrscr ;
screen.gotoxy(1,1);

 Initialisation(IObase);

 NoReadings := VarLength;

 get_filename;
 Assign(f1,filename);
 Rewrite (f1);
 initialise_arrays;

 {
 if TestCycle Then begin
   CheckOutputTime ;
   key.readkey ;
   exit;
 end;
 }

 datacount:=0;
 counter:=0;
 adc_calibration;
 Screen.writeln('');
 Screen.writeln(' Please Wait,  Sampling in process ... ');
 IF ToScreen1 then begin
   Writeln(' The option to display the output has been disabled ... ');
 end;
```

```
Screen.writeln('');
{beep;}

done     :=false;  { block of code for creating a pause facility }
counter  := 0 ;
datacount := 0 ;
j        := 0 ;

REPEAT

  datacount := datacount+1;
  counter  := counter+1;

  WriteOutput ;

  IF (datacount = NoReadings) or (Done) then
  begin
   break ;
  end ;

  {Get End Time}
  GetTime(h,m,s,Q);
  a := h ; a :=  a * 10000000 ;
  b := m ; b :=  b *  100000 ;
  c := s ; c :=  c *   1000 ;
  d := q ; d :=  d *     10 ;
  EndTime := a + b + c + d   ;
  Endtime := Endtime + kdelay ;

  {Check if we have passed the End Time of a loop}
  Repeat
    if key.keypressed then checkForInput;
    if done = true then break ;

    GetTime(h,m,s,q);
    a := h ; a :=  a * 10000000 ;
    b := m ; b :=  b *  100000 ;
    c := s ; c :=  c *   1000 ;
    d := q ; d :=  d *     10 ;
    CHECKTI := a + b + c + d ;
  Until CHECKTI >= EndTime     ;


UNTIL (Done) ;

IF (datacount = NoReadings) or (done) then begin

    if not done then begin ;
      beep;
      writeln('Entered number of readings reached.') ;
      write('Press any key to continue');
      Key.GetInput;
    end;
```

INITVARS. INC

```
procedure InitVars;
{}
begin

 with Channel do
 begin
   Init(2,2,15,7,'Select Channels using spacebar');
   SetboxOn(True);
   AddItem('Channel ~1~',302,false);
   AddItem('Channel ~2~',273,false);
   AddItem('Channel ~3~',275,false);
   AddItem('Channel ~4~',275,false);
   SetID(1);
 end;

 with VarLength do
 begin
   Init(60,6,8);
   SetLabel('Enter number of readings : ');
   SetValue(1000);
   SetMinMax(0,99999999);
   SetRules(EraseDefault);
   SetId(2)
 end;

 with VarDelay do
 begin
   Init(60,8,8);
   SetLabel('Enter Sample Interval in milliseconds : ');
   SetValue(1000);
   SetMinMax(0,99999999);
   SetRules(EraseDefault);
   SetId(3)
 end;

 with VarIObase do
 begin
   Init(60,4,8);
   SetLabel('Base Address : ');
   SetValue(528);
   SetRules(EraseDefault);
   SetId(4)
 end;

 with ToScreen do
 begin
   Init(2,10,45,4,'Display Option using spacebar');
   SetboxOn(true);  AddItem('Do not write output to Screen',302,false);
   SetID(5);
 end;
```

```
    OK.Init(55,11,'  ~O~K  ',Finished);
    OK.SetHotkey(280);
    OK.SetID(6);
    Cancel.Init(55,13,' C~a~ncel ',Escaped);
    Cancel.SetHotkey(286);
    Cancel.SetID(7);

    Keys.Init;

  end; {InitVars}

  procedure DisposeVars;
  {}
  begin
    Channel.Done;
    OK.Done;
    Cancel.Done;
    Keys.Done;
    VarLength.Done;
    VarDelay.Done;
    VarIObase.done;
    Toscreen.done;
  end; {DisposeVars}


  Procedure DoOptions;
  Begin
    InitVars;
    screen.ShadFillBox(3,21,78,23,Yellow,2);
    screen.writeAt(24,22,Black,' Use the [TAB] Key to change Options ');
    with Manager do
    begin
      Init;
      Win^.SetSize(5,4,75,19,1);
      Win^.SetTitle(' Enter Your Options ');
      AddItem(Keys);
      AddItem(Channel);
      Additem(VarIOBase);
      Additem(Varlength);
      Additem(VarDelay);
      Additem(ToScreen);
      AddItem(OK);
      AddItem(Cancel);
      win^.GrowDraw;
      Result := Go;
      Win^.Remove;
      if Result = Finished then
      begin
        GotoXY(1,18);
      end;
```

```
    Channel1  := Channel.Getvalue(1) ;
    Channel2  := Channel.Getvalue(2) ;
    Channel3  := Channel.Getvalue(3) ;
    Channel4  := Channel.Getvalue(4) ;
    ToScreen1 := ToScreen.Getvalue(1) ;
    DisposeVars;
    Done;
  end;
end;

Procedure DoProgram ;
begin
 DoKurt(Channel1,Channel2,Channel3,Channel4,VarLength.Getvalue,VarDelay.Getvalue,
VarIOBase.getvalue,toscreen1);
end;
```

MENU. PAS

```
program DemoMenuSeven;
{DEMMN7 - using EZPull objects}
USES  DOS, CRT,
    totMENU, totFAST,totio1,Kurt,About,output,totio2;

var
 Menu: EZPullArrayOBJ;
 Choice: word;

 Channel ,ToScreen : CheckIOOBJ;
 OK,Cancel : Strip3dIOOBJ;
 Keys: ControlKeysIOOBJ;
 Manager: WinFormOBJ;
 Result: tAction;
 VarLength ,
 VarDelay  ,
 VarIObase : IntIOOBJ;
 Channel1 , Channel2 , Channel3 , Channel4  : Boolean ;
 Fn : String;

{$I InitVars.INC}


procedure CreateMenu;
{}
var
 Mtxt: Array[1..6] of string[90];
begin
  MTxt[1] := '\ Main Menu "System Commands';
  MTxt[2] := ' ~O~ptions       "Set Run Options "100';
  MTxt[3] := ' ~R~un Program    "            "101';
  MTxt[4] := ' ~V~iew Output    "            "102';
  MTxt[5] := ' ~A~bout         "Who, Why And What"s this all about"103';
  MTxt[6] := ' ~E~xit          "Leave this program"999';
  with Menu do
  begin
    Init;
    AssignList(MTxt,6,90);
  end;
end; {CreateMenu}

begin
  TestCycle := false ;
  Screen.PartClear(1,2,80,24,white,'°'); {paint the screen}
  Screen.PartClear(1,1,80,1,31,' ');
  Screen.PartClear(1,25,80,25,31,' ');
  Screen.WritePlain(9,25,'³');
```

```
    Limitations;

    CreateMenu;
    with Menu do
    begin
      Choice := Push(13,0,0);   {Pass Enter to make menu pull down}
  {     Done; }
    end;
    GotoXY(25,15);

    Repeat

     if Choice = 100 then DoOptions ;

     If Choice = 101 then DoProgram ;

     If Choice = 102 then Begin
                        write('Enter Filename : ');
                        readln(Fn);
                        ReadOutput(Fn);
                      end;

     If Choice = 0   then exit ;

     If Choice = 999 then break ;

     If Choice = 103 then About1 ;

     IF Choice = 104 then begin
                        TestCycle1  ;
                      end;
     Choice := 0 ;
     Screen.PartClear(1,2,80,24,white,'°'); {paint the screen}
     Screen.PartClear(1,1,80,1,31,' ');
     Screen.PartClear(1,25,80,25,31,' ');
     Screen.WritePlain(9,25,'³');

     Choice := MENU.Push(13,0,0);   {Pass Enter to make menu pull down}

   Until Choice = 999 ;

   MENU.DONE;
   ClrScr;
   Write('Thanks for using this software and the K.April I/O Card.');

end.
```

ABOUT. PAS

```
UNIT ABOUT ;
{$o+}
interface

PROCEDURE ABOUT1 ;
PROCEDURE Limitations ;
implementation
uses totmsg ;

procedure ABOUT1 ;
Var
  MsgWin   : MessageOBJ;
begin
   with MsgWin do
        begin
          Init(1,' About ');
          AddLine('');
          AddLine('      This software was       ');
          Addline('      developed for the       ');
          Addline('      Measurement and         ');
          Addline('     Instrumentation Lab      ');
          Addline('    toward a MSc(Elec. Eng)    ');
          AddLine('         at U.C.T             ');
          Addline('                              ');
          Addline('        Written by            ');
          Addline('                              ');
          Addline('      Kurt .A. April          ');
          Addline('');
          Show ;
        end;
end;

procedure Limitations ;
Var
  MsgWin   : MessageOBJ;
begin
  with MsgWin do
  begin
    Init(1,' Limitations ');
    AddLine('');
    Addline(' The maximum sample rate is dependent on the speed ');
    Addline('        of the processor chip used            ');
    AddLine('');
    Show ;
  end;
end;

end .
```

OUTPUT. PAS

```
unit output;
{$o+}
interface

Procedure ReadOutput(DefaultFile : string);

implementation


Uses DOS,CRT,
   totFAST, totINPUT, totLINK, totLIST, totSTR;

Procedure ReadOutput(DefaultFile : string);
var
  BWin: BrowseFileOBJ;
  RetCode: integer;
  Filename: string;

begin

  FileName := DefaultFile;

  screen.ShadFillBox(3,21,78,23,Yellow,2);
  screen.writeAt(24,22,Black,'     Press [Esc] to quit       ');

  with BWin do
  begin
    Init;
    Win^.SetSize(5,4,75,19,1);
    Retcode := AssignFile(Filename);
    if Retcode in [0,2] then
      Go
    else
    begin
      Writeln('Unable to find file: ',Filename,'.');
      Key.DelayKey(2000);
    end;
    Done;
  end;
end;

end.
```

TEST. PAS

```
{$N+}
USES dos, CRT;
VAR H , M ,S , Q ,
  HH,MM,SS,HHUND : WORD ;
  CHECKTI : longint ;
  endtime , a , b ,c ,d , kdelay : longint ;

BEGIN
        kdelay := 1000 ;
        CLRSCR ;
        GetTime(h,m,s,Q);
        a := h ; a := a * 10000000 ;
        b := m ; b := b *  100000 ;
        c := s ; c := c *   1000 ;
        d := q ; d := d *     10 ;
        EndTime := a + b + c + d ;
        Endtime := Endtime + kdelay  ;

        Repeat
         GetTime(h,m,s,q);
         a := h ; a := a * 10000000 ;
         b := m ; b := b *  100000 ;
         c := s ; c := c *   1000 ;
         d := q ; d := d *     10 ;
         CHECKTI := a + b + c + d ;
        Until CHECKTI >= EndTime ;
        writeln((CHeckti - ENDtime):20) ;
END.
```

APPENDIX A

2. SOFTWARE GRAPHICS

These are graphic representations of the actual software package, i.e., if one enters the program, these graphics will appear on the computer monitor in the sequence shown. The various prompts that the user is confronted with are shown in these graphics. Facilities such as pull-down menus, use of a mouse, colour, user-defined options, and the like, has been included.

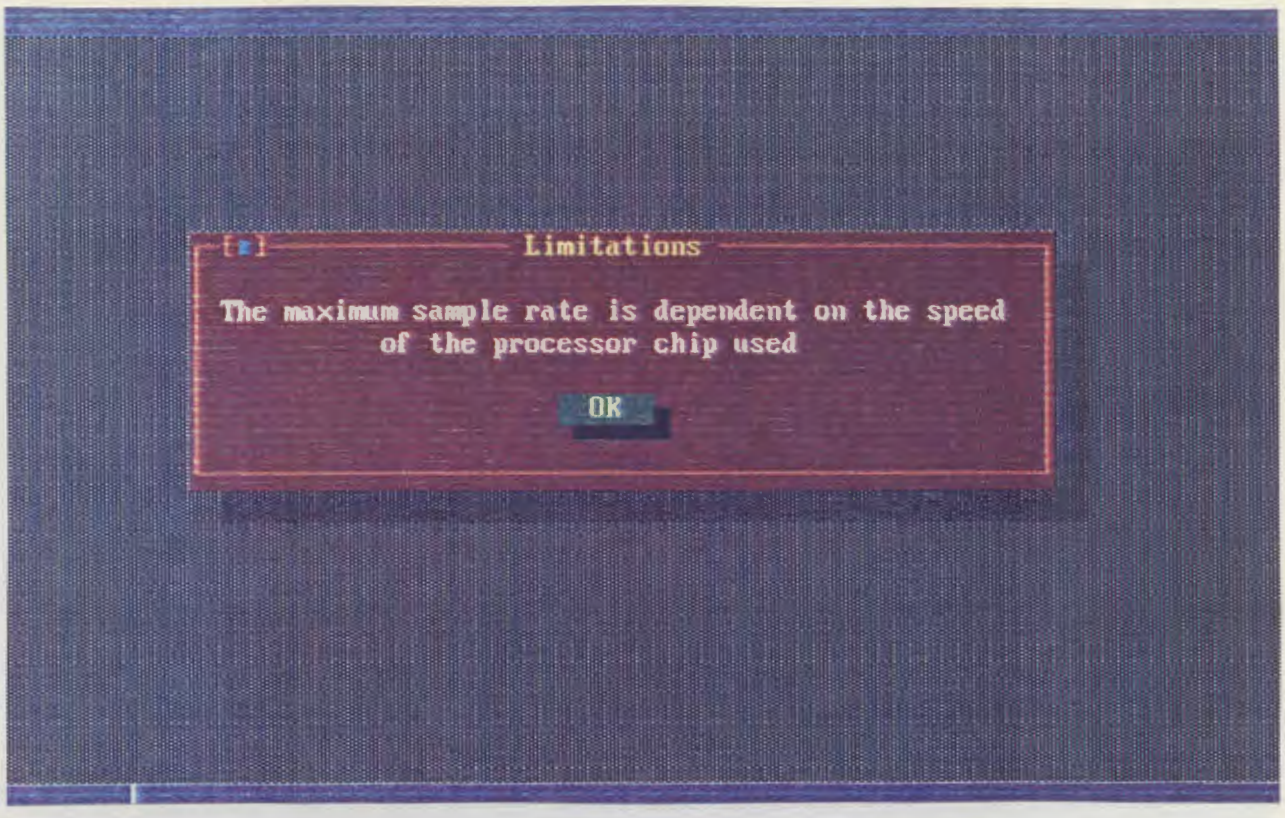

On entering the program (by typing "MENU"), the above graphic will be the first message displayed to the user. It informs the user that the speed at which the A/D can sample is dependent on the speed of the processor been used by the computer.

After hitting the <ENTER> key, or clicking on <OK> with a mouse, the Main Menu screen appears. A pull-down menu prompts the user to make one of the 5 choices shown above. A help line has been provided at the bottom of the screen, informing the user of what each of the options achieves.

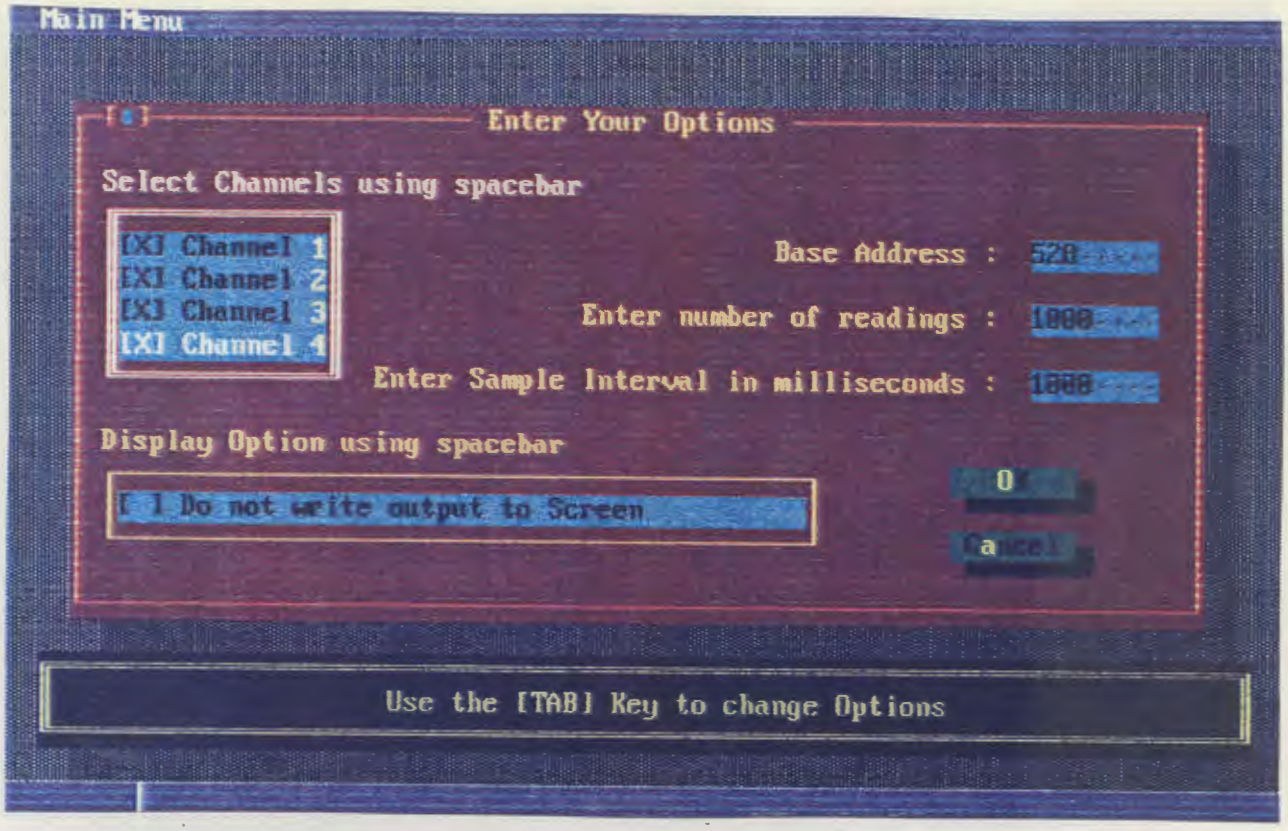

Having chosen <OPTIONS> option, the user is confronted with this screen. Any one of the four channels may be selected with the aid of the spacebar, the base address of free-I/O space for the use of the card may be selected by the user, the number of samples and sample interval may be set by the user, and the user has the option of displaying the output to the screen or not. By enabling the "DO NOT WRITE TO THE SCREEN" option, faster sampling rates may be achieved.

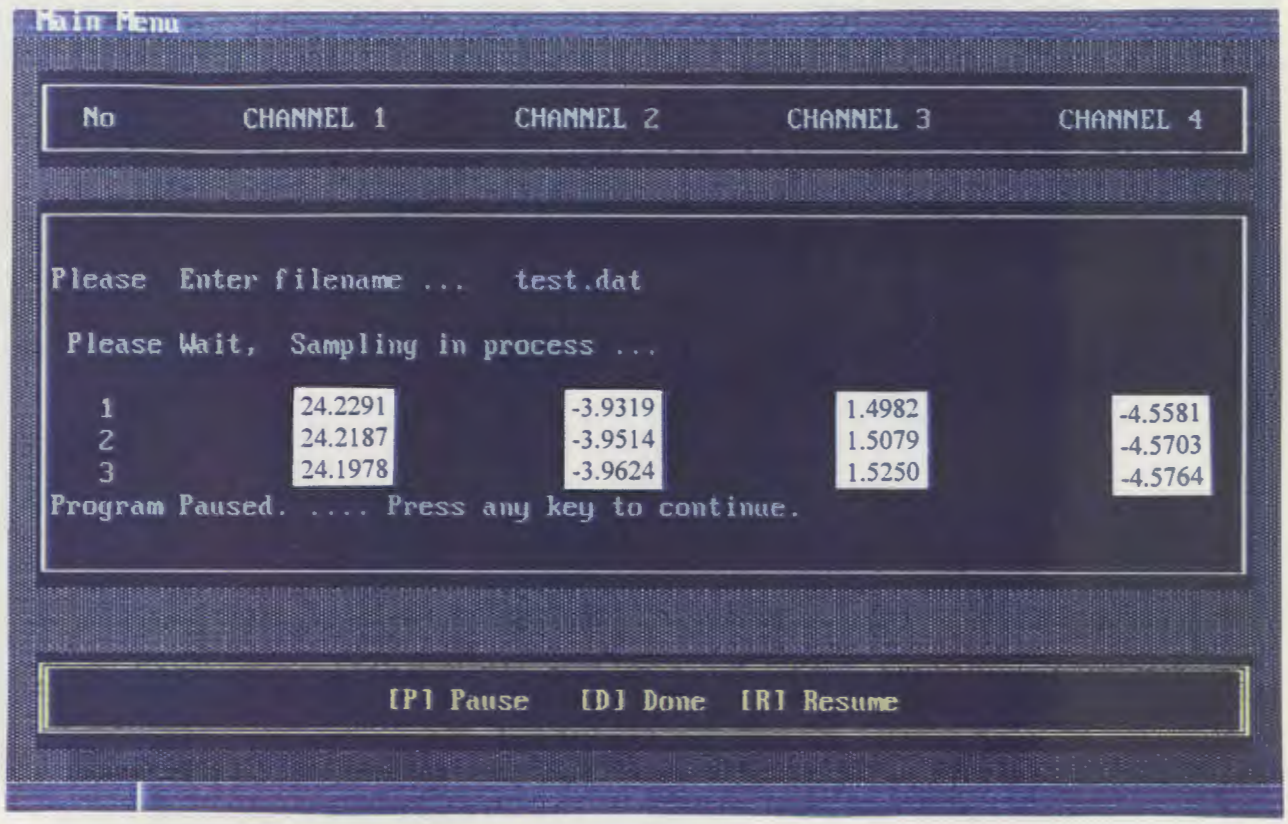

Once the user sets the required options before running the program, in the <OPTIONS> screen, s/he may move on to the <RUN PROGRAM> option. Here the user is prompted to enter a filename into the computer. The screen displays the channels that were selected, as well as real-time data as measurements are taken. The user has the option to <PAUSE> the program, and then <RESUME> running the program.....this feature has been found to be extremely useful in a laboratory environment.

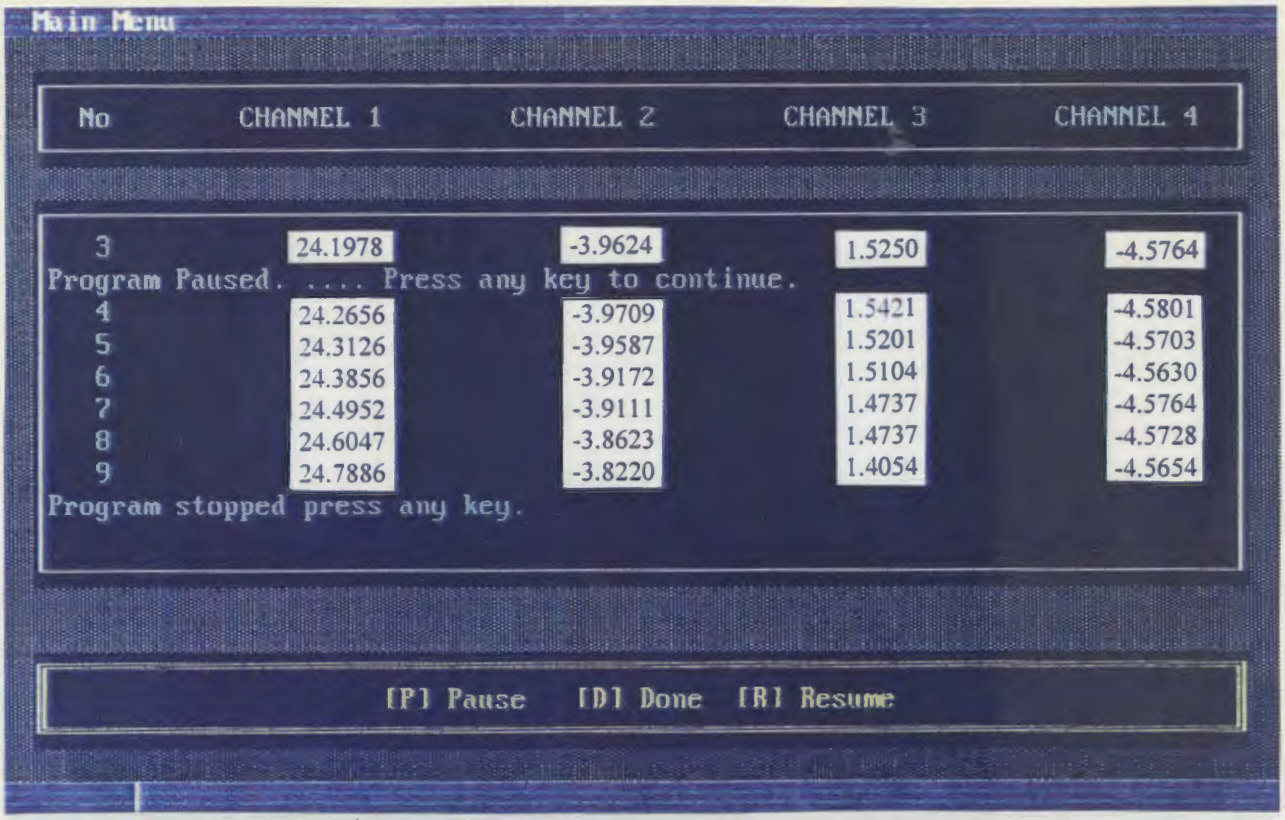

The program will stop for the following reasons (under normal running conditions) : (a) the user has pressed "P" to <PAUSE> the program, (b) the entered number of readings has been reached, or (c) the user has selected "D" to terminate the program. Messages will inform the user of all three "situations" described.

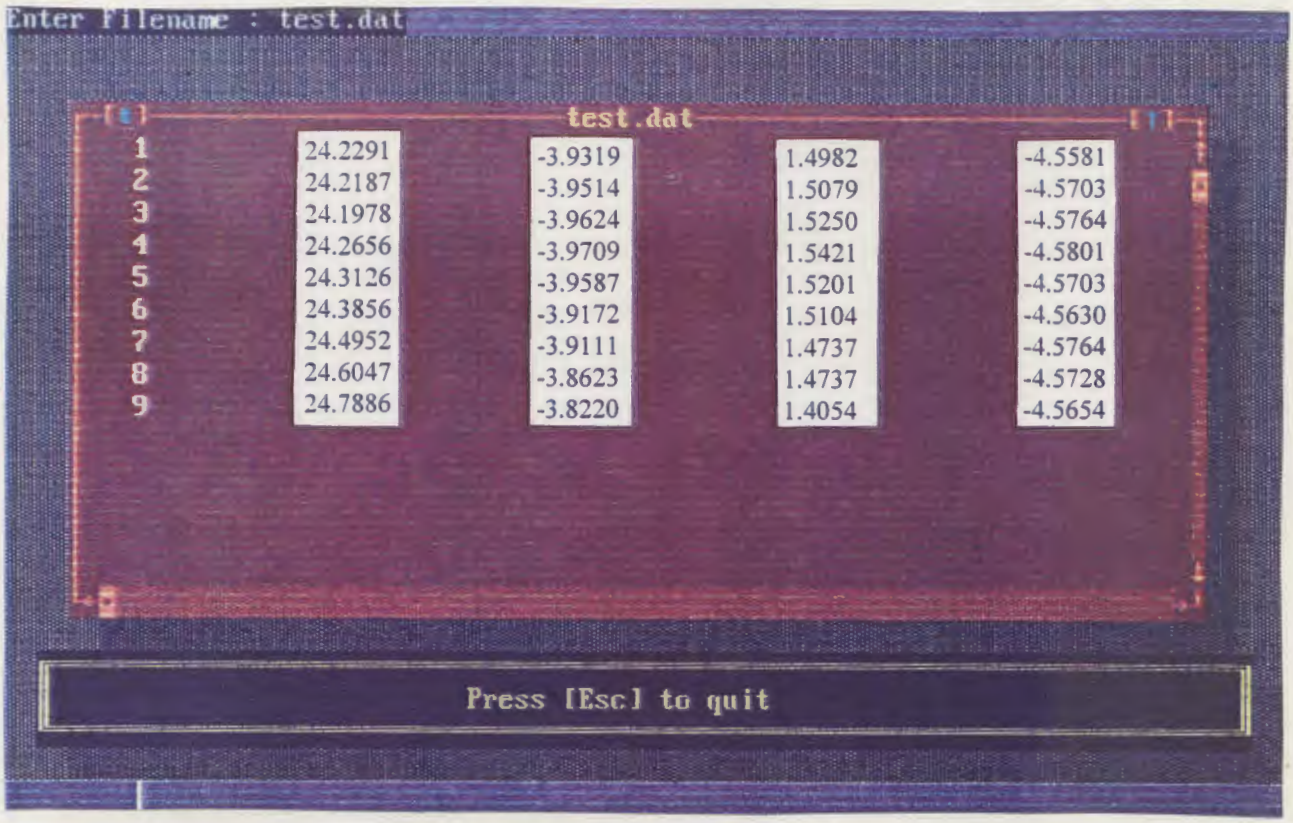

Having taken the necessary readings and measurements, the user then has the facility to view the output, by selecting <VIEW OUTPUT> in the Main Menu. Data can be scrolled through with the use of the arrow keys on a keyboard, or by clicking (with a mouse) on the provided "scroll channel" on the right-hand side of the screen.

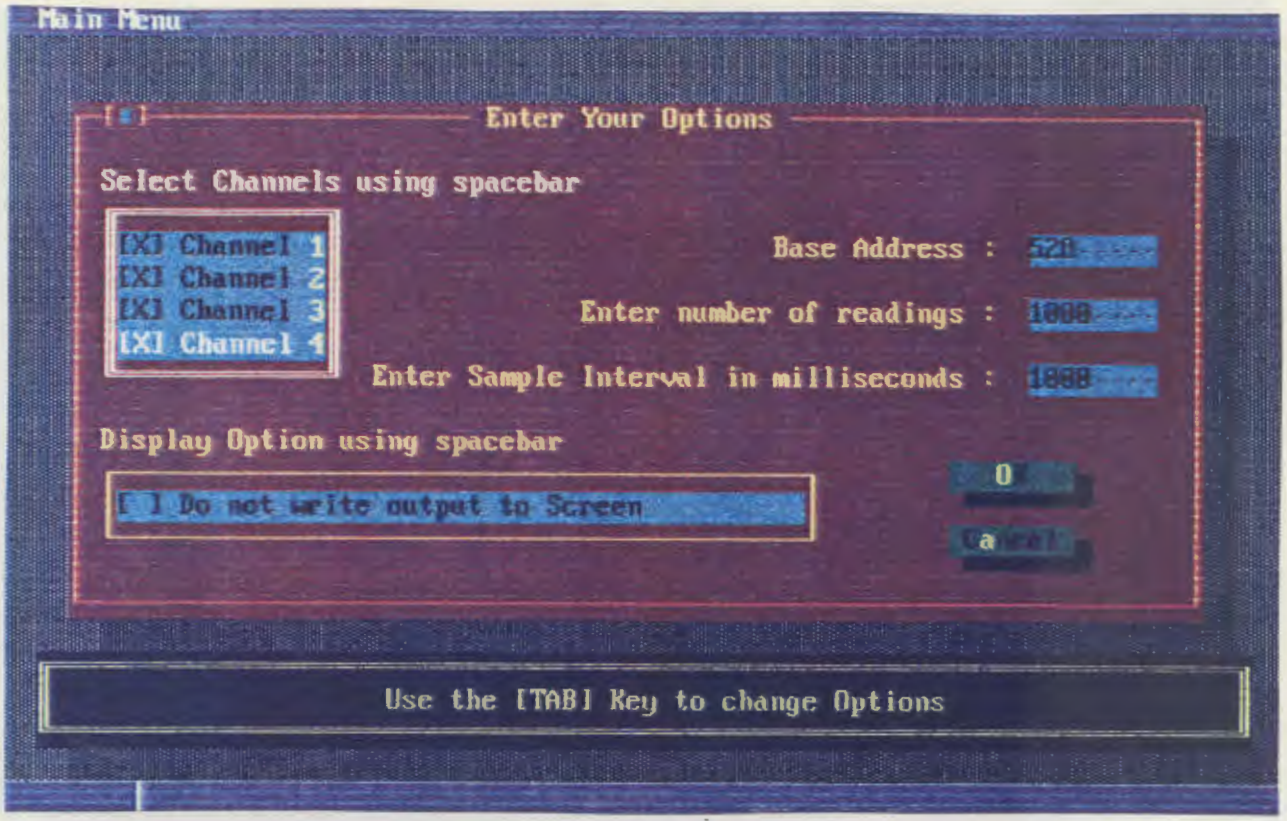

Having chosen <OPTIONS> option, the user is confronted with this screen. Any one of the four channels may be selected with the aid of the spacebar, the base address of free-I/O space for the use of the card may be selected by the user, the number of samples and sample interval may be set by the user, and the user has the option of displaying the output to the screen or not. By enabling the "DO NOT WRITE TO THE SCREEN" option, faster sampling rates may be achieved.

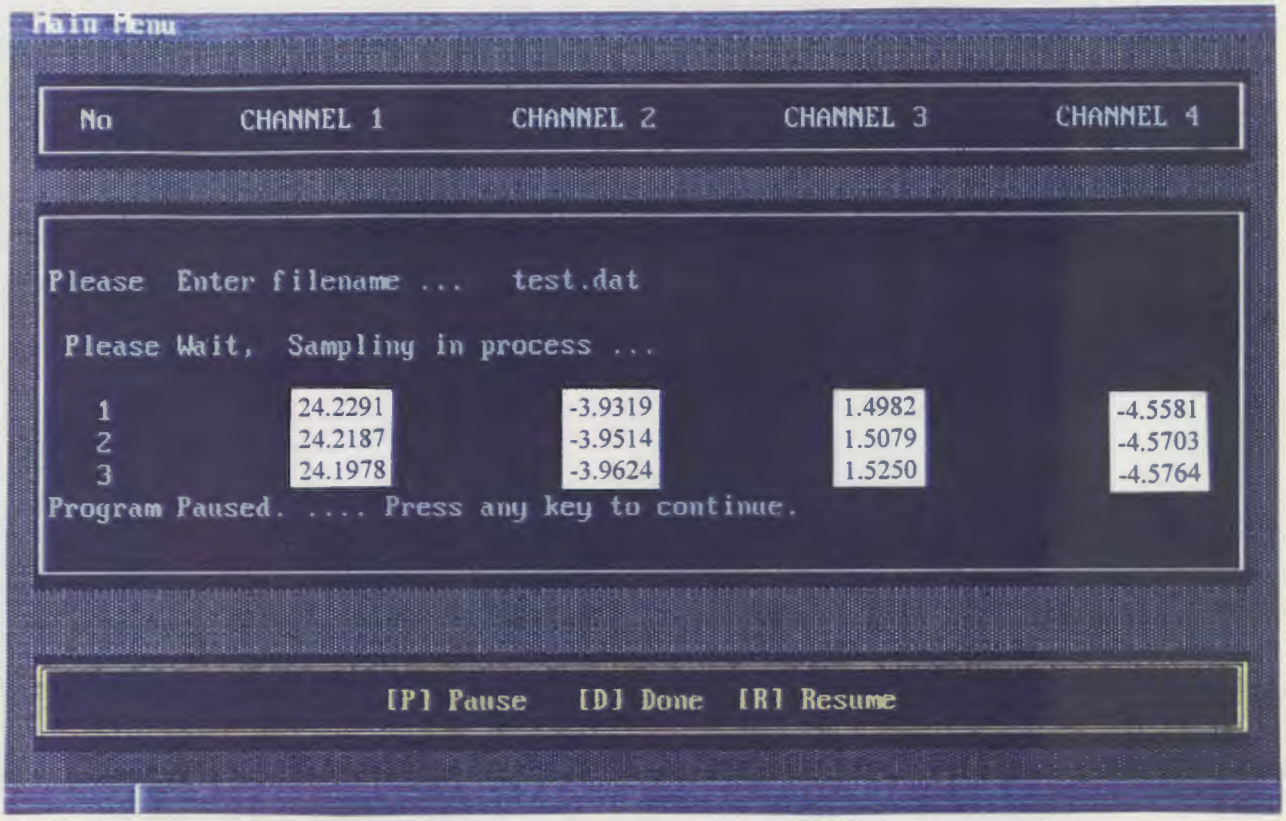

Once the user sets the required options before running the program, in the <OPTIONS> screen, s/he may move on to the <RUN PROGRAM> option. Here the user is prompted to enter a filename into the computer. The screen displays the channels that were selected, as well as real-time data as measurements are taken. The user has the option to <PAUSE> the program, and then <RESUME> running the program.....this feature has been found to be extremely useful in a laboratory environment.

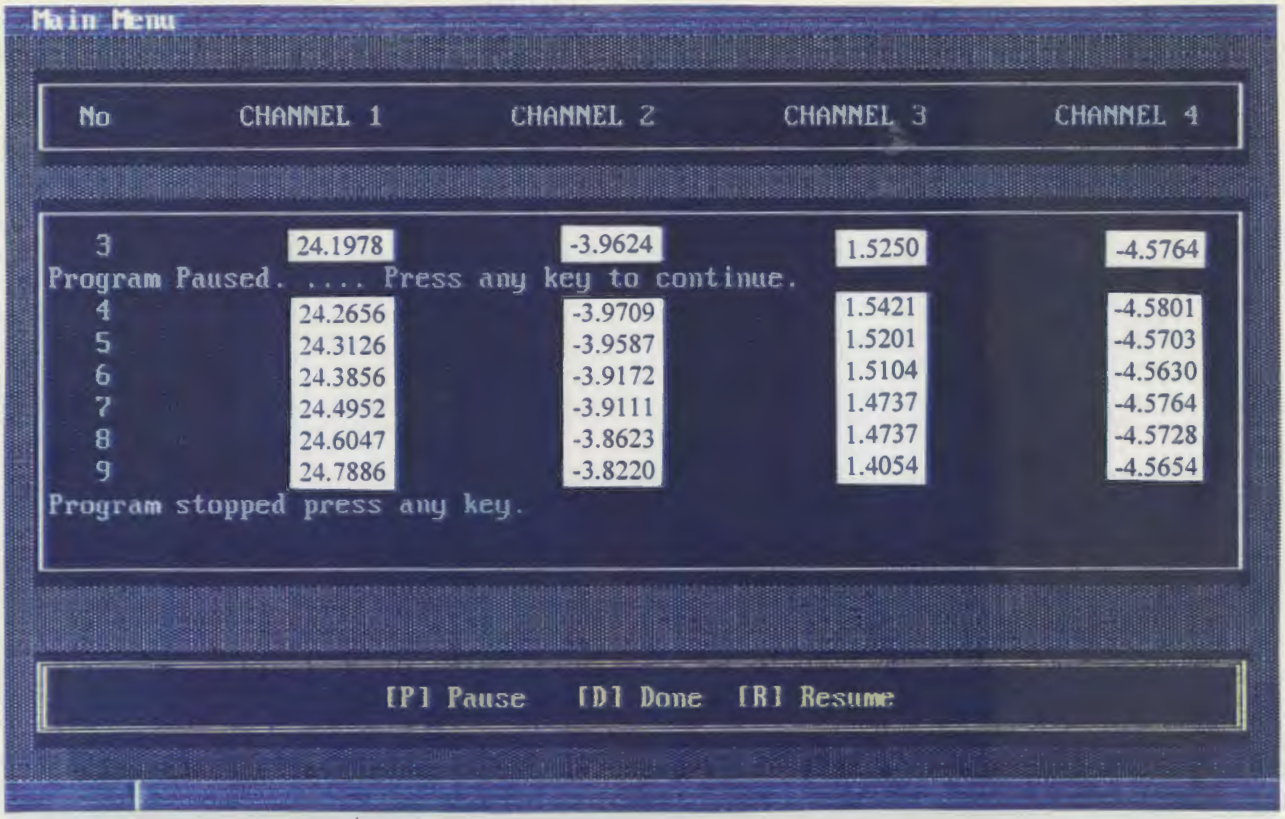

The program will stop for the following reasons (under normal running conditions) : (a) the user has pressed "P" to <PAUSE> the program, (b) the entered number of readings has been reached, or (c) the user has selected "D" to terminate the program. Messages will inform the user of all three "situations" described.

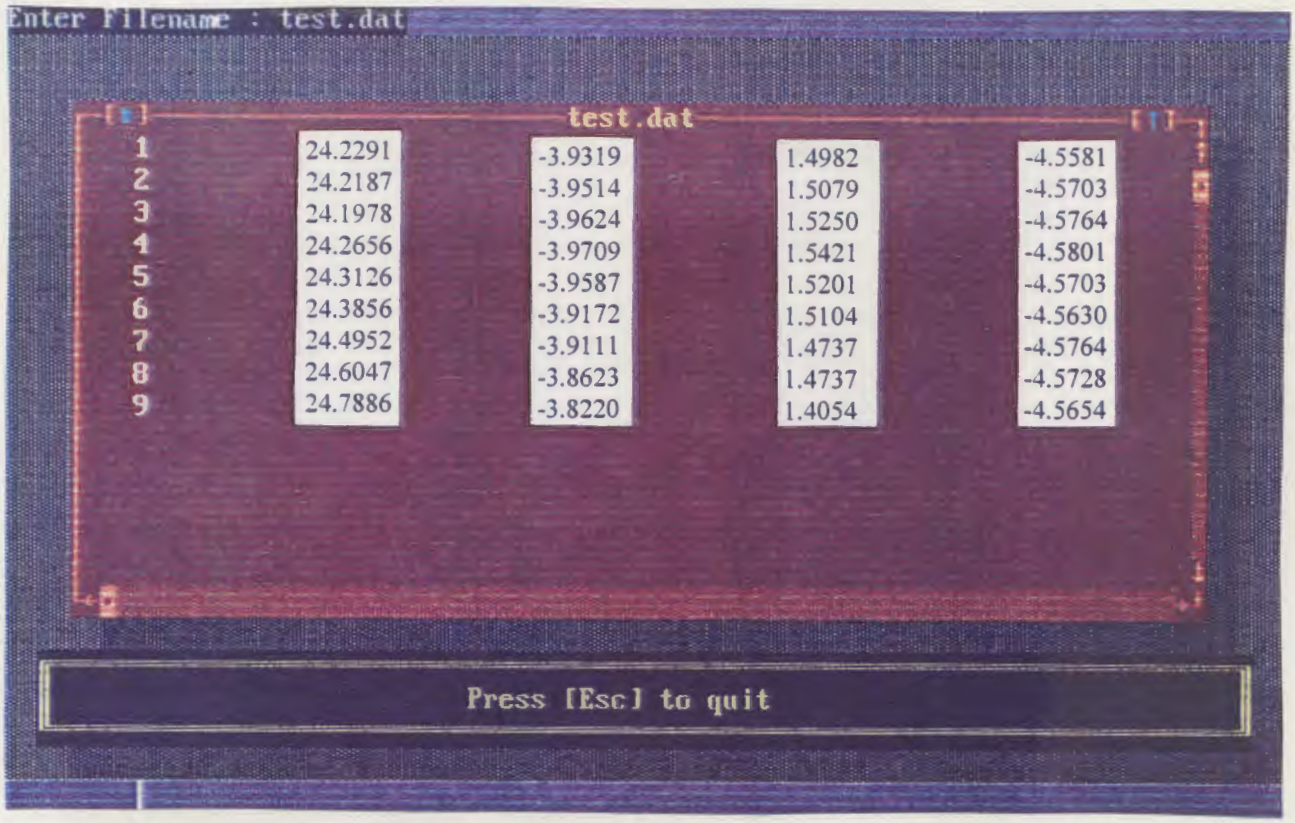

Having taken the necessary readings and measurements, the user then has the facility to view the output, by selecting <VIEW OUTPUT> in the Main Menu. Data can be scrolled through with the use of the arrow keys on a keyboard, or by clicking (with a mouse) on the provided "scroll channel" on the right-hand side of the screen.

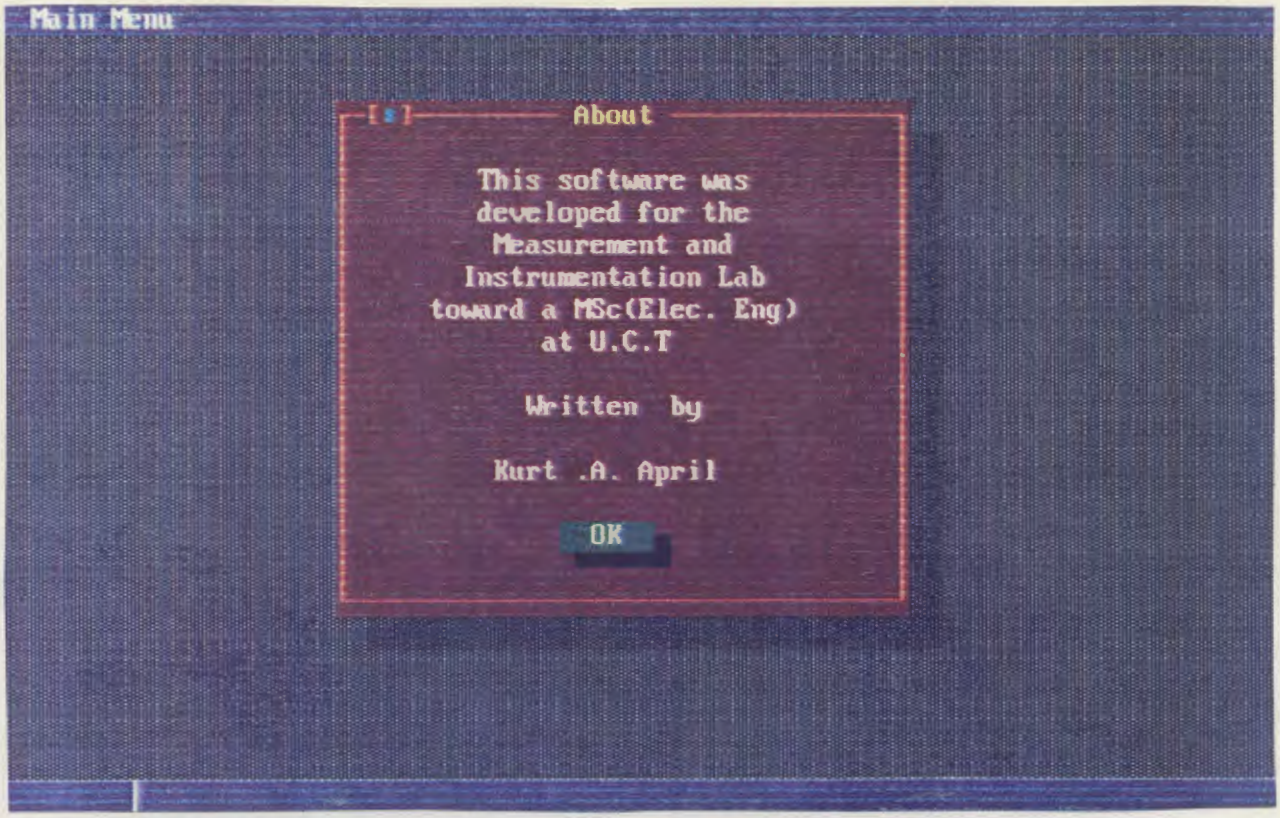

An <ABOUT> option has been provided to inform the user about the "who", and "for what" concerning the software.

APPENDIX B

PHOTOGRAPHS :

Photograph Bα : This double sided printed circuit board is a bottom view of the 12-bit PC-interface card. The only components on this side (for the sake of saving space) are the red dipswitch, and the LM7905 (-5V) regulator. Also evident in this photograph in the protruding input jack, mounted on the top side of the board. The dimensions of the card is 135mm × 110mm, and the card plugs directly into the I/O bus of any computer. Notice the widespread ground throughout the board, which reduces the amount of noise.

Photograph Bβ : This photograph shows the two resistors that were used during the investigation into the temperature coefficients of metal-film resistors and carbon film resistors. They are both 100Ω resistors, and the 5% tolerance carbon film resistor is shown on the left, whilst the 1% tolerance metal-film resistor is shown on the right. Notice the difference in the size of the two resistors. Also included in the photograph is the LM35 temperature sensor, which was employed in virtually all the experiments. This 3-legged device provides a voltage output with +10mV/°C slope.....it has an internal offset such that the output is 0 volts at 0°C.

Photograph Bχ: The three devices shown are the AD633, the LF351 high speed, JFET-input operational amplifier, and the AD620 high accuracy, instrumentation amplifier. The LF351 is normally used in applications such as high speed integrators, fast D/A converters, sample-and-hold circuits, and many other circuits requiring low input offset voltage, low input bias current, high input impedance, high slew rate and wide bandwidth. The high accuracy AD620, with its low offset voltage, high common-mode rejection and extremely low offset drift of 0.6μV/°C, is ideally suited for use in precision data acquisition systems such as transducer interfaces.

Photograph Bδ : The two voltage regulators that were studied, i.e., the LM7805 (+5V) regulator, and the LM7905 (-5V) regulator. Both these regulators exhibited parabolic output responses to increased temperature. Other regulators in the series were also tested, but the LM7805 had by far the most stable characteristics.

Photograph Bε : The MPX100AP pressure sensor, which was used during experiments with the "weather station". The MPX100AP sensor is a silicon piezo-resistive pressure sensor. It provides a very accurate and linear voltage output, which increases with increasing pressure relative to ambient pressure (approximately 100kPa) applied to the pressure side of the device.

Photograph Bϕ : The white 5W resistors is similar to the "heater resistors" used during experiments conducted and components to establish their temperature coefficients. The plate, onto which the unit-under-test was secured, was heated with the aid of two (white 5W) 100Ω resistors, which were connected in parallel to a 30V power supply. The 1.5μF Wima polyester capacitor (red) was studied for its thermal properties. Notice the bulky size of the capacitor.

Photograph Bγ : A "mixed bag" of components and devices that were used, and studied, during experiments.

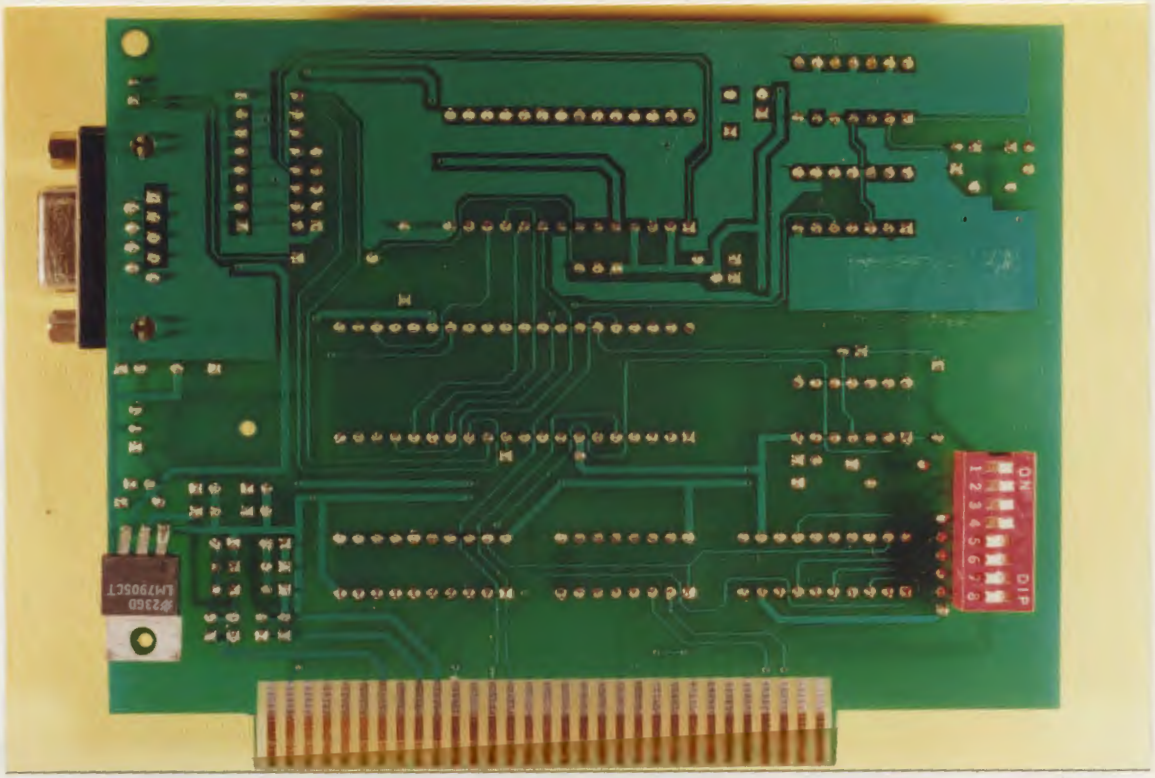

Photograph Bα : This double sided printed circuit board is a bottom view of the 12-bit PC-interface card. The only components on this side (for the sake of saving space) are the red dipswitch, and the LM7905 (-5V) regulator. Also evident in this photograph in the protruding input jack, mounted on the top side of the board. The dimensions of the card is 135mm × 110mm, and the card plugs directly into the I/O bus of any computer. Notice the widespread ground throughout the board, which reduces the amount of noise.

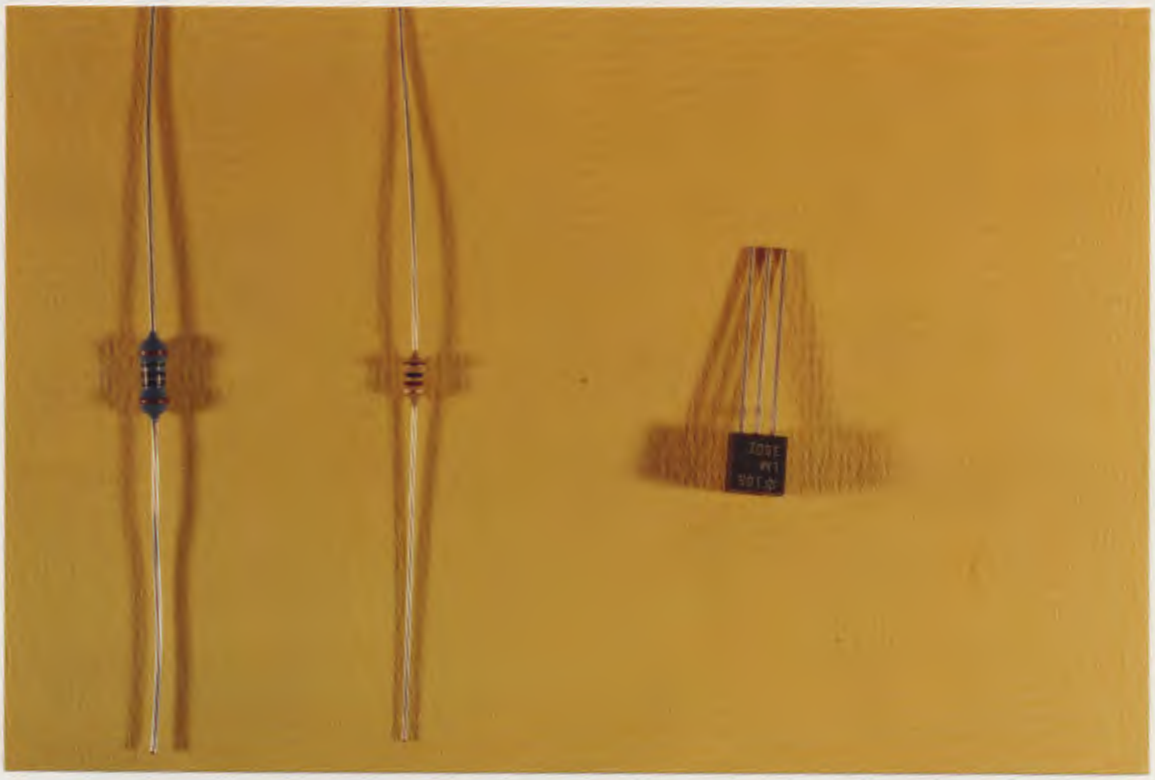

Photograph Bβ : This photograph shows the two resistors that were used during the investigation into the temperature coefficients of metal-film resistors and carbon film resistors. They are both 100Ω resistors, and the 5% tolerance carbon film resistor is shown on the left, whilst the 1% tolerance metal-film resistor is shown on the right. Notice the difference in the size of the two resistors. Also included in the photograph is the LM35 temperature sensor, which was employed in virtually all the experiments. This 3-legged device provides a voltage output with +10mV/°C slope.....it has an internal offset such that the output is 0 volts at 0°C.

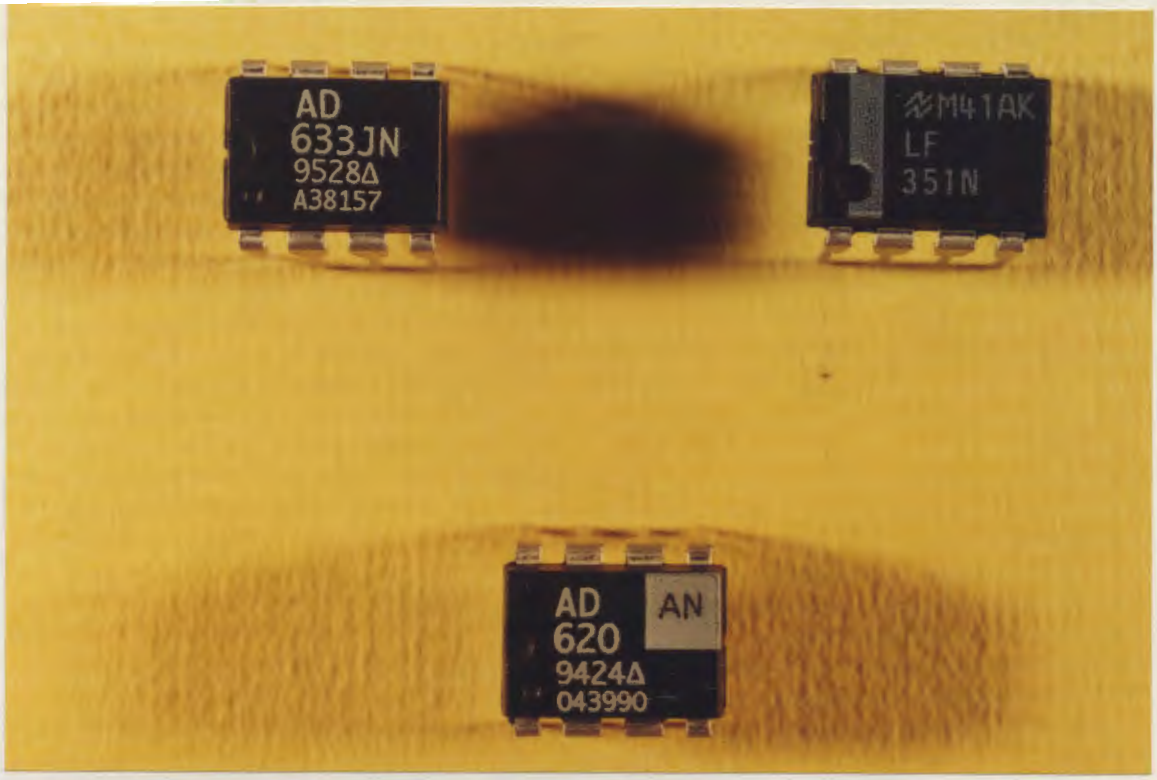

Photograph Bχ: The three devices shown are the AD633, the LF351 high speed, JFET-input operational amplifier, and the AD620 high accuracy, instrumentation amplifier. The LF351 is normally used in applications such as high speed integrators, fast D/A converters, sample-and-hold circuits, and many other circuits requiring low input offset voltage, low input bias current, high input impedance, high slew rate and wide bandwidth. The high accuracy AD620, with its low offset voltage, high common-mode rejection and extremely low offset drift of 0.6μV/°C, is ideally suited for use in precision data acquisition systems such as transducer interfaces.

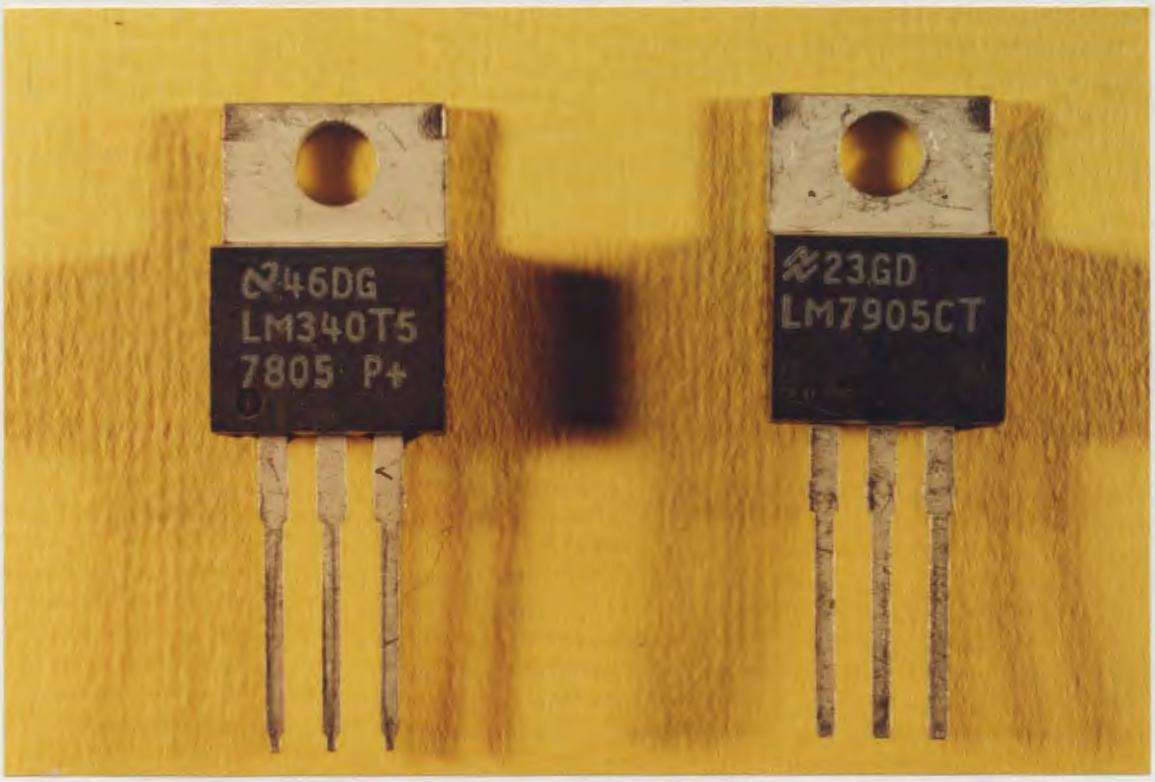

Photograph Bδ : The two voltage regulators that were studied, i.e., the LM7805 (+5V) regulator, and the LM7905 (-5V) regulator. Both these regulators exhibited parabolic output responses to increased temperature. Other regulators in the series were also tested, but the LM7805 had by far the most stable characteristics.

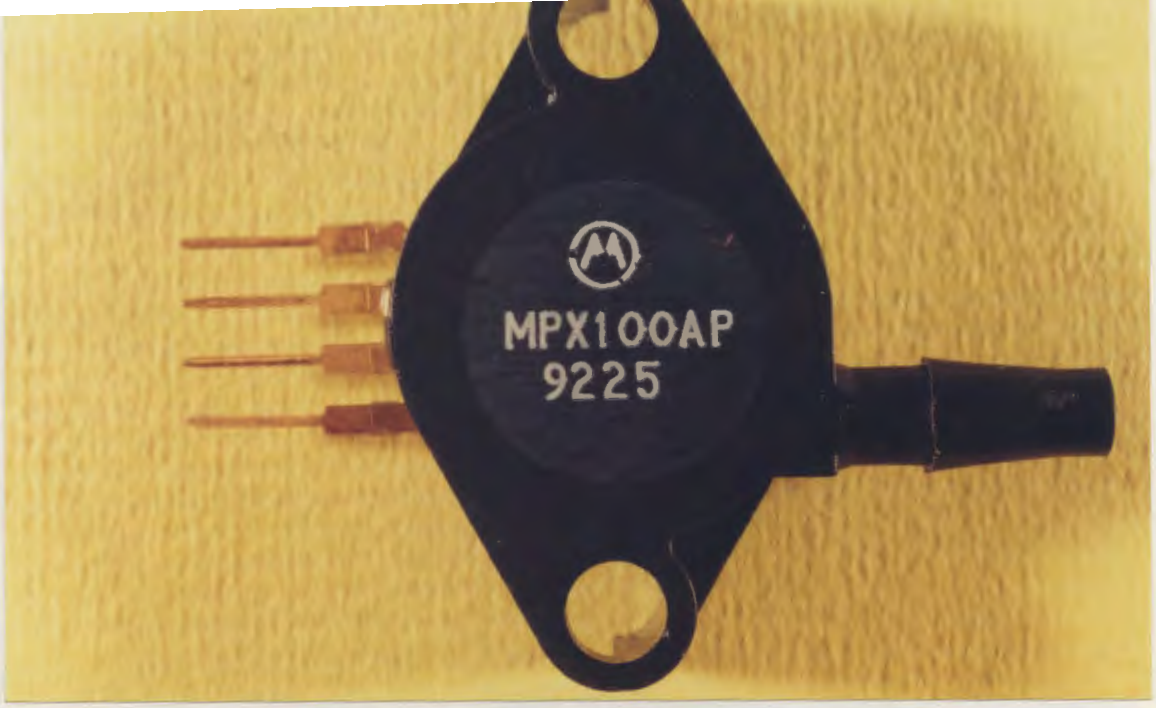

Photograph Bε : The MPX100AP pressure sensor, which was used during experiments with the "weather station". The MPX100AP sensor is a silicon piezo-resistive pressure sensor. It provides a very accurate and linear voltage output, which increases with increasing pressure relative to ambient pressure (approximately 100kPa) applied to the pressure side of the device.

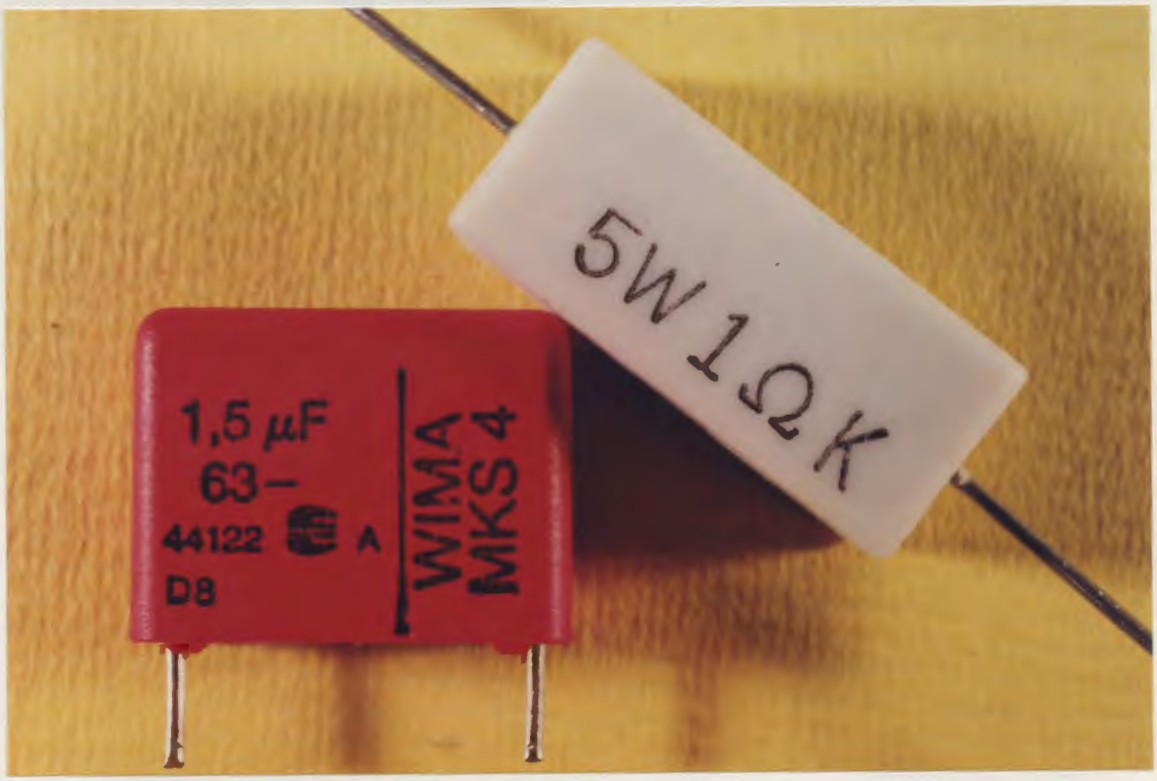

Photograph Bϕ : The white 5W resistors is similar to the "heater resistors" used during experiments conducted and components to establish their temperature coefficients. The plate, onto which the unit-under-test was secured, was heated with the aid of two (white 5W) 100Ω resistors, which were connected in parallel to a 30V power supply. The 1.5µF Wima polyester capacitor (red) was studied for its thermal properties. Notice the bulky size of the capacitor.

APPENDIX C

CIRCUIT DIAGRAMS

A. Complete circuit diagram of the Measurement-Card which uses a 12-bit Analogue-to-Digital Converter, and interfaces to a personal computer.

B. Circuit diagram of the Resistor-Inductor-Capacitor (RLC) Network which was used to filter out unwanted noise on the power rails of the personal computer. This filter network is built onto the Measurement-Card, close to the connector end of the card which plugs directly into the I/O bus of the PC.

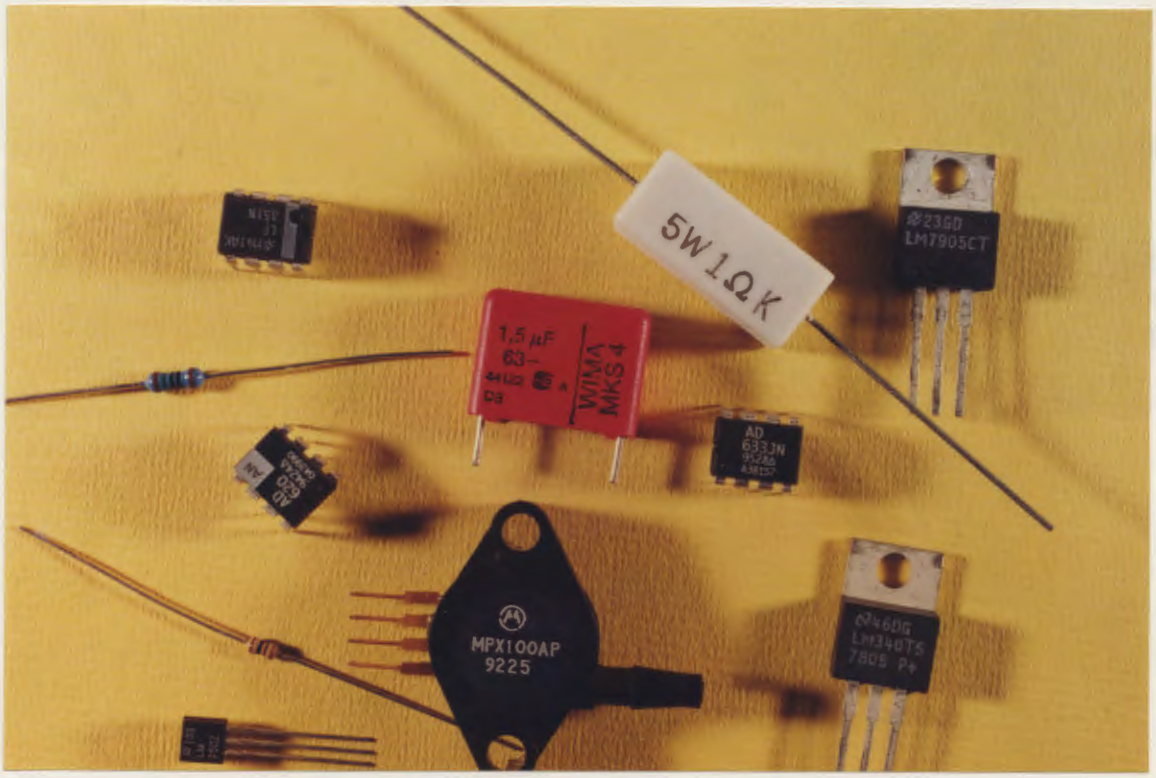

Photograph Bγ : A "mixed bag" of components and devices that were used, and studied, during experiments.

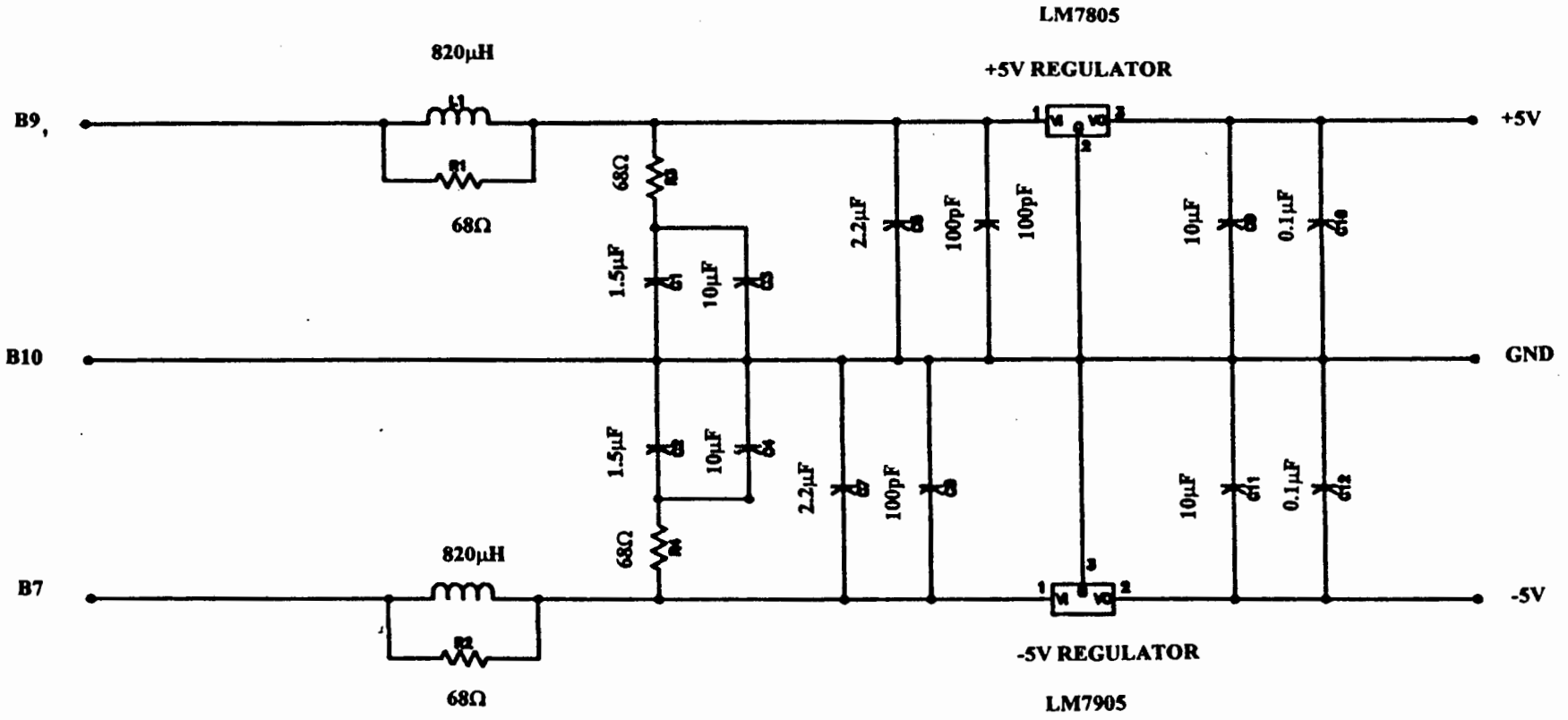

RLC Network to filter out noise on the power rails of a personal computer. This filter set-up can be used, with advantage, on any computer using I/O peripherals.

REFERENCES

1. Advantech, **Total Solution for PC-Based Industrial and Lab Automation**, Solution Guide, Volume 51, 1996.

2. Budzilovich, P.N., **Electrical Noise**, IEEE Paper, Volume 16, May 1980, pp. 85 - 89.

3. **Dictionary of Scientific and Technical Terms**, McGraw-Hill, Second Edition, 1978.

4. Dorf, R. C., **Electrical Engineering Handbook**, CRC Press, Ann Arbor, 1993, pp. 5-33 and pp. 447-451.

5. Doyle, F. E., and Byrom, G. T., **Instrumentation Temperature**, Robert Cunningham & Sons Publishers, London, 1970, pp. 5 -40

6. Enke, C.G., **Data Domains -An analysis of Digital and Analogue Instrumentation Systems and Components**, Anal. Chem., Volume 43, January 1971, pp. 69 - 80.

7. Gydien, M.Z., **Temperature Dependence of Piezo-Ceramic Capacitors and Ferrite Pit Core Inductors**, University of Cape Town, November 1994, pp. 1-25.

8. Handscombe, E., **Electrical Measuring Instruments**, Wykeham Publications, London, 1970, pp. 1-9 and pp. 50-54.

9. Hashemia, H. M., and Peterson, K. M., **Assuring accurate Temperature Measurement**, Intech, (36) 1989, pp. 30-63.

10. McGee, T. D., **Principles and Methods of Temperature Measurement**, John Wiley & Sons, New York, 1988, pp. 500-529.

11. Leigh, J. R., **Temperature Measurement and Control**, Peregrinus Publishers, London, 1988, pp. 22-54.

12. Prefumo, J. P. G., **Transient Response of Temperature Sensors**, University of Cape Town, April 1994, Chapter 2, pp. 2-12.

13. Shambrook, K. P., **Signal Processing Techniques for Temperature Measurement**, American Institute of Physics, (5) 1982, pp. 1160-1172.

14. Smith, R. J., **Circuits, Devices and Systems**, John Wiley & Sons, New York, Fourth Edition, 1984, pp. 58-88 and pp. 435-464.

15. Wildhack, W., **National Conference on Instrumentation**, Proc. 1953.

BIBLIOGRAPHY

1. April, K. A., **A study of the fundamental performance and limitations of Analogue-to-Digital Converters**, University of Cape Town, November 1994.

2. Arthur, K., **Transducer Measurements**, Tektronix, Oregan, First Edition, 1970.

3. Cerni , R. H., and Foster, L. E., **Instrumentation for Engineering Measurement**, John Wiley & Sons, New York, 1962.

4. Department of Instrumentation and Analytical Science UMIST, **Instrumentation and Analytical Science**, Peter Peregrinus Ltd., London, 1989.

5. De Sa, A., **Principles of Electronic Instrumentation**, Routledge, Chapman and Hall, Inc., New York, Second Edition, 1990.

6. Finkel, J., **Computer-Aided Experimentation : Interfacing to Minicomputers**, John Wiley & Sons, New York, 1975.

7. Hill, Winfield and Horowitz, Paul, **The Art of Electronics**, Cambridge University Press, Cambridge, Second Edition, 1989.

8. Kuo, B. C., **Digital Control Systems**, Saunders College Publishing, Florida, 1992.

9. Lion, K. S., **Elements of Electrical and Electronic Instrumentation**, John Wiley & Sons, New York, 1975.

10. Taub, Herbert and Schilling, Donald, **Digital Integrated Electronics**, McGraw-Hill, Kogakusha Ltd., Tokyo, First Edition, 1977.

11. Van Putten, Anton F. P., **Electronic Measurement Systems**, Prentice Hall International (UK) Ltd., Hertfordshire, First Edition, 1988.

12. Williams, B. W., **Power Electronics**, The Macmillan Press Ltd., Hong Kong, Second Edition, 1993.

13. Zuch, Eugene L., **Data Acquisition and Conversion Handbook**, 8th Edition, Datel Publishing, Mansfield, Massachusetts, 1988.

APPENDIX B

PHOTOGRAPHS :

Photograph Bα : This double sided printed circuit board is a bottom view of the 12-bit PC-interface card. The only components on this side (for the sake of saving space) are the red dipswitch, and the LM7905 (-5V) regulator. Also evident in this photograph in the protruding input jack, mounted on the top side of the board. The dimensions of the card is 135mm × 110mm, and the card plugs directly into the I/O bus of any computer. Notice the widespread ground throughout the board, which reduces the amount of noise.

Photograph Bβ : This photograph shows the two resistors that were used during the investigation into the temperature coefficients of metal-film resistors and carbon film resistors. They are both 100Ω resistors, and the 5% tolerance carbon film resistor is shown on the left, whilst the 1% tolerance metal-film resistor is shown on the right. Notice the difference in the size of the two resistors. Also included in the photograph is the LM35 temperature sensor, which was employed in virtually all the experiments. This 3-legged device provides a voltage output with +10mV/°C slope.....it has an internal offset such that the output is 0 volts at 0°C.

Photograph Bχ: The three devices shown are the AD633, the LF351 high speed, JFET-input operational amplifier, and the AD620 high accuracy, instrumentation amplifier. The LF351 is normally used in applications such as high speed integrators, fast D/A converters, sample-and-hold circuits, and many other circuits requiring low input offset voltage, low input bias current, high input impedance, high slew rate and wide bandwidth. The high accuracy AD620, with its low offset voltage, high common-mode rejection and extremely low offset drift of 0.6μV/°C, is ideally suited for use in precision data acquisition systems such as transducer interfaces.

Photograph Bδ : The two voltage regulators that were studied, i.e., the LM7805 (+5V) regulator, and the LM7905 (-5V) regulator. Both these regulators exhibited parabolic output responses to increased temperature. Other regulators in the series were also tested, but the LM7805 had by far the most stable characteristics.

Photograph Bε : The MPX100AP pressure sensor, which was used during experiments with the "weather station". The MPX100AP sensor is a silicon piezo-resistive pressure sensor. It provides a very accurate and linear voltage output, which increases with increasing pressure relative to ambient pressure (approximately 100kPa) applied to the pressure side of the device.

Photograph Bϕ : The white 5W resistors is similar to the "heater resistors" used during experiments conducted and components to establish their temperature coefficients. The plate, onto which the unit-under-test was secured, was heated with the aid of two (white 5W) 100Ω resistors, which were connected in parallel to a 30V power supply. The 1.5μF Wima polyester capacitor (red) was studied for its thermal properties. Notice the bulky size of the capacitor.

Photograph Bγ : A "mixed bag" of components and devices that were used, and studied, during experiments.